NCHRP

Final Report

Comparing the Corrosion Protection of Hot Dip Batch versus Hot Dip Continuously Galvanized W-Beam Guardrail Sections

Project Number: 20-07/Task 333
Task 16 Deliverable

Submitted:

November 2014

Contractor:

Elzly Technology Corporation

Executive Summary

Testing was performed to compare the corrosion performance of batch hot dip galvanized (B-HDG) and continuous hot dip galvanized (C-HDG) Type I and II coated guardrails. Type I coating has a minimum specified average coating thickness which is half that of Type II. Testing was conducted in an accelerated corrosion test chamber meeting the characteristics of General Motors Test Procedure GMW 14872 [1], Cyclic Corrosion Laboratory Test. This specification is widely used in the automotive industry for predicting the behavior of steel and zinc coated steel materials in the automotive environment.

Test articles were coated to the Type I and II standard per AASTHO M180 [2] by the B-HDG and C-HDG methods (four total combinations). Test article configurations included one-meter long straight samples, one-meter long spliced guardrail sections, and small coupons cut from production guardrail. The test articles were exposed for a period of 120-cycles, with evaluations every 30-cycles.

The corrosion performance of coatings produced by B-HDG and C-HDG processes was similar provided the galvanizing thicknesses were similar. Corrosion of the factory edges of each sample was similar amongst all samples, despite the fact that edges of the C-HDG guardrails are fabricated after galvanizing while B-HDG guardrails are galvanized after fabricating. The most significant steel substrate corrosion, as measured by depth of pitting, was on the mating surfaces of the splice and under fasteners. The splice interface of B-HDG and C-HDG exhibited measurable pitting which was comparable for the two processes. An order of magnitude increase in pit depth was observed for the thinner (Type I) coating versus the thicker (Type II) coating.

The B-HDG Type I samples tested exhibited thickness in excess of 4 oz/ft^2, more than twice the thickness of the C-HDG Type I samples. Because AASHTO M-180 only requires a *minimum* coating weight, the thicker B-HDG and thinner C-HDG both meet the Type I specification requirement. Discussions with industry representatives confirm that it is difficult to achieve the lower, Type I coating thickness in the batch hot dip process. Because Type I coating produced using the B-HDG process is inherently thicker than that of Type I produced using the C-HDG process, it exhibited better corrosion performance. This should not be misinterpreted to mean that B-HDG is intrinsically better than C-HDG. If the thickness issue is a concern to the community, a maximum weight for Type I coating could be added to the specification.

Strategies to combat corrosion in the splice should be considered in areas where corrosion limits service life of the guardrails. The metallic mating surfaces experience an accelerated form of corrosion called crevice corrosion. Crevice corrosion is traditionally combated by using a dielectric (barrier) coating, though other strategies such as additional sacrificial coating may prove effective.

The data in this report provide the basis for making material selection choices based on relative corrosivity, however a more specific correlation between environmental characteristics and corrosion performance would require the analysis of data in the literature and/or further testing.

Table of Contents

Executive Summary ii
Table of Contents iii
Table of Figures iv
Introduction 1
Background 2
Experimental Approach 6
Test Chamber Construction and Validation 7
Sample Preparation 9
Sample Exposure Orientation 10
Results and Discussion 13
Un-exposed Sample Characterization 13
Pre-Conditioned Samples 18
Test Chamber Process Control 19
Exposed Guardrail Corrosion Performance 21
Overall Visual Analysis 21
Splice Interface 28
ASTM A90 Coupon Performance 32
Pre-Conditioned Coupon Performance 35
Zinc Mass Loss 37
Corrosion Acceleration 38
Conclusions 40
Recommendations 41
References 42
Appendix A 44

Table of Figures

Figure 1: Corrosion rate of bare Cold Rolled Steel (CRS) and zinc after accelerated corrosion tests and field exposures [4]..... 3
Figure 2: Crevice Corrosion at Bolt / Guardrail Interface..... 3
Figure 3: Crevice Test Coupon..... 4
Figure 4: Galvanized Crevice Coupons..... 5
Figure 5: Temperature and Relative Humidity Data for GMW14872 Stages..... 8
Figure 6: Steel Control Coupon Mass Loss Following Exposure to 6 Cycles..... 8
Figure 7: Schematic Showing Test Specimen Fabrication Method..... 9
Figure 8: Schematic Showing Coupon Sample Location..... 10
Figure 9: Representative Mounting Rack (design and actual)..... 10
Figure 10: Guardrails as Placed in GMW14872 Chamber..... 11
Figure 11: View of Guardrail Assemblies in Closed GMW14872 Chamber..... 11
Figure 12: Manual Application of GMW14872 Solution on Guardrail Surfaces..... 12
Figure 13: DFT Measurement Locations..... 14
Figure 14: Batch Hot Dip Galvanizing Type I..... 14
Figure 15: Batch Hot Dip Galvanizing Type II..... 15
Figure 16: Continuous Hot Dip Galvanizing Type I..... 15
Figure 17: Continuous Hot Dip Galvanizing Type II..... 15
Figure 18: Zinc Coating Thickness (bars indicate one standard deviation from the average)..... 16
Figure 19: Average B-HDG Coating Intermetallic Layer Thicknesses..... 17
Figure 20. Negative Chromate Present Test..... 18
Figure 21. Confirmation of Test Accuracy..... 18
Figure 22: Average, Min and Max DFT on Pre-Conditioned Samples..... 19
Figure 23: Representative Pre-Conditioned Samples (B-HDG left, C-HDG right)..... 19
Figure 24: 10-Cycle Iterative Steel Mass Loss Data for Test Control Coupons..... 20
Figure 25: Cumulative Steel Mass Loss Data for Test Control Coupons..... 20
Figure 26: Condition of B-HDG Type I Spliced Guardrail after 120-Cycles in GMW14872..... 21
Figure 27: Condition of B-HDG Type II Spliced Guardrail after 120-Cycles in GMW14872..... 22
Figure 28: Condition of B-HDG Type I Straight Guardrail after 120-Cycles in GMW14872..... 22

Figure 29: Condition of B-HDG Type II Straight Guardrail after 120-Cycles in GMW14872 ... 23
Figure 30: Spangle on B-HDG Samples ... 23
Figure 31: Example of Red Rust Forming from Iron in the Iron-Zinc Phases ... 24
Figure 32: Condition of C-HDG Type I Spliced Guardrail after 120-Cycles in GMW14872 ... 24
Figure 33: Condition of C-HDG Type II Spliced Guardrail after 120-Cycles in GMW14872 ... 25
Figure 34: Condition of C-HDG Type I Straight Guardrail after 120-Cycles in GMW14872 ... 25
Figure 35: Condition of C-HDG Type II Straight Guardrail after 120-Cycles in GMW14872 ... 26
Figure 36: Edge Corrosion on B-HDG Spliced Samples ... 27
Figure 37: Edge Corrosion on C-HDG Spliced Samples ... 28
Figure 38: Condition at Splice Interface of B-HDG Samples ... 29
Figure 39: Condition at Splice Interface of C-HDG Samples ... 30
Figure 40: Examples of Metal Loss on Mating Surface of Spliced Samples ... 30
Figure 41: Depth of Attack Evaluated at Mated Surfaces ... 31
Figure 42: Representative Condition of Guardrail/Splice Bolt Interface on B-HDG Samples ... 31
Figure 43: Representative Condition of Guardrail/Splice Bolt Interface on C-HDG Samples ... 32
Figure 44: Representative B-HDG Coupons throughout the Test Period ... 33
Figure 45: Representative C-HDG Coupons throughout the Test Period ... 33
Figure 46: Calculated Coating Thickness from ASTM A90 Coupon Samples ... 34
Figure 47: Microscopy of C-HDG Type I Pre-Exposure (Left) and After 120-Cycles (Right) ... 34
Figure 48: Microscopy of B-HDG Type II Pre-Exposure (Left) and After 120-Cycles (Right) ... 35
Figure 49: Estimated Surface Area Percentage Exhibiting Red Rust ... 35
Figure 50: Representative Pre-Conditioned B-HDG Coupons throughout the Test Period ... 36
Figure 51: Representative Pre-Conditioned C-HDG Coupons throughout the Test Period ... 36
Figure 52: Zinc Coating Loss calculated from Coupon Mass Loss ... 37
Figure 53: Estimated Average Zinc Loss Rate as a Function of Measurement Method ... 38
Figure 54: Time to First Maintenance Prediction (American Galvanizers Association [13]) ... 39

Introduction

This is the final report for NCHRP Project Number: 20-07/Task 333, *Comparing the Corrosion Protection of Hot Dip Batch versus Hot Dip Continuously Galvanized W-Beam Guardrail Sections*. The objective of this research was to determine and compare the corrosion resistance of guardrail materials prepared by each of two (2) processes using accelerated corrosion testing. The two (2) different processes for applying a zinc coating to steel are:

1. Batch hot dip galvanizing (B-HDG)
2. Continuous hot dip galvanizing (C-HDG)

Galvanized guardrail manufactured to American Association of State Highway and Transportation Officials (AASHTO) designation M-180 [2] is used by all state highway agencies. Four types and two classes of guardrail are provided for in the specification as follows:

Type I – Zinc coated, 550 g/m² (1.80 oz/ft²) minimum single spot
Type II – Zinc coated, 1100 g/m² (3.60 oz/ft²) minimum single spot
Type III – Beams to be painted
Type IV – Beams of corrosion resistant steel

Class A – Base metal nominal thickness – 2.67 mm (0.105 in)
Class B – Base metal nominal thickness – 3.43 mm (0.135 in)

For Type I and Type II guardrails, many agencies permit batch hot dip (B-HDG) and continuous hot dip galvanizing (C-HDG) processes. The difference in corrosion performance among guardrails produced using the two processes for both types was investigated during this project.

During this project, accelerated laboratory testing of guardrail materials was conducted to the General Motors Test Procedure GMW 14872, Cyclic Corrosion Laboratory Test [1]. Test articles were coated to the Type I and II standard per AASTHO M180 by the B-HDG and C-HDG methods (four total combinations). Test article configurations included one-meter long straight samples, one-meter long spliced guardrail sections, and small coupons cut from production guardrail. The test articles were exposed for a period of 120-cycles, with evaluations every 30-cycles. The following sections address the details regarding the approach and the results following 120-cycles of testing.

Background

Analysis of material corrosion resistance has long been an important research field in product development, and natural environmental exposure has been the standard form of testing. For corrosion resistant materials like galvanized steel, natural environmental exposure tests often take too long to test a material to failure. For this reason, accelerated corrosion tests have been developed. Continuous salt spray testing first became widely adopted as a corrosion test in 1939 when the American Society of Testing and Materials (ASTM) first published ASTM B117, *"Standard Practice for Operating Salt Spray (Fog) Apparatus."*

Research into the corrosion resistance properties of batch hot dip galvanized versus continuously galvanized W-beam guardrail sections was previously evaluated using the salt fog method [3]. This testing failed to show any difference in the performance of the two materials after a substantial exposure period of 5,000 hours (208 days).

Salt fog testing has been shown to have a poor correlation with natural environments for galvanized steel due to the corrosion resistance mechanism of zinc. The auto industry, which relies heavily on zinc-coatings for their automobile rust-through warranties, regularly uses Cyclic Corrosion Testing (CCT) (as opposed to *continuous* exposure) as the "de-facto" standard for material performance. Many of these tests function on the same premise: a specimen is placed inside a chamber where it undergoes a multi-cycle test. Typically, samples are sprayed wet with a near-neutral pH, salt-containing electrolyte, exposed to a high humidity environment with an elevated temperature, and subsequently exposed to a low humidity, high heat "dry-off" cycle. Each testing method will vary the time, temperature, humidity and electrolyte content to produce a unique result.

Figure 1 shows metal loss results from different automotive manufacturer CCTs [4]. The data compares various automotive CCTs with field exposure and continuous salt spray similar to the B117 test (ISO 9227). The data show that the GM 9540P test (presently incorporated into GMW14872) process closely represents the corrosion rates for steel and zinc materials when compared to on-vehicle coupons exposed in areas subject to periodic deicing salts. In addition to automotive manufacturers, the United States military also regularly uses the GMW14872 CCT to predict service life of various coatings and materials exposed on tactical vehicles. In the above-reported test data, the GMW14872 testing was conducted for 40 "cycles" (i.e., 40 days) and was found to be equivalent to nominally one year of natural exposure, an acceleration factor of approximately 10. The military testing for coated galvanized materials estimates that 150 cycles is equivalent to 25 years, an acceleration factor of 60.

In one year of exposure, the zinc loss was 6.7 µm (0.27 mils) for the coupons exposed to deicing salts and 2.5 µm (0.10 mils) for the zinc exposed to the marine site. Other extensive testing has been carried out on zinc materials in a variety of environments. Among the harsher environments were "industrial" sites near Pittsburgh, PA, Chicago, IL, and Newark, NJ. Exposure tests at these locations have shown the worst case zinc metal loss is about 5 µm/yr (0.2 mils/year) [5][6].

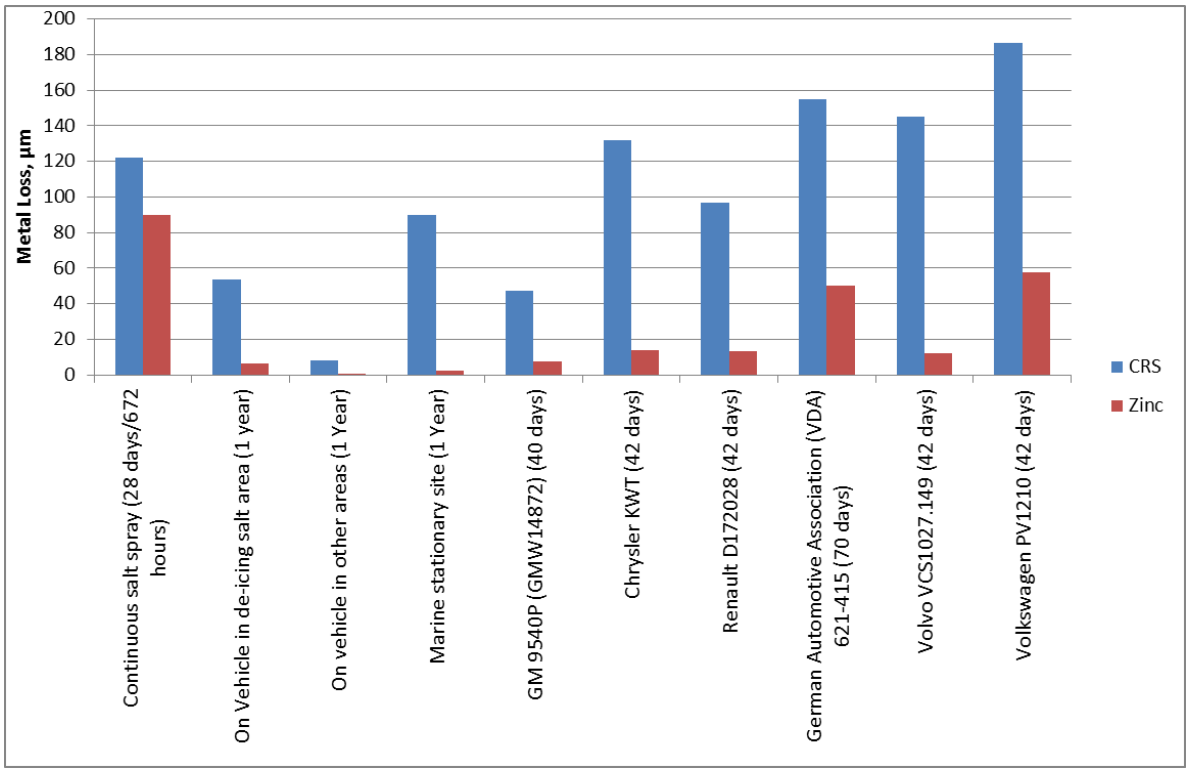

Figure 1: Corrosion rate of bare Cold Rolled Steel (CRS) and zinc after accelerated corrosion tests and field exposures [4].

The form and magnitude of corrosion are also going to be dependent on the exposure configuration of the guardrail and any of its appurtenances. Figure 1 presented corrosion loss for zinc materials directly exposed (flat specimens) to the different environments. Figure 2 shows corrosion occurring within a crevice formed at a joint between a fastener and the guardrail material – both the fastener and the guardrail are corroding at this interface. A similar condition exists at the mating surfaces of a splice joint.

Figure 2: Crevice Corrosion at Bolt / Guardrail Interface

Data from the US Army Pacific Rim Corrosion Research Program (PRCRP) included comparisons of accelerated testing and outdoor exposure for galvanized steel and zinc including boldly exposed and crevice samples [7]. The PRCRP included studies of crevices for their unique corrosion effects. Figure 3 shows the simple crevice samples. The samples were G60 galvanized steel. G60 is a continuous galvanizing process with a coating weight of 0.60 oz/ft^2 (about 1 mil). The panel was painted in all areas other than the "test area," a circular unpainted area (exposing the galvanizing) covered with another flat, painted, G60 galvanized plate. A 0.25 mm shim separated the two plates.

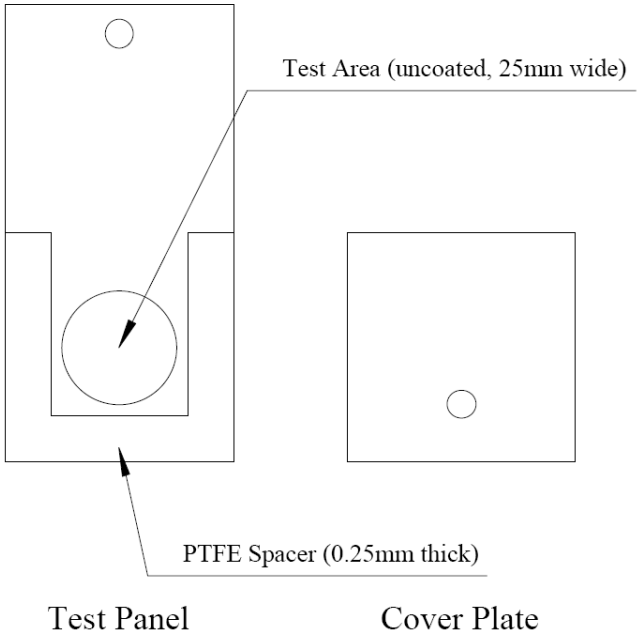

Figure 3: Crevice Test Coupon

Figure 4 shows a comparison of corrosion observed on the crevice samples from 1 year of exposure at a marine site in Sea Isle City, NJ and in the SAE J2334 CCT. SAE J2334 CCT is similar to the GMW14872 testing. The results show the corrosion loss of the galvanized steel to be more than 7 mils; this is in excess of the original zinc thickness. The underlying steel is actively corroding. Similar results are obtained in the CCT, wherein a similar degree of corrosion appears to occur between 16 and 32 cycles. This is a similar magnitude of cycles as suggested by the round-robin testing of different CCTs illustrated in Figure 1, where 40 cycles of the GMW14872 were equivalent to one year of on-vehicle exposure.

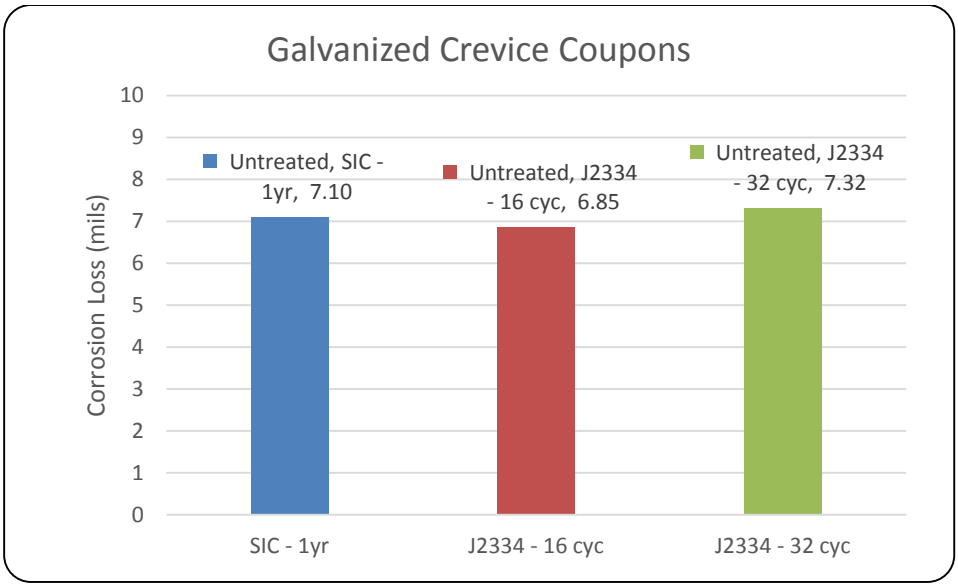

Figure 4: Galvanized Crevice Coupons

Experimental Approach

Testing consisted of exposing eight (8) Type I and Type II guardrail samples, representing both B-HDG and C-HDG, to a GMW14872 accelerated corrosion environment. Four (4) samples were 1-meter straight samples with no joint and four (4) were 1-meter joined (spliced) samples, as listed in Table 1. All samples were cut from 12.5-ft W-beam guardrails prepared to the M 180 specification.

Table 1: Full Size Sample Test Matrix

Process	Type	Form
B-HDG	I	1-meter sample, no joints
B-HDG	II	1-meter sample, no joints
B-HDG	I	1-meter joined sample
B-HDG	II	1-meter joined sample
C-HDG	I	1-meter sample, no joints
C-HDG	II	1-meter sample, no joints
C-HDG	I	1-meter joined sample
C-HDG	II	1-meter joined sample

A suite of coupons, cut from the same guardrails as the full size samples, were also exposed for the purposes of ASTM A90 coating mass analysis and testing with pre-conditioned, reduced initial coating thickness samples.

Samples were evaluated non-destructively and metallurgically to characterize the condition of the test samples as received and at periodic inspections points throughout the test. Table 2 outlines the evaluation methods for the test samples at each evaluation period. Following testing, the full sized spliced samples were disassembled for further evaluation.

Table 2: Evaluation Methods for Each Inspection Interval

Inspection Interval	Full Size Samples		As received condition				Reduced Initial Thickness	
	Visual (Including Photographs)	Non-Destructive Thickness	Visual (Including Photographs)	Coating Mass Loss (ASTM A90)	Non-Destructive Thickness	Microscopy	Visual (Including Photographs)	Non-Destructive Thickness
Pre-exposure	X	X	X	X	X	X	X	X
30-cycles	X	X	X	X	X		X	X
60-cycles	X	X	X	X	X	X	X	X
90-cycles	X	X	X	X	X		X	X
120-cycles	X	X	X	X	X	X	X	X

The following subsections provide details on the construction and validation of the test chamber as well as galvanized guardrail test sample preparation and configuration.

Test Chamber Construction and Validation

There are three (3) stages to the GMW14872 test – Ambient, Humid and Dry. Each stage requires specific temperature and humidity ranges as listed in Table 3.

Table 3: Parameters Required by GMW14872

Stage	Temperature, °C	Relative Humidity, %RH
Ambient	25 ± 3	45 ± 10
Humid (1-hr transition time allowed)	49 ± 2	~100
Dry (3-hr transition time allowed)	60 ± 2	≤ 30

During the Ambient Stage, the guardrails were placed in a 10-ft x 8-ft storage shed which contains environmental controls to maintain temperature and relative humidity levels. For the two remaining cycles, the guardrails were moved to a custom fabricated 6-ft x 4-ft test chamber. A steam generator maintained the requirements for the Humid Stage inside the test chamber. A temperature controller managed a solenoid valve on the generator to sustain the temperature and humidity requirements. Electric resistance heaters worked in conjunction with a venting system to reduce the humidity levels and increase the temperature during the Dry Stage.

A custom control unit was designed to allow the Humid and Dry Stages to run automatically. A microprocessor and a series of relays power the components systematically to create the necessary environments. To ensure that the proper environmental parameters described in GMW14872 were met, temperature and relative humidity data was tracked throughout the test period for all three stages. Figure 5 shows representative data for a single cycle, demonstrating the compliance with the required conditions listed in Table 3.

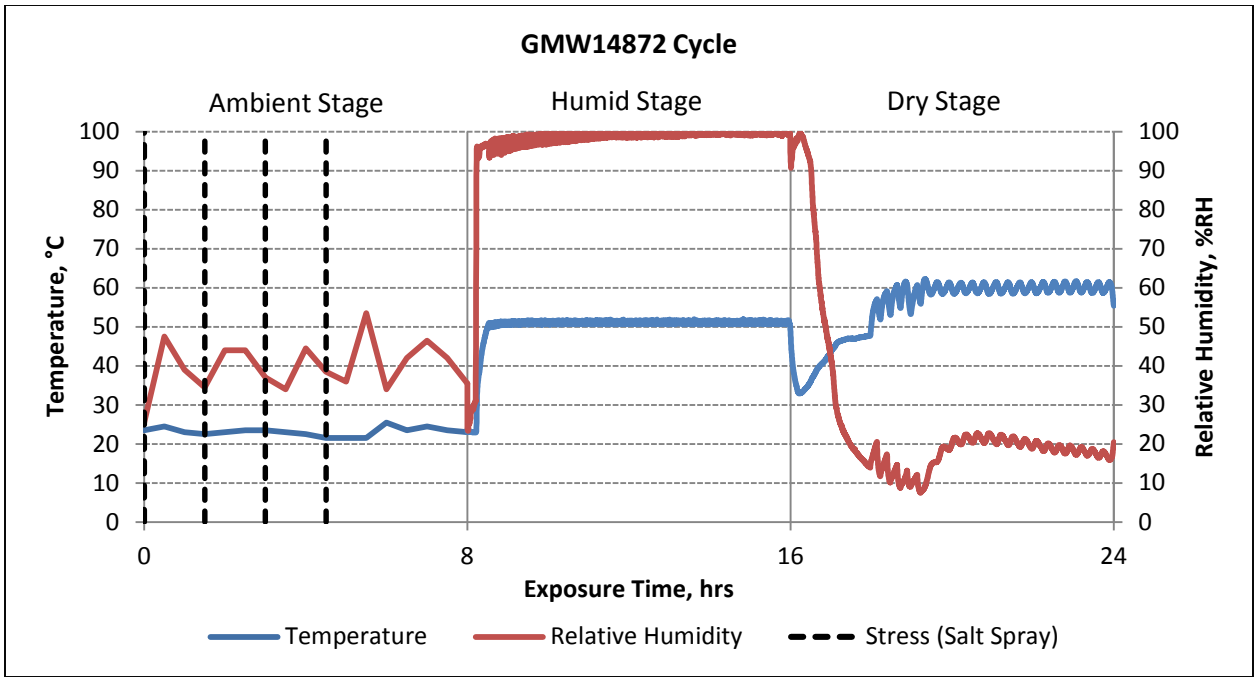

Figure 5: Temperature and Relative Humidity Data for GMW14872 Stages

After the individual stages were operational, three 1-inch x 2-inch x 0.125-inch cold-rolled steel test coupons (purchased from ACT Test Panels, stated to meet the requirements of GMW14872) were subjected to six (6) cycles of testing to validate proper operation. The GMW14872 mass loss target for steel coupons after 6±1 cycles is 0.84±0.14 g (for reference, this corresponds to an average target penetration rate of 1.4 mils per 6 cycles). Figure 6 shows that the mass loss measured for the three (3) coupons fall within the target range.

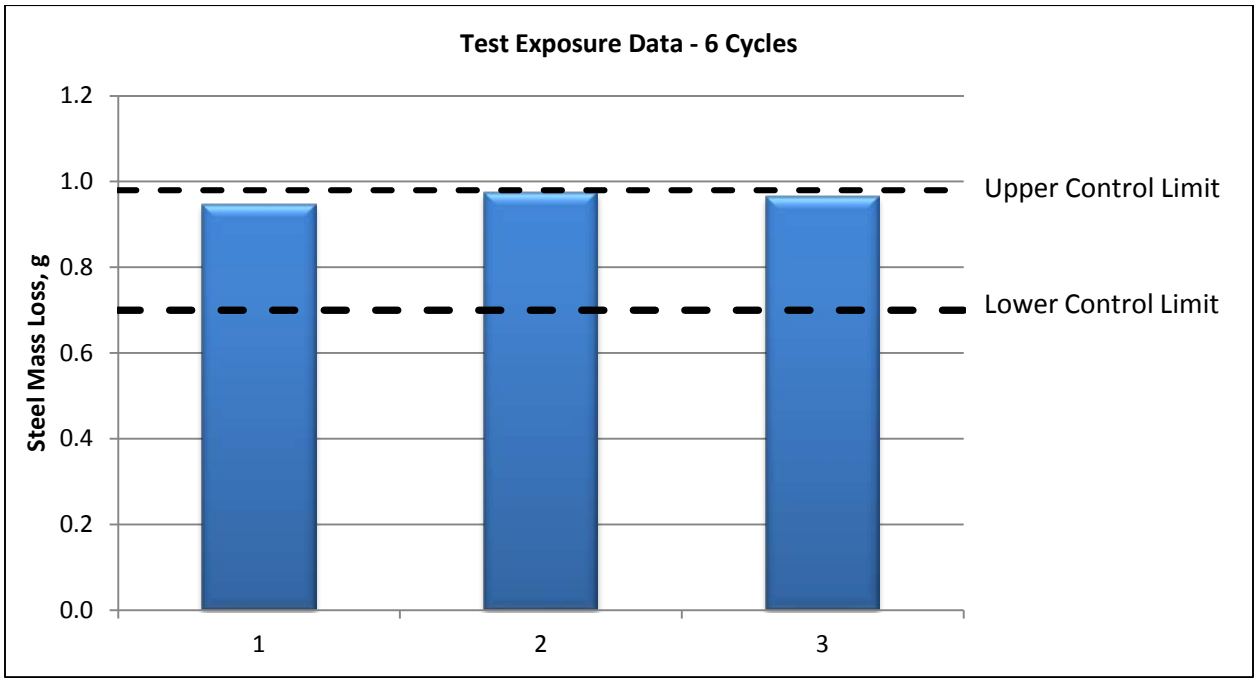

Figure 6: Steel Control Coupon Mass Loss Following Exposure to 6 Cycles

Sample Preparation

Two, 12.5-foot lengths of Type I and Type II hot dip continuous galvanized and batch hot dip galvanized guardrail were obtained from commercial suppliers for testing. Samples meeting AASHTO M180 were requested. Coating weights were measured for validation and are presented in the Results and Discussion section of this report.

For each guardrail material, coating thickness measurements were made using an electronic thickness gage to determine which of the two samples had the most consistent and representative coating thickness. The selected guardrail section was machined into the required sample sizes as described below. The remaining guardrail was held in reserve.

Figure 7 shows how the test pieces were cut from the samples. The factory ends of the guardrail (shown in gray) were used for the joined test sample. The straight test sample was cut from the middle of the guardrail (shown in blue). Twenty (20) coupons were removed from the remaining piece of guardrail (shown in red). All cut edges on B-HDG samples resulting from test sample fabrication were touched up with a zinc-rich primer and were neglected during corrosion evaluations.

Figure 8 shows a detail of where the test coupons were removed. These coupons were used for the preconditioned coupon tests and the ASTM A90 tests. The drawing shows a piece nominally 2 by 2½ inches (5 square inches) removed from a flat section of the guardrail.

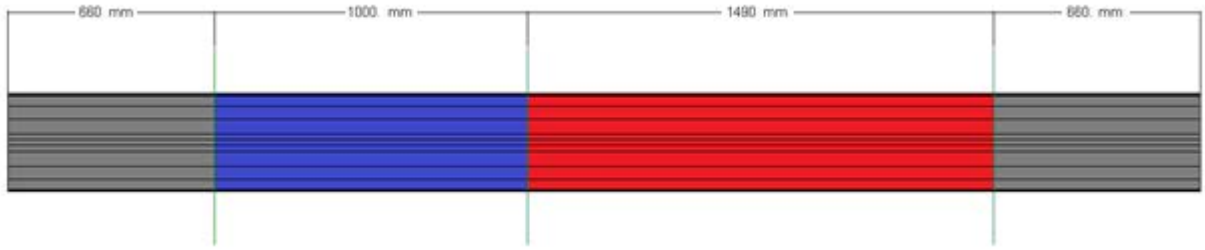

	Ends cut off to create overlapped sample • Factory edges used at overlap • Cut edges will be finished with zinc-rich primer
	1-m Section used for non-overlapped sample • Cut edges on B-HDG samples finished with zinc-rich primer
	Remaining material used to fabricate 2-in x 2.5-in test coupons for mechanical stripping test and as-received ASTM A-90 tests

Figure 7: Schematic Showing Test Specimen Fabrication Method

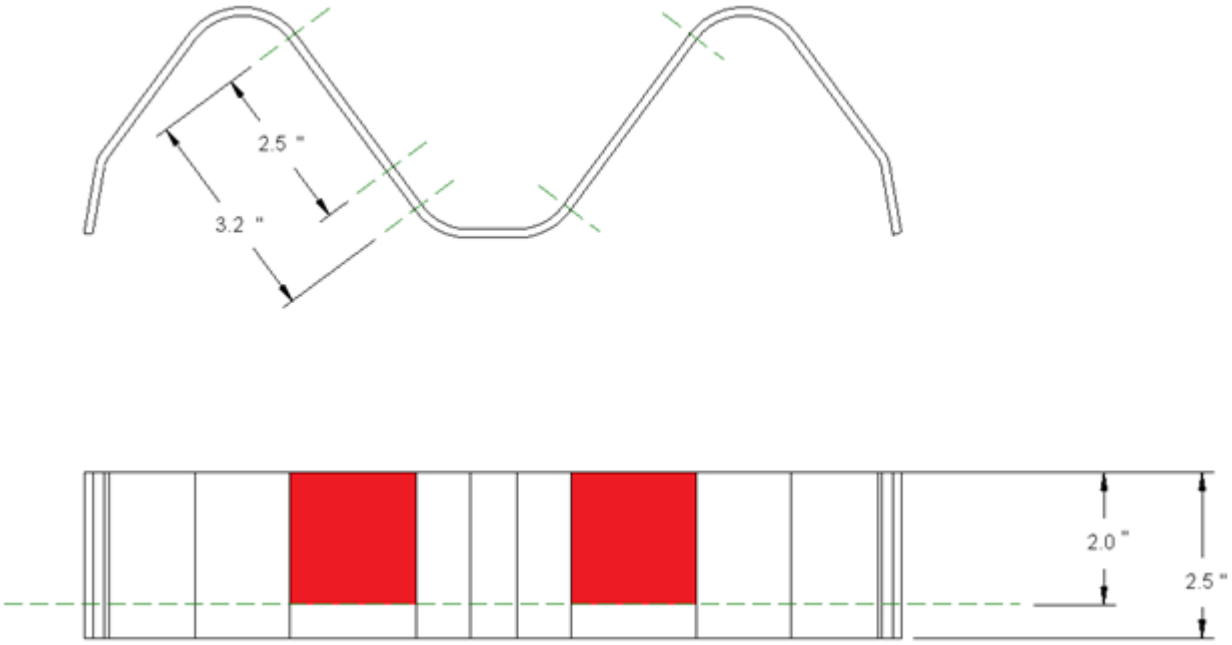

Figure 8: Schematic Showing Coupon Sample Location

Sample Exposure Orientation

To adequately represent the pertinent characteristics with respect to guardrail mounting and orientation, four (4) test racks were fabricated, each of which holds two (2) test articles (spliced and straight). Standard splice and post bolts, conforming to ASTM A307 and galvanized per ASTM A153 were utilized for the overlapped guardrail sections. Galvanized carriage bolts, also conforming to ASTM A307 and galvanized per ASTM A153 were used for mounting purposes where post bolts could not be utilized. Only the splice and post bolts were considered during evaluations. Figure 9 shows a representative mounting rack.

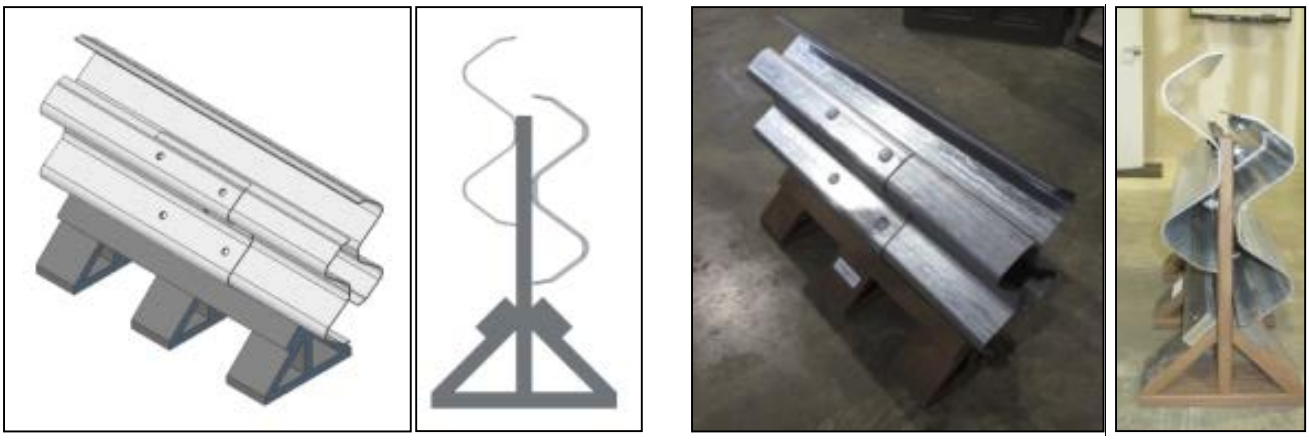

Figure 9: Representative Mounting Rack (design and actual)

Research has shown that test spacing as close as one inch does not impact accelerated corrosion test results, provided the components are not shielded from the salt spray application process [8].

Therefore, samples were placed in the test chamber such that a minimum of 1-inch spacing was allowed between samples. Steel mass loss samples (used for test chamber process control only), ASTM A90 and pre-conditioned coupons cut from other guardrail sections were placed on a table next to the guardrail racks. Figure 10 and Figure 11 show the placement and orientation of guardrails in both an open and closed chamber. The positions of each guardrail rack were rotated every 30 cycles to avoid any potential exposure bias.

Figure 10: Guardrails as Placed in GMW14872 Chamber

Figure 11: View of Guardrail Assemblies in Closed GMW14872 Chamber

During the Ambient Stage, GMW14872 salt spray solution was applied manually to all guardrail and coupons samples. This ensures thorough wetting of all guardrail surfaces, interior and exterior, as shown in Figure 12. The solution was sprayed four (4) times at 1.5-hour intervals until the surfaces were dripping wet, as required by the specification. The solution consists of

0.9% Sodium Chloride (NaCl), 0.1% Calcium Chloride ($CaCl_2$), and 0.075% Sodium Bicarbonate ($NaHCO_3$) mixed with ASTM D1193 Type IV reagent water.

Figure 12: Manual Application of GMW14872 Solution on Guardrail Surfaces

Results and Discussion

Un-exposed Sample Characterization

The coating thickness on the received guardrails was measured to characterize the samples and to develop a baseline of coating thickness data. Coating thickness was tracked throughout the exposure period using the same methods. The following three (3) methods were used to determine the coating thickness:

1. ASTM A90 – "Standard Test Method for Weight of Coating on Iron and Steel Articles with Zinc or Zinc-Alloy Coatings" was completed on three unexposed samples for each guardrail. Assured Testing Services performed this test.
2. Electronic Dry Film Thickness (DFT) – Coating thickness measurements were made at locations evenly distributed across each guardrail using an Elcometer 456 electronic coating thickness gage. The device is verified and adjusted with calibrated shims and is calibrated by the manufacturer annually.
3. Microscopy – Two ½-inch long cross sections were evaluated from perpendicular planes on each guardrail. Measurements of galvanizing thickness were made using a metallurgical microscope with digital image analysis software and/or scanning electron microscope (SEM).

Under AASHTO specification M180, galvanized guardrails are classified under two (2) types (Type I and Type II) based on coating weight. Table 4 is the table from M180 indicating the minimum coating weight to qualify for that particular type. Note that no maximum weight is indicated in the table. ASTM A90 (coating weight) measurements were taken from three (3) random samples cut from the guardrails. Table 5 shows these results, all of which meet the minimum for the single-spot test shown in Table 4, verifying that each of the test articles meets the coating weight requirement in AASHTO M180.

Table 4: AASHTO M180 Weight of Coating Requirement

Type	Min Check Limit Single-Spot Test		Min Check Limit Triple-Spot Test	
I	550 g/m^2	1.8 oz/ft^2	610 g/m^2	2.00 oz/ft^2
II	1100 g/m^2	3.6 oz/ft^2	1220 g/m^2	4.00 oz/ft^2

Table 5: ASTM A90 Test Results

Type	Sample 1	Sample 2	Sample 3	Average	Pass/Fail
B-HDG Type I	4.33 oz/ft^2	4.52 oz/ft^2	3.36 oz/ft^2	4.07 oz/ft^2	Pass
B-HDG Type II	5.10 oz/ft^2	5.08 oz/ft^2	5.05 oz/ft^2	5.08 oz/ft^2	Pass
C-HDG Type I	2.49 oz/ft^2	2.70 oz/ft^2	2.39 oz/ft^2	2.53 oz/ft^2	Pass
C-HDG Type II	4.21 oz/ft^2	3.97 oz/ft^2	4.06 oz/ft^2	4.08 oz/ft^2	Pass

Five (5) electronic coating thickness measurements (DFT) were taken on all spliced and straight guardrail samples at three (3) locations along their length as shown in Figure 13. Table 6 shows the DFT data for each coating type.

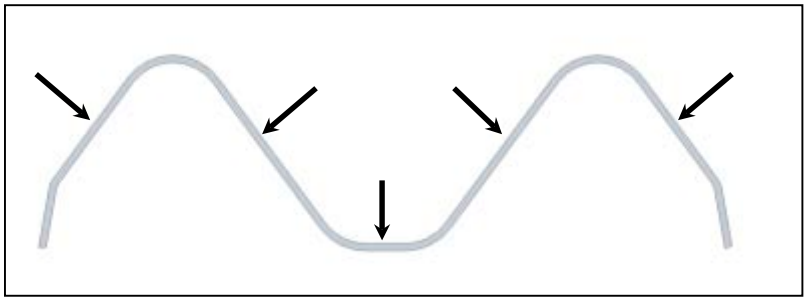

Figure 13: DFT Measurement Locations

Table 6: Electronic Dry Film Thickness Measurements

Type	DFT, mils			
	AVG	MIN	MAX	STDEV
B-HDG Type I	2.74	1.87	4.67	0.62
B-HDG Type II	4.27	3.07	5.70	0.50
C-HDG Type I	2.05	1.59	3.58	0.34
C-HDG Type II	3.37	2.06	5.17	0.49

Initial coating thicknesses were measured using optical microscopy and scanning electron microscopy. Samples were cut using a slow speed (diamond blade) metallurgical saw (which minimizes sample deformation, flaking, etc.), potted in epoxy and polished to allow coating thickness measurements to be taken. Figure 14, Figure 15, Figure 16 and Figure 17 show representative images of each type of guardrail. A complete set of SEM micrographs are provided in Appendix A.

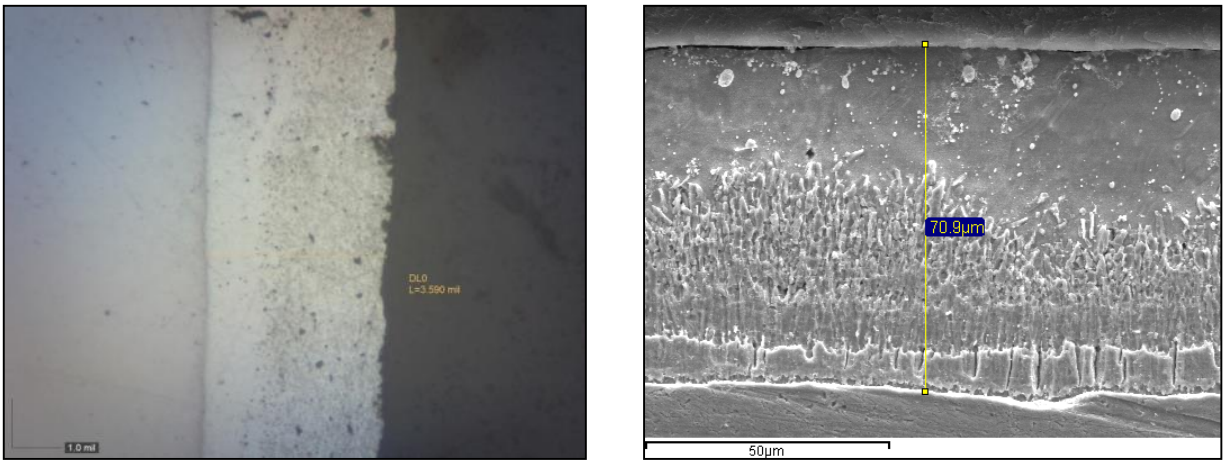

Figure 14: Batch Hot Dip Galvanizing Type I

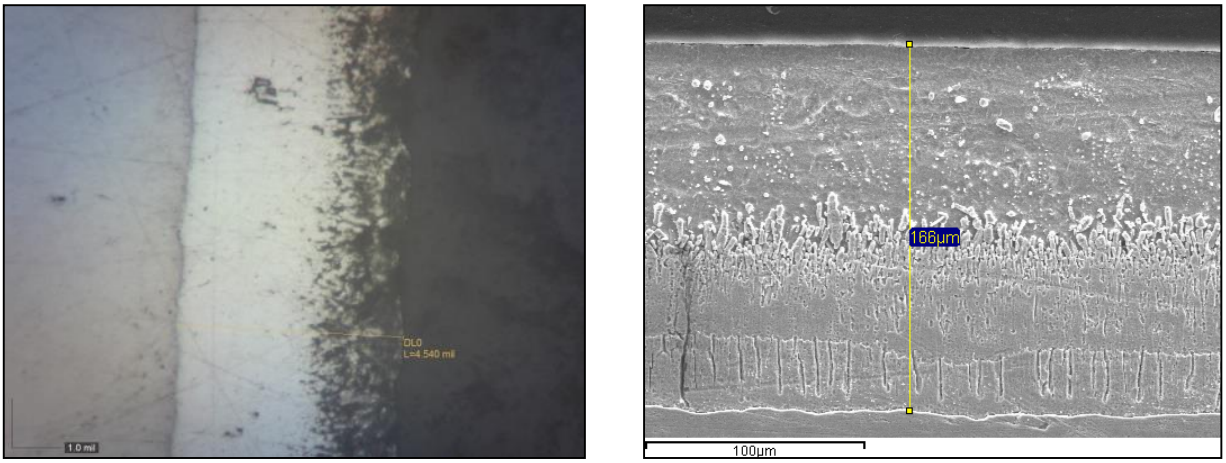

Figure 15: Batch Hot Dip Galvanizing Type II

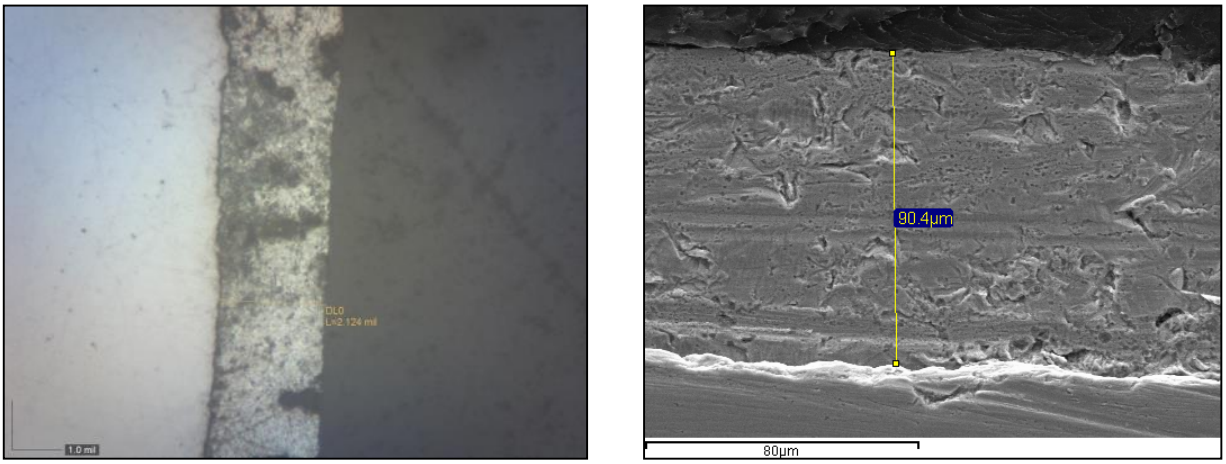

Figure 16: Continuous Hot Dip Galvanizing Type I

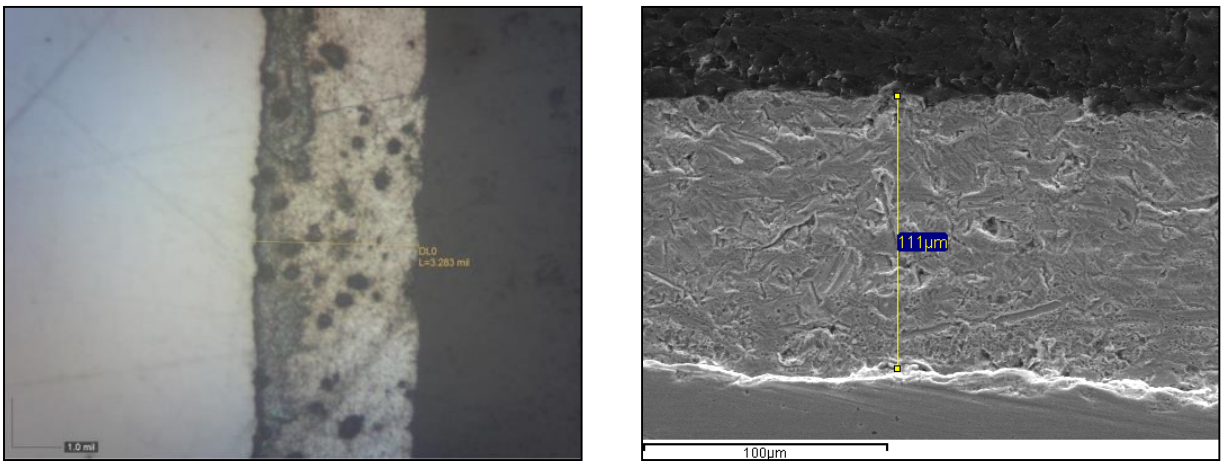

Figure 17: Continuous Hot Dip Galvanizing Type II

Figure 18 illustrates the coating thicknesses from all four (4) measurement methods. A mathematical estimate for the coating thickness based on the ASTM A90 testing (averaged from three coupons per coating type) is included for comparison purposes. This estimate was

calculated using equations 1 and 2 from ASTM A123. The equations provide an average thickness per side by assuming uniform coating thickness across the sample.

$$oz/ft^2 = \mu m \times 0.02316; \quad mils = \mu m \times 0.03937 \qquad (1)$$

$$\text{total mils (both sides)} = oz/ft^2 \times 1.7 \qquad (2)$$

The error bars in Figure 18 indicate plus or minus one standard deviation from the average measured value. Dotted lines indicate the coating thickness equivalent required for Type I and Type II coatings calculated using the M180 minimum coating mass requirements and the above equations. The data confirm that the guardrails all meet the required minimum coating thickness. The data suggest that the B-HDG process produces a thicker coating than the C-HDG process for both Type I and Type II coatings. The elevated thickness of the B-HDG samples is not surprising. Thicknesses are routinely exceeded by galvanizers due to the nature of the B-HDG process [9]. Discussions with industry representatives confirm that it is difficult to achieve the lower, Type I coating thickness in the batch hot dip process.

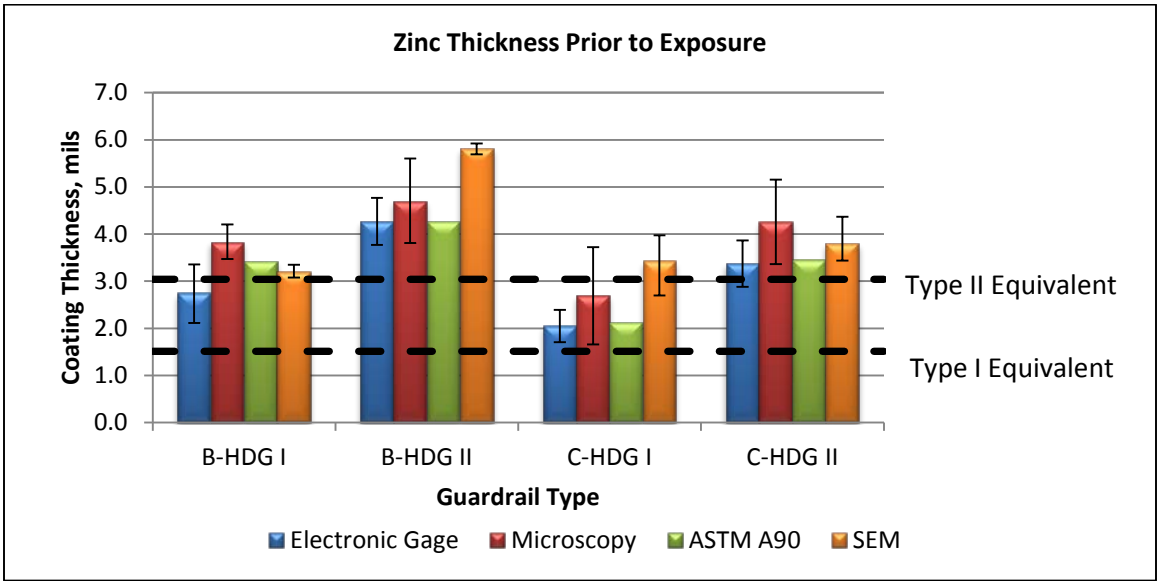

Figure 18: Zinc Coating Thickness (bars indicate one standard deviation from the average)

The SEM images in Appendix A were used to determine the alloy layer thicknesses for the B-HDG coatings. Each visually discernable layer was measured. The decreased zinc concentrations indicated in the EDX spectra (also in Appendix A) corroborate the visual delineations in the micrographs. Due to the semi-quantitative nature of the EDX process (with an accuracy of ±10 %), the intermetallic layer compositions could not be quantitatively identified accurately. Table 7 lists the averages and standard deviations for the intermetallic layer thickness values measured on the B-HDG samples during SEM analysis. Figure 19 visually demonstrates the average layer thicknesses.

Table 7: B-HDG Intermetallic Layer Thickness Values

Layer	B-HDG I		B-HDG II	
	AVG	STDEV	AVG	STDEV
Eta	1.992	0.377	2.719	0.273
Zeta	1.131	0.392	2.004	0.396
Delta	0.337	0.040	1.002	0.095
Gamma	0.043	0.018	0.065	0.015

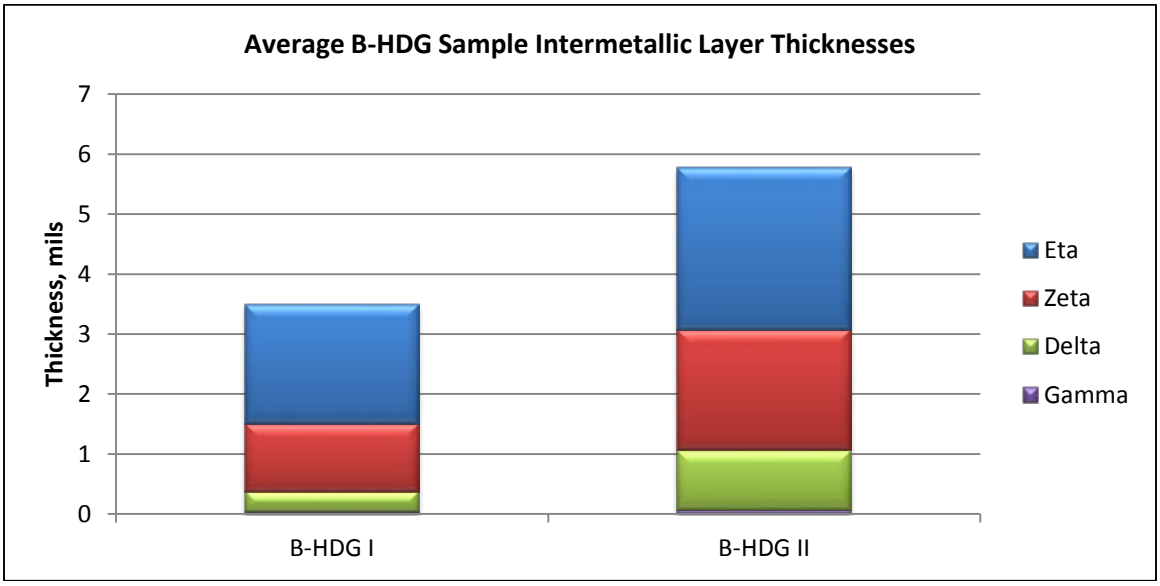

Figure 19: Average B-HDG Coating Intermetallic Layer Thicknesses

Prior to testing, test articles were tested for the presence of chromates on the surface. Tests were completed using Chromate Check™ swabs. These swabs produce an instant, non-destructive test result. The swab was rubbed on the surface of the test article, and its color observed. No color change indicates no chromates are present. The same swab was then rubbed on a confirmation card that would cause it to turn purple, indicating that the test was valid. In the event the swab did not change color when rubbed on the confirmation card, the test would be declared invalid and a second test would be conducted with a new swab. Figure 20 and Figure 21 show representative images of the negative test results and the positive test confirmation.

No chromates were found on the C-HDG Type I or II and the B-HDG Type II Samples. However, chromates were detected on the B-HDG Type I samples. The chromate process is typically a means to protect samples while in storage (nominally 6-weeks). Due to the accelerated nature of the GMW14872 test, chromates were no longer detectable after one cycle. After the first cycle, the B-HDG Type I and Type II samples were similar in appearance. The observations suggested that the initially detectable chromates would not influence the results.

Figure 20. Negative Chromate Present Test

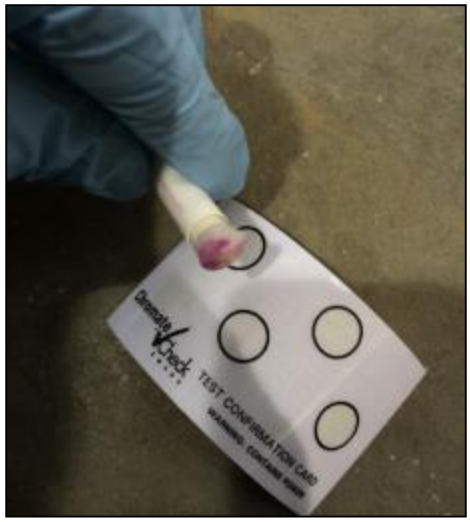

Figure 21. Confirmation of Test Accuracy

Pre-Conditioned Samples

Various mechanical and chemical means were considered to remove a portion of galvanized coating before exposure inside the simulated corrosive environment. Each of the methods resulted in an uneven final thickness (perhaps due in part to uneven initial conditions). Based on preliminary testing, abrasive blasting with fine grit aluminum oxide media (230-325 grit) was used to remove some of the galvanized coating prior to testing. Each coupon was blasted using the same pattern (horizontally followed by vertically in a checkerboard like pattern). After each evolution of blasting, five (5) dry film thickness measurements were performed. This process was repeated until less than 1 mil was achieved on at least two (2) of the five (5) locations. Each blasting pass required approximately one (1) minute, after which the sample was not noticeably warm. Therefore, we do not believe that the time or temperature was sufficient for any alloying effect.

Figure 22 shows the average, minimum and maximum dry film thickness measurements taken on the pre-conditioned samples. The resulting surfaces had uneven coating thickness between 0.04 and 6.4 mils. Figure 23 shows examples of the pre-conditioned samples. The B-HDG samples tended to have more steel/alloy layer exposed than the C-HDG samples. Table 8 shows the number of individual measurements falling into various ranges. At each inspection period coating thickness was again measured at each location to try to attempt to detect changes in behavior associated with the interface between the zinc and steel.

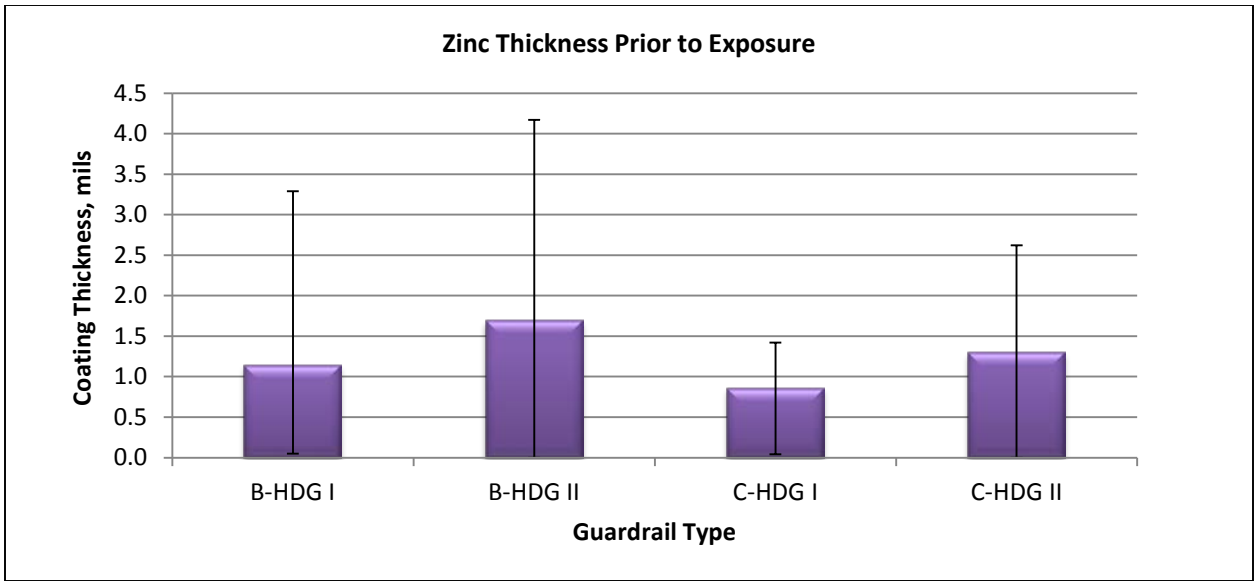

Figure 22: Average, Min and Max DFT on Pre-Conditioned Samples

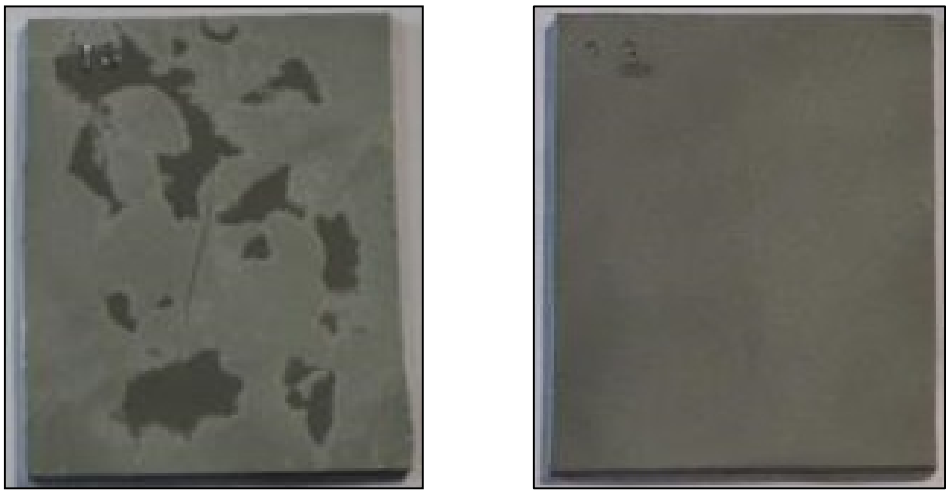

Figure 23: Representative Pre-Conditioned Samples (B-HDG left, C-HDG right)

Table 8: Range of Reduced Thicknesses

Thickness, mils	B-HDG I	B-HDG II	C-HDG I	C-HDG II
< 0.25	6	3	6	3
.25 ≥ x < .5	6	5	4	5
.5 ≥ x < .75	3	10	1	5
.75 ≥ x >1	9	10	7	7
1 ≥ x > 1.25	7	16	2	4
≥ 1.25	19	6	30	26

Test Chamber Process Control

The GMW14872 test exposure conditions are verified by monitoring mass loss of steel coupons. Target ranges for the number of cycles necessary to meet the required mass loss ranges are listed

in the specification. To ensure proper exposure test conditions, duplicate 1-inch x 2-inch x 0.125-inch cold-rolled steel uncoated mass loss coupons (purchased from ACT Test Panels, stated to meet the requirements of GMW14872) were exposed and removed every 20 cycles to track overall corrosion progression. Additional duplicate coupon sets were removed and replaced every 10 cycles to track interim corrosion. Figure 24 shows the iterative 10-cycle steel mass loss data and Figure 25 shows the cumulative target steel mass loss range (in green) and the data measured. The elevated mass loss between cycles 40 and 50 may be due to increased ambient time (without solution spray) during repairs to the test chamber. The cumulative mass loss data demonstrate that the test has been performed in accordance with the requirements.

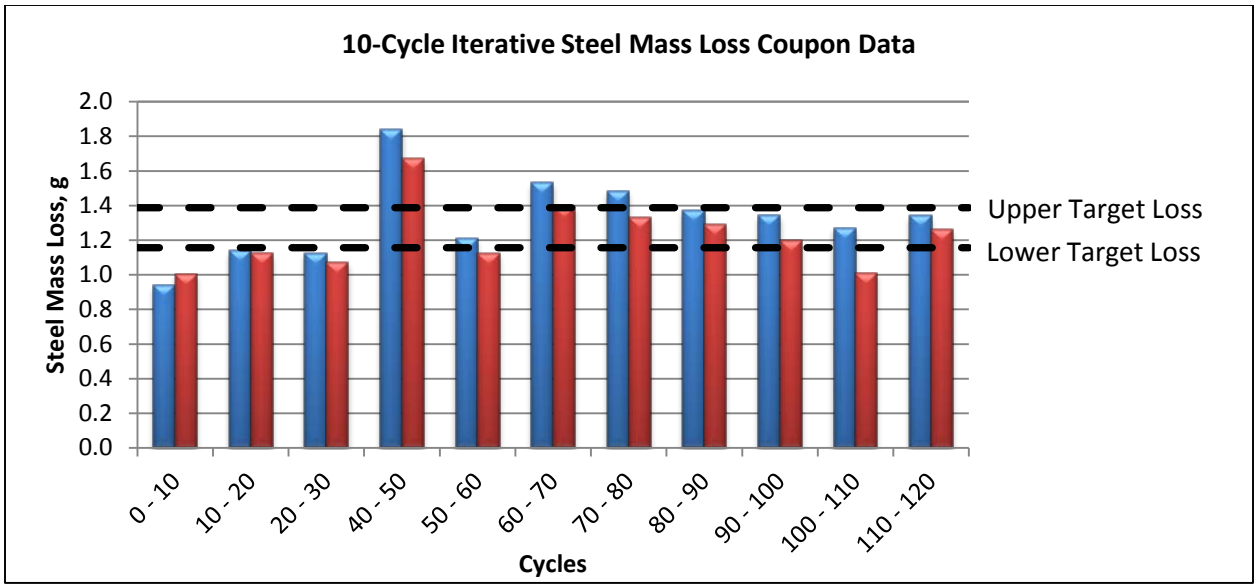

Figure 24: 10-Cycle Iterative Steel Mass Loss Data for Test Control Coupons

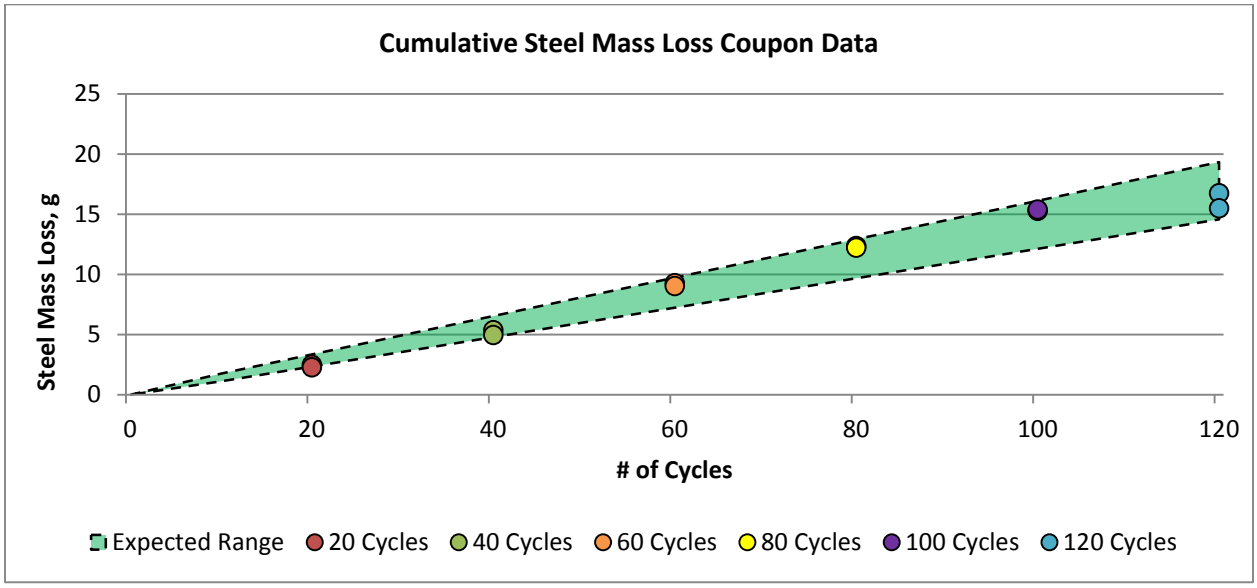

Figure 25: Cumulative Steel Mass Loss Data for Test Control Coupons

Exposed Guardrail Corrosion Performance

Overall Visual Analysis

Figure 26 through Figure 29 show the conditions of the B-HDG spliced and straight guardrails after 120-cycles of exposure in the GMW14872 chamber. All surfaces of the B-HDG guardrails exhibited white zinc corrosion product. Additionally, following 120-cycles of exposure, spots of red rust were observed scattered across each of the B-HDG samples. The red rust spots were initially observed during the 30-cycle inspection and progressed to encompass more of the guardrail surface throughout the duration of the test. The rusting seemed to begin at the bottom surface and progress toward the top surfaces. Less red rust was observed on the Type II (thicker) samples than on Type I (thinner) samples.

B-HDG Type I

Figure 26: Condition of B-HDG Type I Spliced Guardrail after 120-Cycles in GMW14872

B-HDG Type II

Figure 27: Condition of B-HDG Type II Spliced Guardrail after 120-Cycles in GMW14872

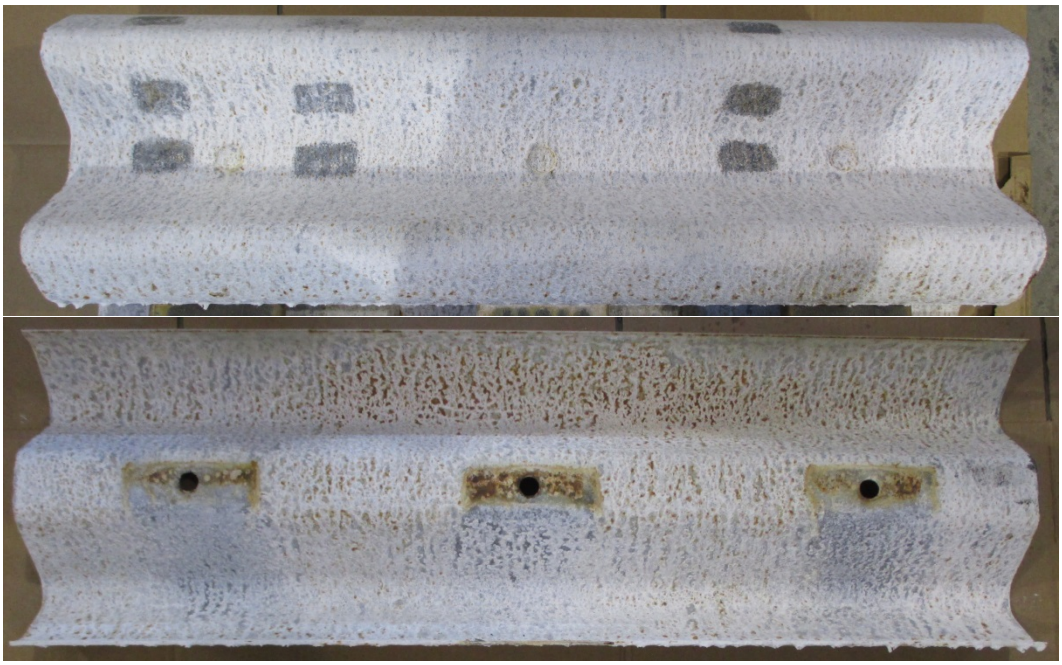

B-HDG Type I

Figure 28: Condition of B-HDG Type I Straight Guardrail after 120-Cycles in GMW14872

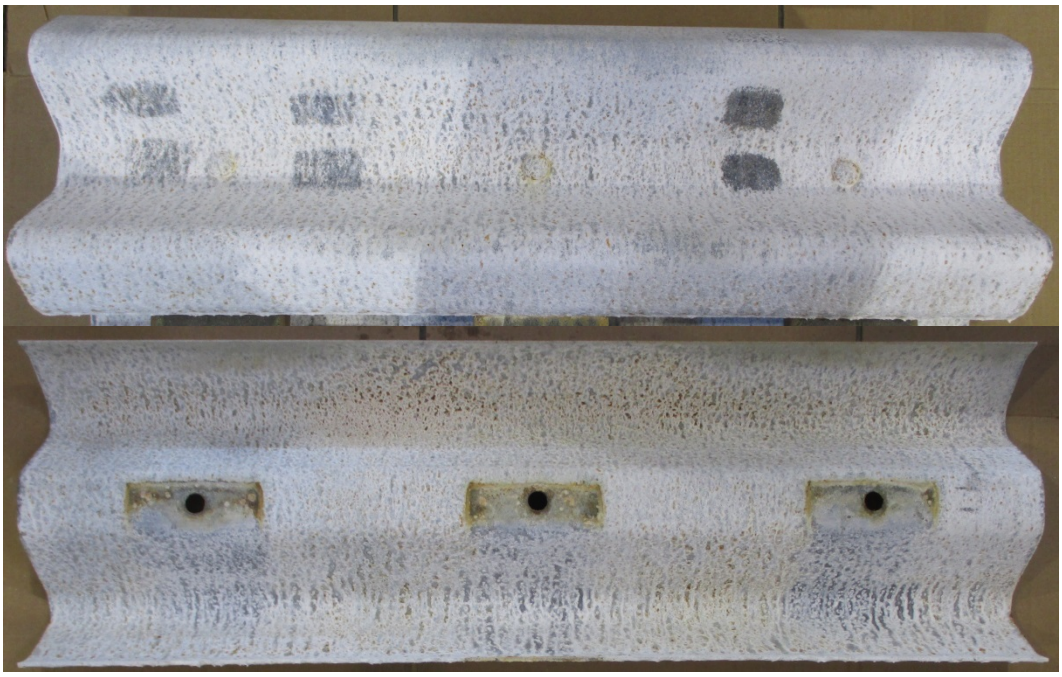

B-HDG Type II

Figure 29: Condition of B-HDG Type II Straight Guardrail after 120-Cycles in GMW14872

Aside from at edges and mated interfaces, the red rust does not appear to be substrate corrosion, but likely results from oxidation of iron in the intermetallic layers [10]. The scattered nature of the observed red rust may be the result of the thinner grain boundaries of the spangle (observed pre-exposure and shown in Figure 30) [11-12]. The center areas of the spangle have thicker coating in which the eta layer would last longer. Figure 31 shows an example of the red rust observed and the condition after corrosion product removal with glass bead media. No measurable steel pitting is evident. Pitting of the steel substrate was observed on areas of the factory edges at the splice interface and at the interfaces to the mounting posts. Less pitting was observed on the Type II (thicker) samples than on Type I (thinner) samples.

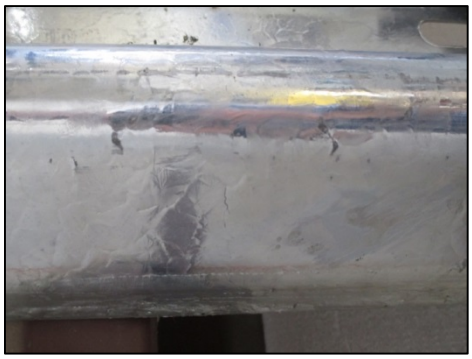

Figure 30: Spangle on B-HDG Samples

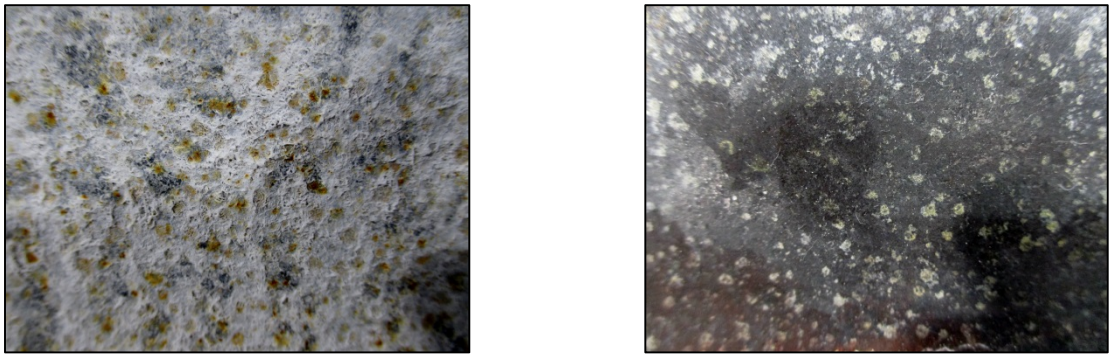

Figure 31: Example of Red Rust Forming from Iron in the Iron-Zinc Phases

Figure 32 through Figure 35 show the condition of the spliced and straight C-HDG guardrail samples. All surfaces of the C-HDG guardrails exhibited white zinc corrosion product. Additionally, following 120-cycles of exposure, varying degrees of red rust were observed on each of the C-HDG samples. Less rusting was observed on the Type II (thicker) samples than on Type I (thinner) samples. Red rusting associated with steel substrate corrosion and pitting was observed at areas on the factory edges at the splice interface and at the interfaces to the mounting posts. Furthermore, significant rust-through was observed on the bottom surface of the Type I guardrails.

C-HDG Type I

Figure 32: Condition of C-HDG Type I Spliced Guardrail after 120-Cycles in GMW14872

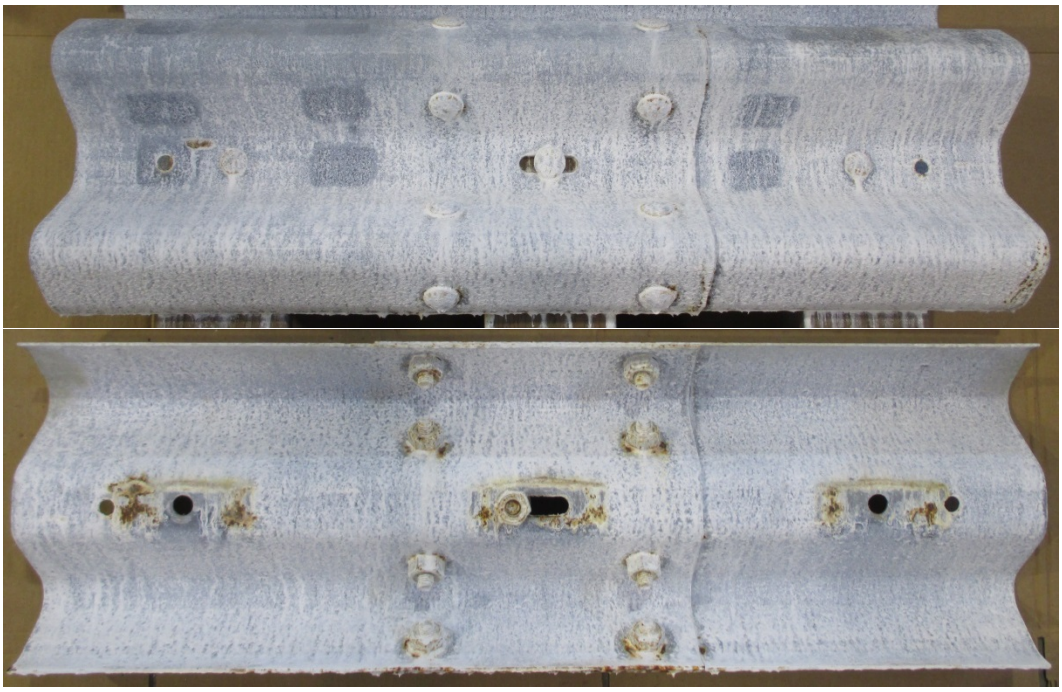

C-HDG Type II

Figure 33: Condition of C-HDG Type II Spliced Guardrail after 120-Cycles in GMW14872

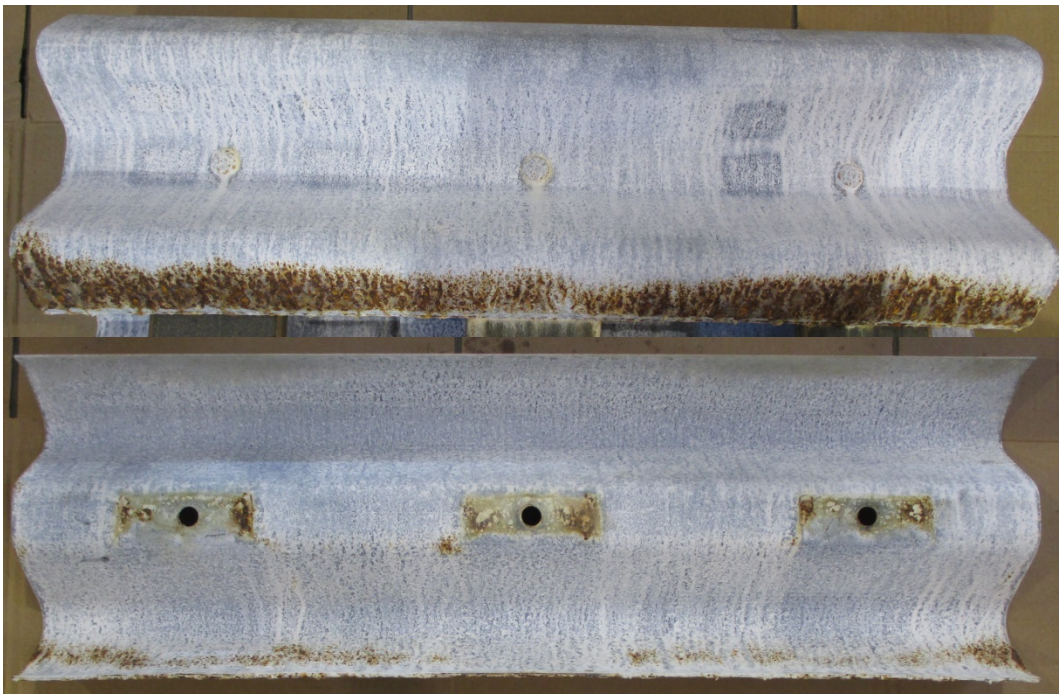

C-HDGI Type I

Figure 34: Condition of C-HDG Type I Straight Guardrail after 120-Cycles in GMW14872

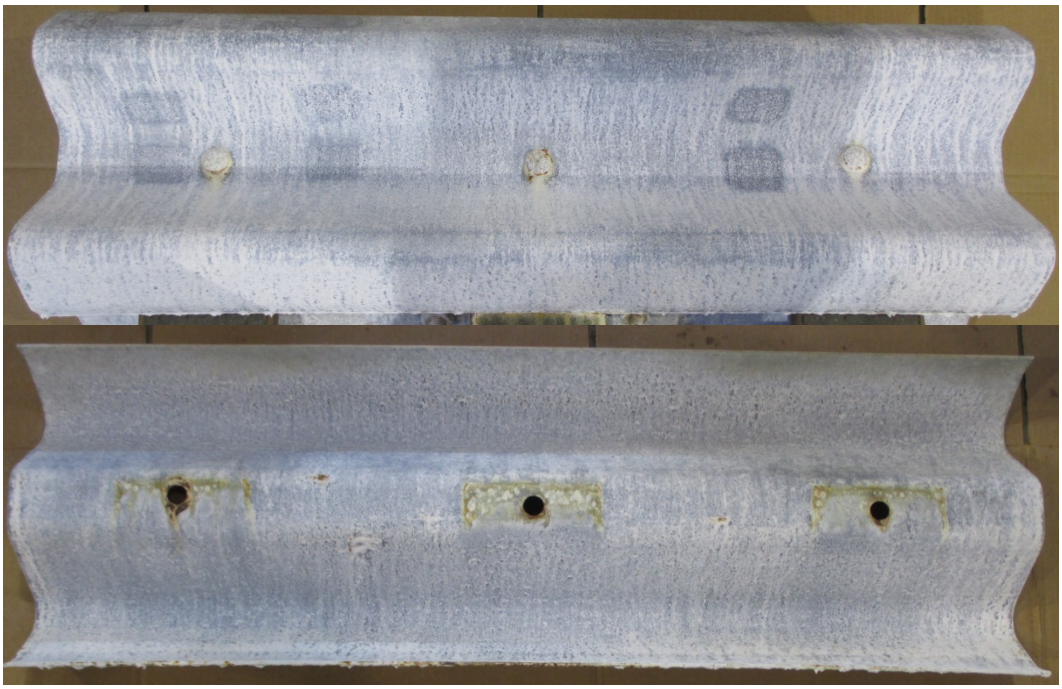

C-HDG Type II

Figure 35: Condition of C-HDG Type II Straight Guardrail after 120-Cycles in GMW14872

Figure 36 and Figure 37 more closely demonstrate the corrosion observed at the factory edges of each of the spliced guardrails. The Type I samples generally exhibited more substrate corrosion than the Type II samples for both coating types. The C-HDG samples exhibited similar corrosion to the B-HDG samples, despite the fact that these edges are uncoated. While the coating thickness on the edges of the B-HDG samples was not specifically measured prior to testing, the samples were carefully handled and there was no remarkable evidence of damage prior to testing.

B-HDG Type I

B-HDG Type II

Figure 36: Edge Corrosion on B-HDG Spliced Samples

C-HDG Type I

C-HDG Type II

Figure 37: Edge Corrosion on C-HDG Spliced Samples

Splice Interface

Figure 38 and Figure 39 show the conditions of the mated surfaces of the spliced guardrails after exposure. There was less visible surface rusting on the mating surface of the Type II samples than Type I samples for both galvanizing processes. The C-HDG samples had less visible surface rusting than the B-HDG samples.

Each of the mated surfaces was glass bead blasted to evaluate metal loss by measuring pit depths. There were deeper pits on the Type I samples than the Type II samples. However, the C-HDG samples and B-HDG samples had comparable depth of attack for samples of the same Type. This suggests that the visible surface rusting on the B-HDG samples looks more severe due to iron from the intermetallic layers. Figure 40 shows examples of metal loss on the respective Type I samples.

Due the curvature of the samples, depth of attack was difficult to measure, but attempts were made with a pit depth gauge (measurements are approximate). Figure 41 shows a cumulative distribution of measurable depth of attack for each guardrail type.

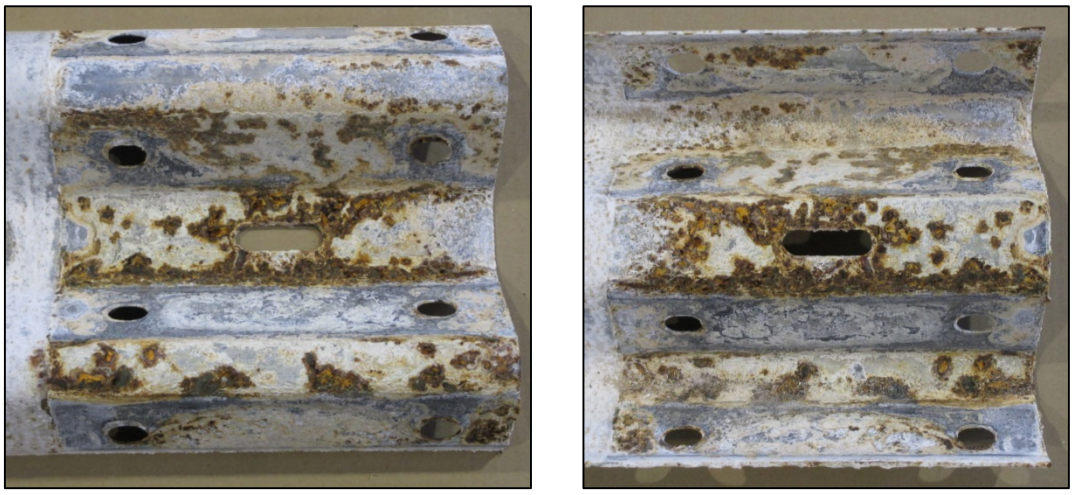

B-HDG I

B-HDG II

Figure 38: Condition at Splice Interface of B-HDG Samples

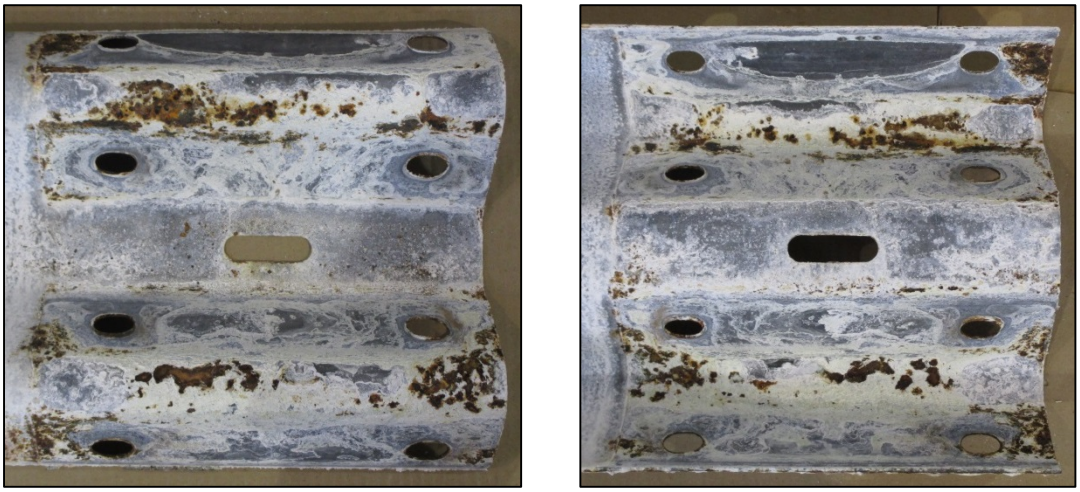

C-HDG I

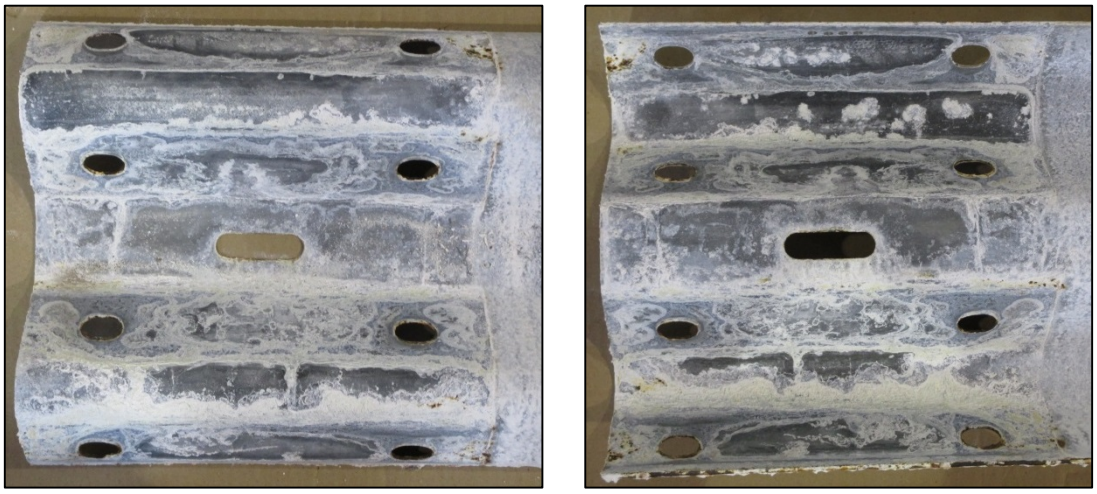

C-HDG II

Figure 39: Condition at Splice Interface of C-HDG Samples

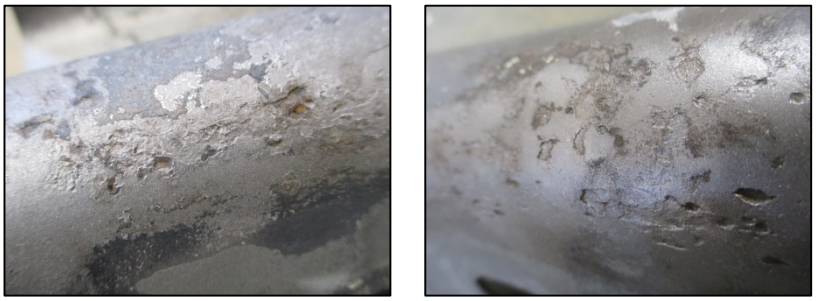

B-HDG I C-HDG I

Figure 40: Examples of Metal Loss on Mating Surface of Spliced Samples

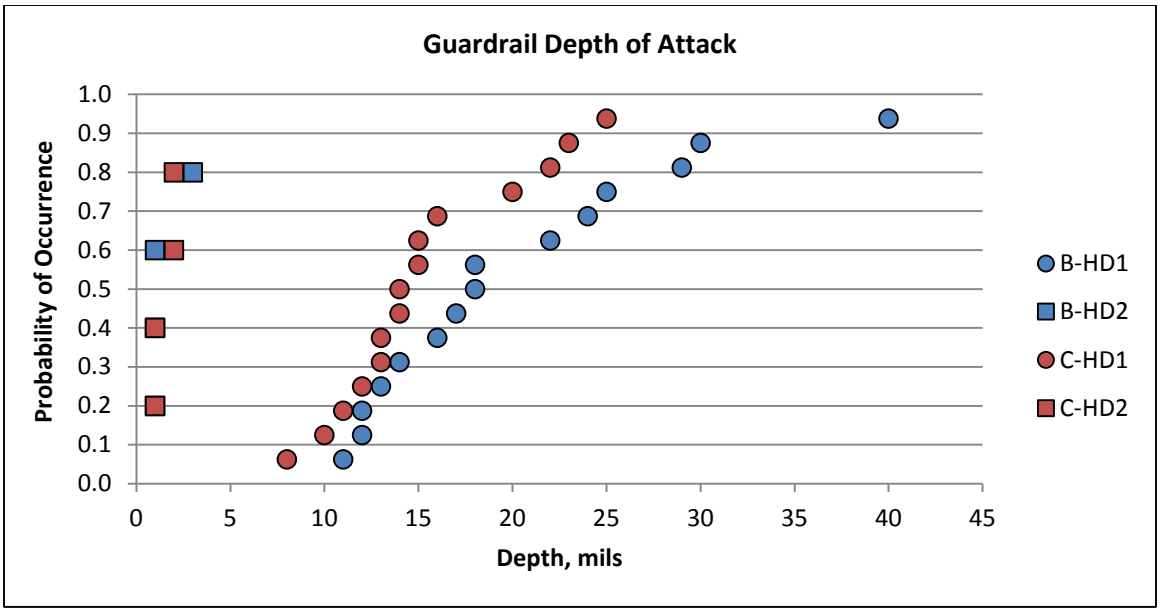

Figure 41: Depth of Attack Evaluated at Mated Surfaces

Figure 42 and Figure 43 show representative condition of the guardrail at a splice bolt interface for B-HDG and C-HDG samples. The B-HDG samples had less red rust and pitting at interfaces to the splice bolts than C-HDG samples. Depth of attack was most severe on the C-HDG I sample, but it was not enough to compromise the structural integrity of the guardrail.

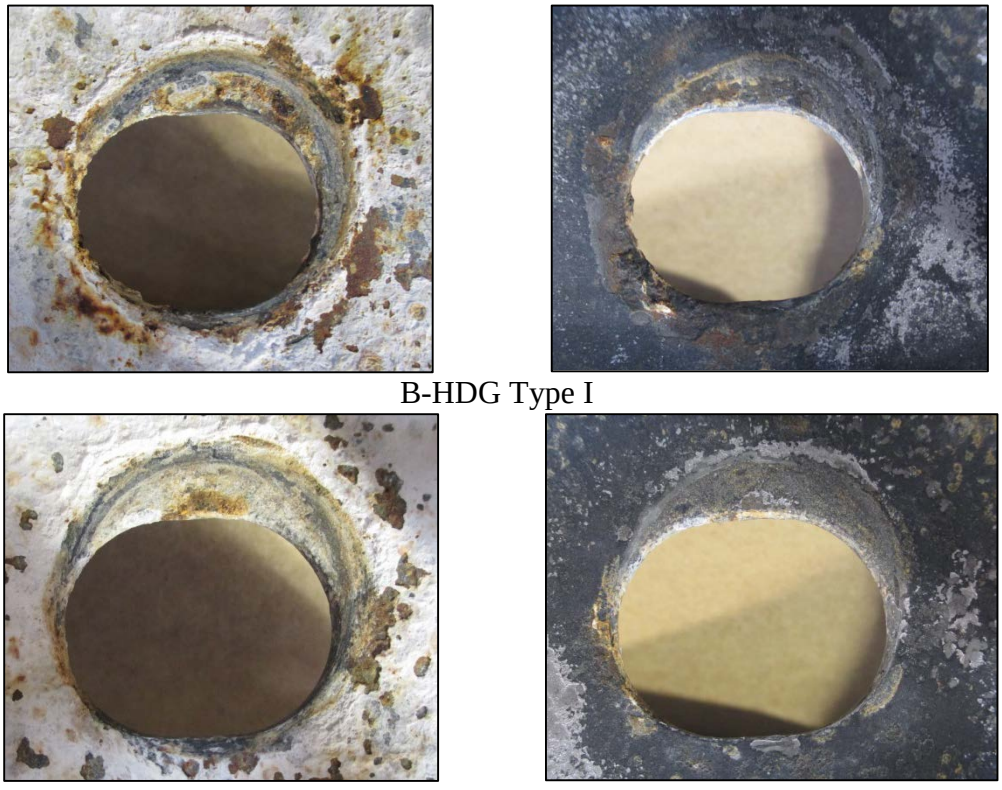

B-HDG Type I

B-HDG Type II

Figure 42: Representative Condition of Guardrail/Splice Bolt Interface on B-HDG Samples

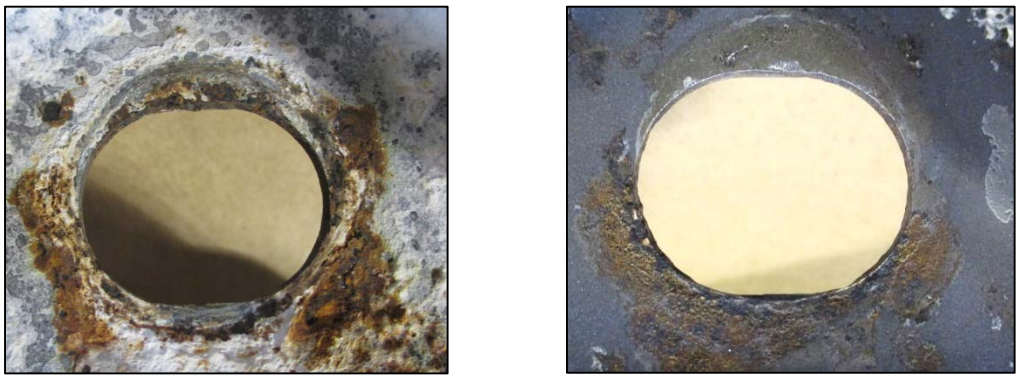

C-HDG Type I

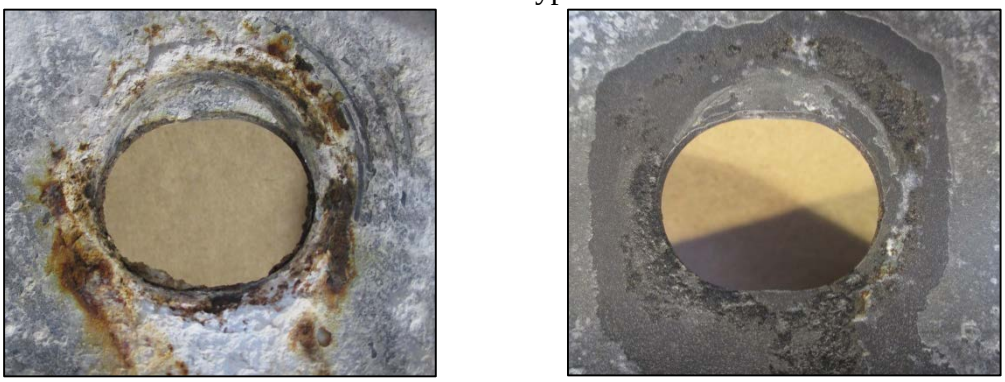

C-HDG Type II

Figure 43: Representative Condition of Guardrail/Splice Bolt Interface on C-HDG Samples

ASTM A90 Coupon Performance

The 2-in x 2.5-in coupons exhibited similar corrosion as their guardrail counterparts, with the C-HDG Type I samples exhibiting the most severe corrosion after 120-cycles. The B-HDG samples further demonstrate the effect of the spangle, with corrosion initially appearing in the area of the grain boundaries before progressing. Figure 44 and Figure 45 show representative photos of one coupon set at each inspection interval.

At each inspection interval, one replicate coupon for each material was removed, blasted with glass bead media to remove corrosion product, and sent for ASTM A90 analysis. The blasting process took approximately two (2) minutes per side to remove the corrosion product. To ensure that no coating was removed during this process, an unexposed coupon of both B-HDG and C-HDG was blasted in one (1) minute intervals up to a maximum of five (5) minutes, and weighed each time. At most, only 0.008 grams (.007 mils) and 0.011 grams (0.009 mils) were removed for B-HDG and C-HDG, respectively, which was considered negligible.

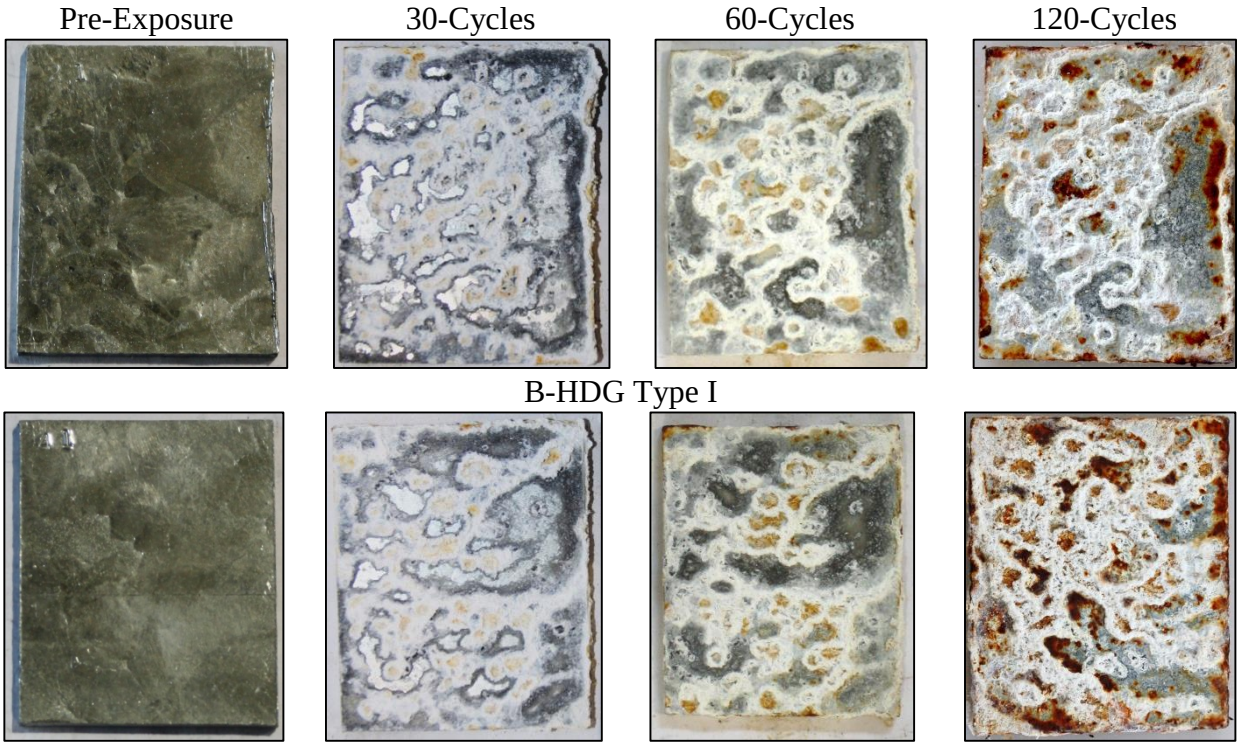

Figure 44: Representative B-HDG Coupons throughout the Test Period

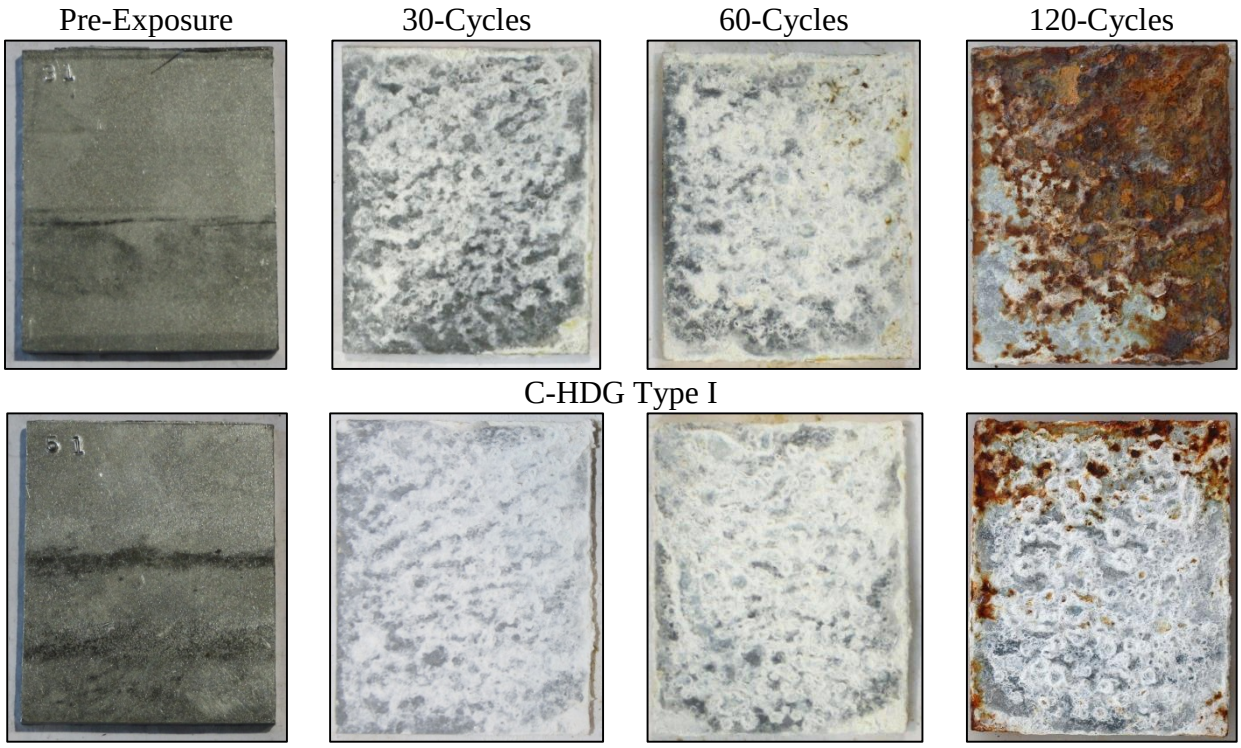

Figure 45: Representative C-HDG Coupons throughout the Test Period

Figure 46 shows the estimated remaining coating thicknesses based on the coating mass results (these calculated coating thickness values assume uniform coating thickness across the sample and are therefore considered only an estimate for comparison purposes.). These data support the microscopy observations, in which little to no coating was visible. Figure 47 and Figure 48 show representative examples of microscopy observations after 120-cycles as compared to pre-exposure. SEM images of all materials after 60 cycles are included in Appendix A.

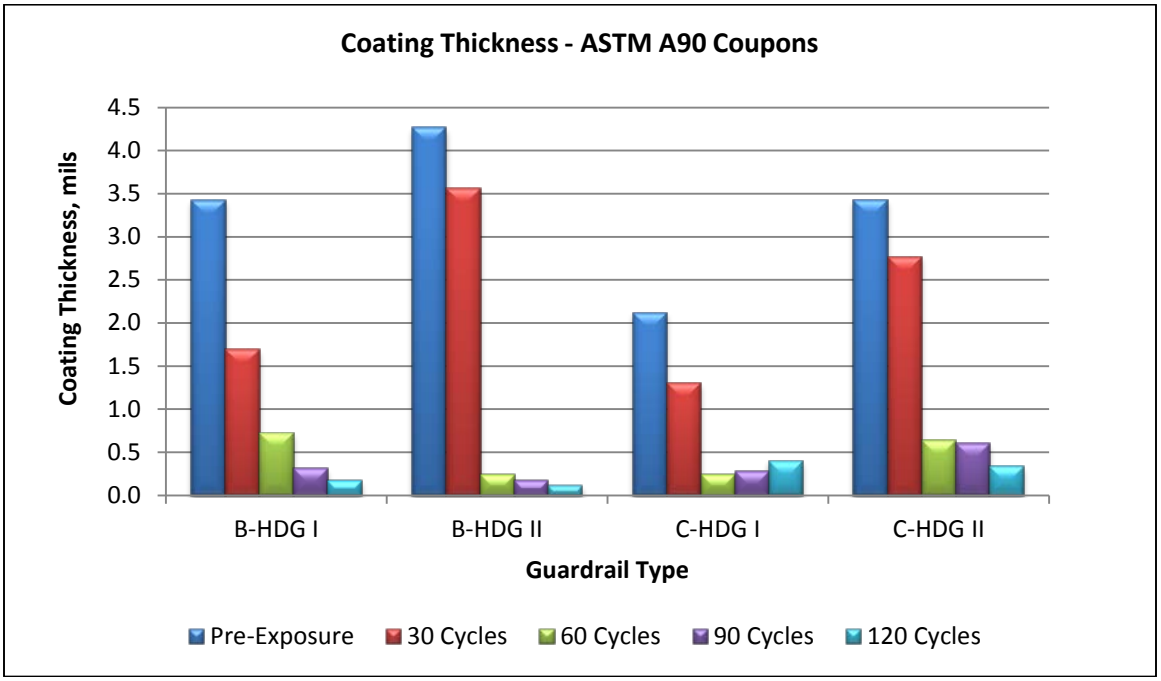

Figure 46: Calculated Coating Thickness from ASTM A90 Coupon Samples

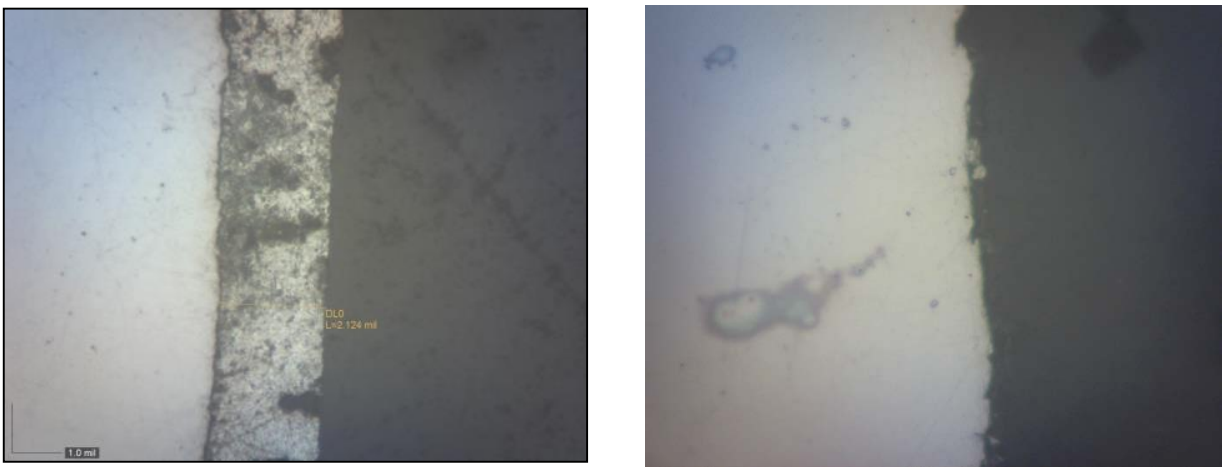

Figure 47: Microscopy of C-HDG Type I Pre-Exposure (Left) and After 120-Cycles (Right)

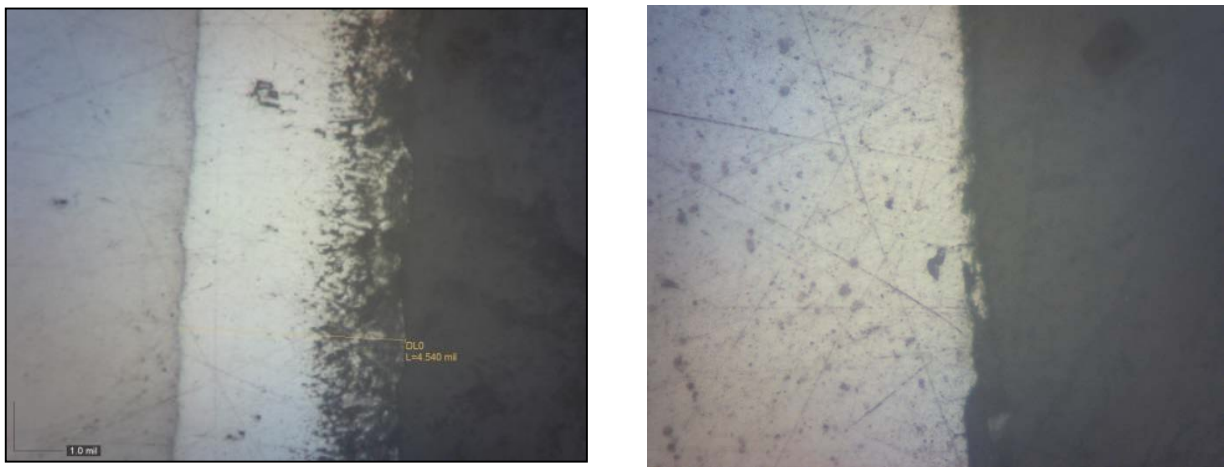

Figure 48: Microscopy of B-HDG Type II Pre-Exposure (Left) and After 120-Cycles (Right)

Figure 49 shows the average percent of red rust estimated visually on the coupon surfaces at each of the evaluation periods. The B-HDG samples exhibited 1-10% surface rust during the early stages of exposure. However, after the final evaluation and sample teardown that most of the observed rust was superficial rust and not the result of measurable substrate corrosion. Visible rust on the C-HDG Type I samples does appear to be the result of substrate corrosion.

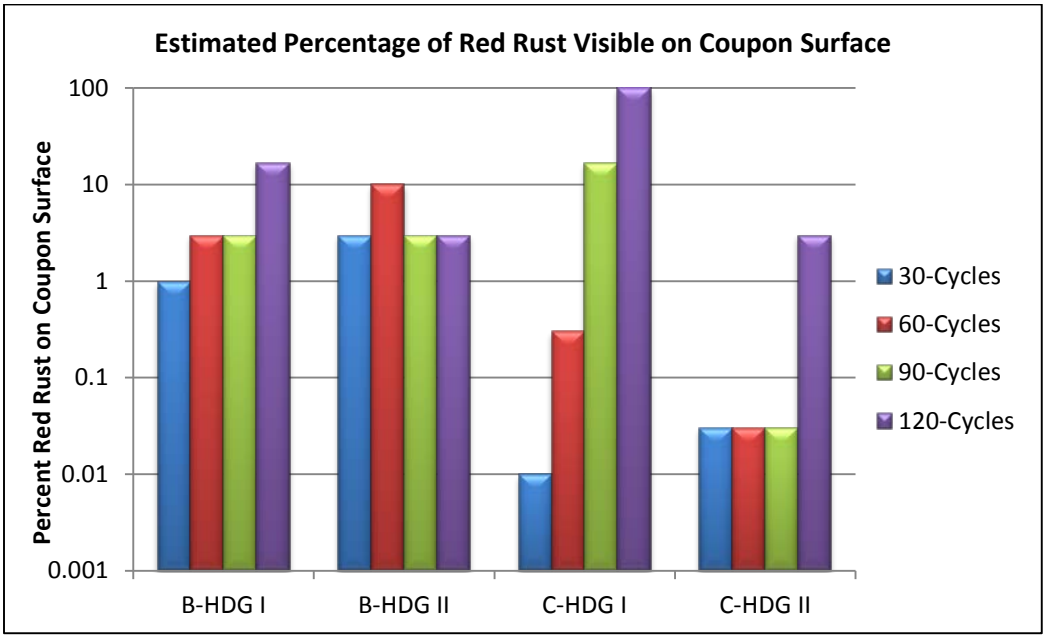

Figure 49: Estimated Surface Area Percentage Exhibiting Red Rust

Pre-Conditioned Coupon Performance

Figure 50 and Figure 51 show representative photos of the pre-conditioned samples before exposure and at the 30, 60, and 120-cycle evaluations. The non-uniform removal of the galvanized coating makes it challenging to draw meaningful conclusions from the data. However, their appearance is consistent with the other observations in this testing.

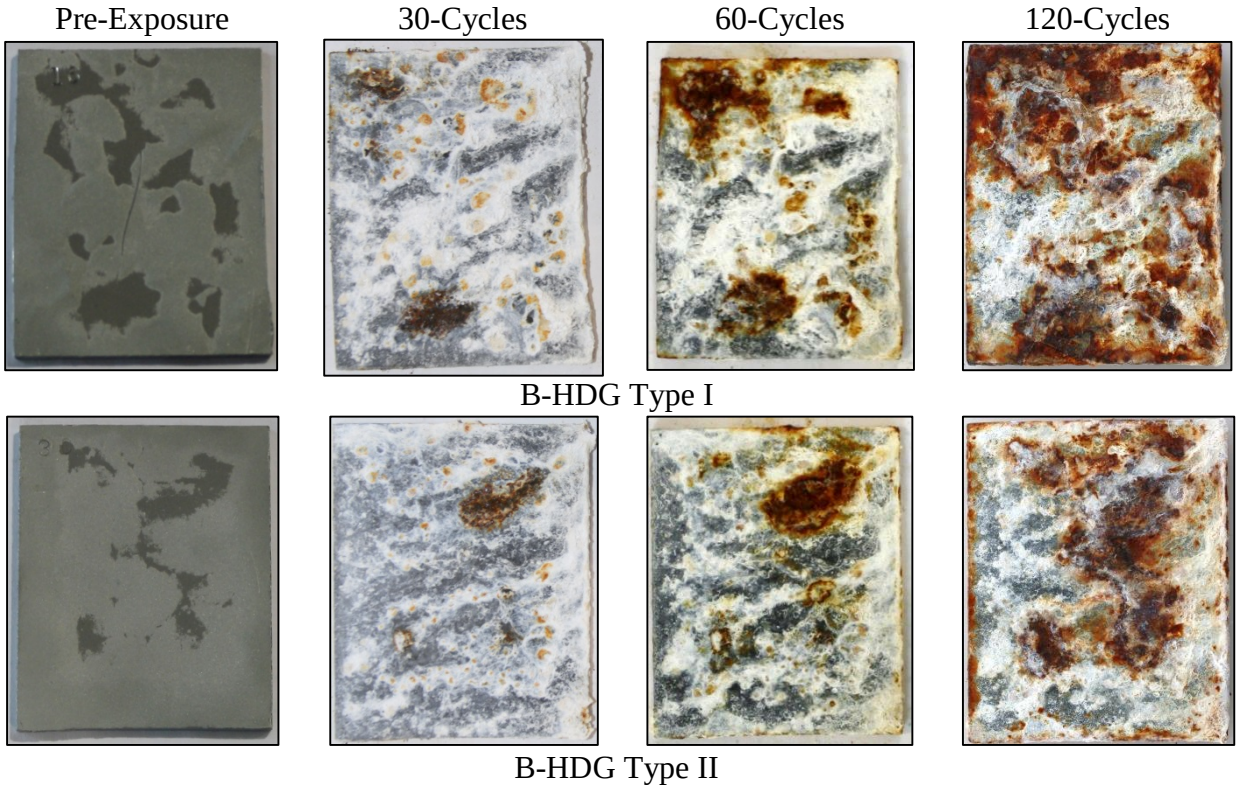

Figure 50: Representative Pre-Conditioned B-HDG Coupons throughout the Test Period

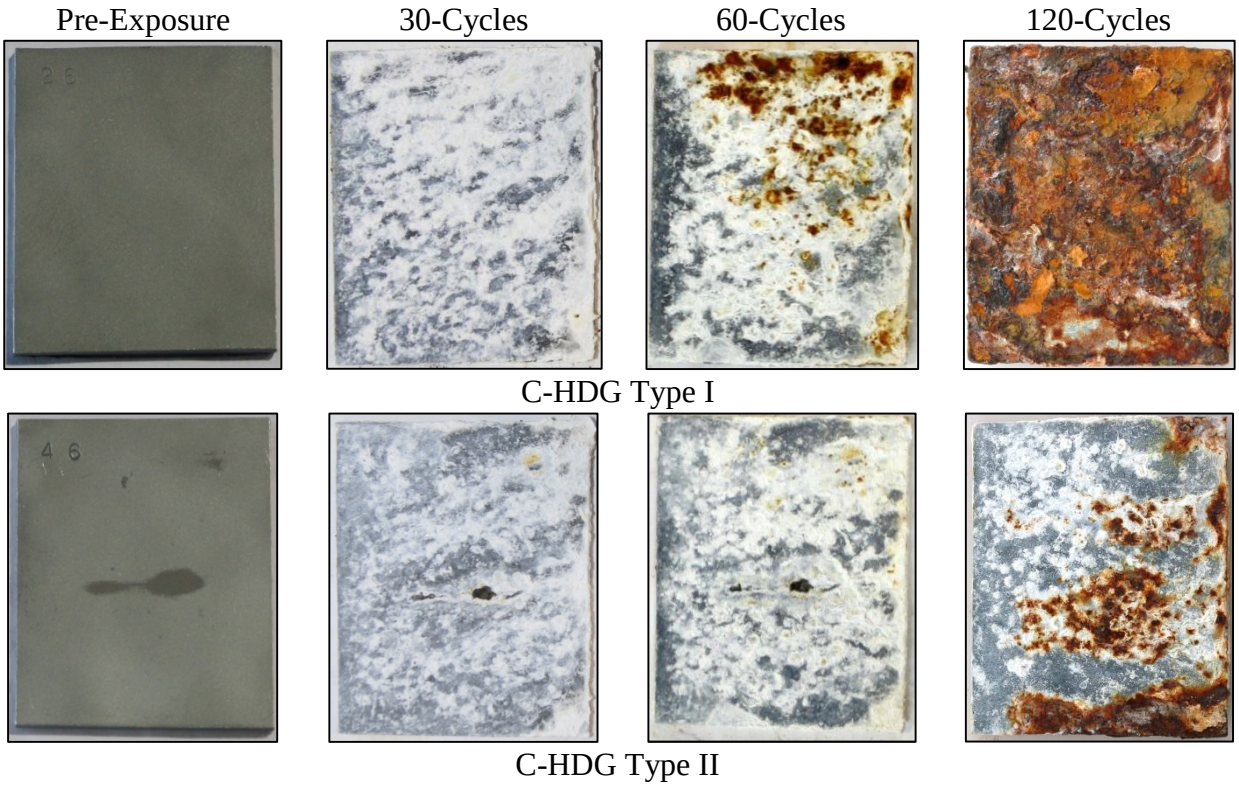

Figure 51: Representative Pre-Conditioned C-HDG Coupons throughout the Test Period

Zinc Mass Loss

After the 60-cycle evaluation, 99.9% pure zinc coupons (1-in x 2-in x .0625-in, purchased from the Metal Samples Company) were exposed with the guardrail samples to determine the corrosion rate of pure zinc in the GMW14872 environment. Figure 52 shows the estimated coating thickness loss calculated from the zinc coupon mass loss. If the linear relationship continues, approximately 3.7 mils (calculated to be approximately 2.2 oz/ft^2) mils would be lost after 120-cycles. This corroborates what was observed on the C-HDG I guardrail and coupons samples, as coating weights on these samples were measured to be close to 2 oz/ft^2 and were the only samples to exhibit significant substrate corrosion on the boldly exposed, unmated surfaces.

Figure 53 shows the estimated average zinc loss based on measurements taken from the ASTM A90 samples and SEM images. The ASTM A90 coating masses were compared for pre-exposure and after 30-cycles of exposure. Data for the longer exposed samples had increased scatter, likely due to increased steel corrosion product present. The SEM measurements were taken pre-exposure and at 60 cycles. Note that the SEM observations are highly localized, thus considerable variability is expected. While there is not enough data to generate an adequate statistical comparison, the observed loss rate observations for the galvanized guardrail seem consistent with the corrosion rate of pure zinc.

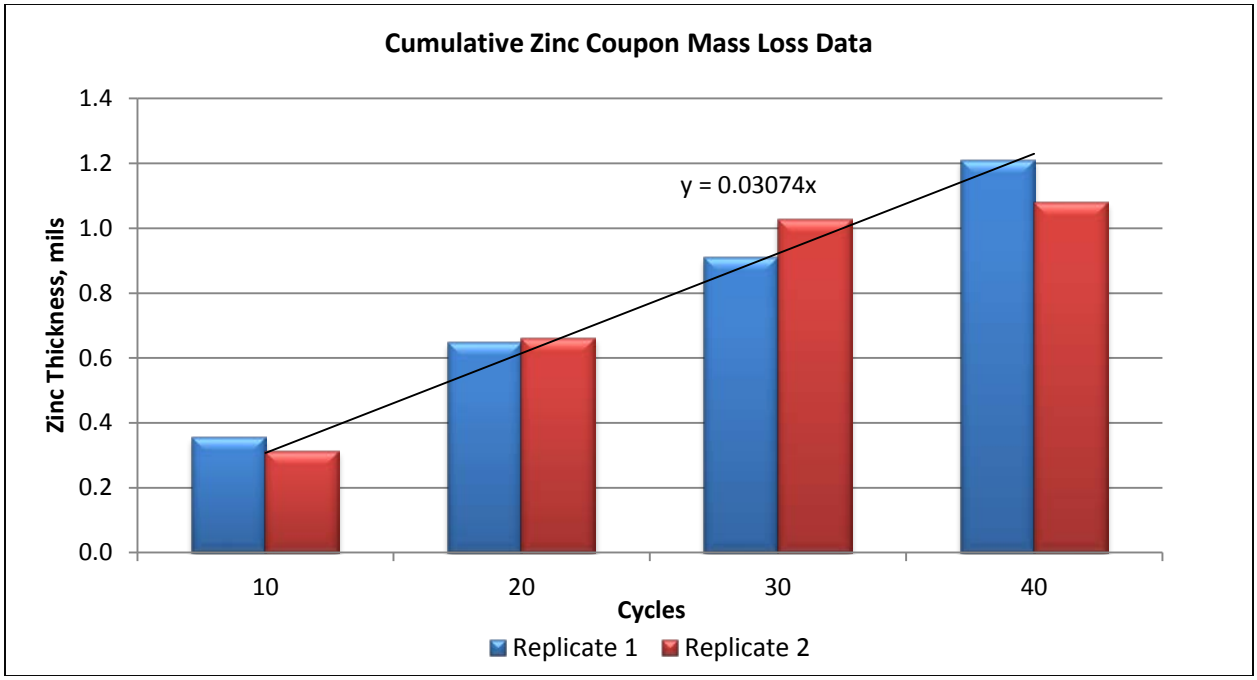

Figure 52: Zinc Coating Loss calculated from Coupon Mass Loss

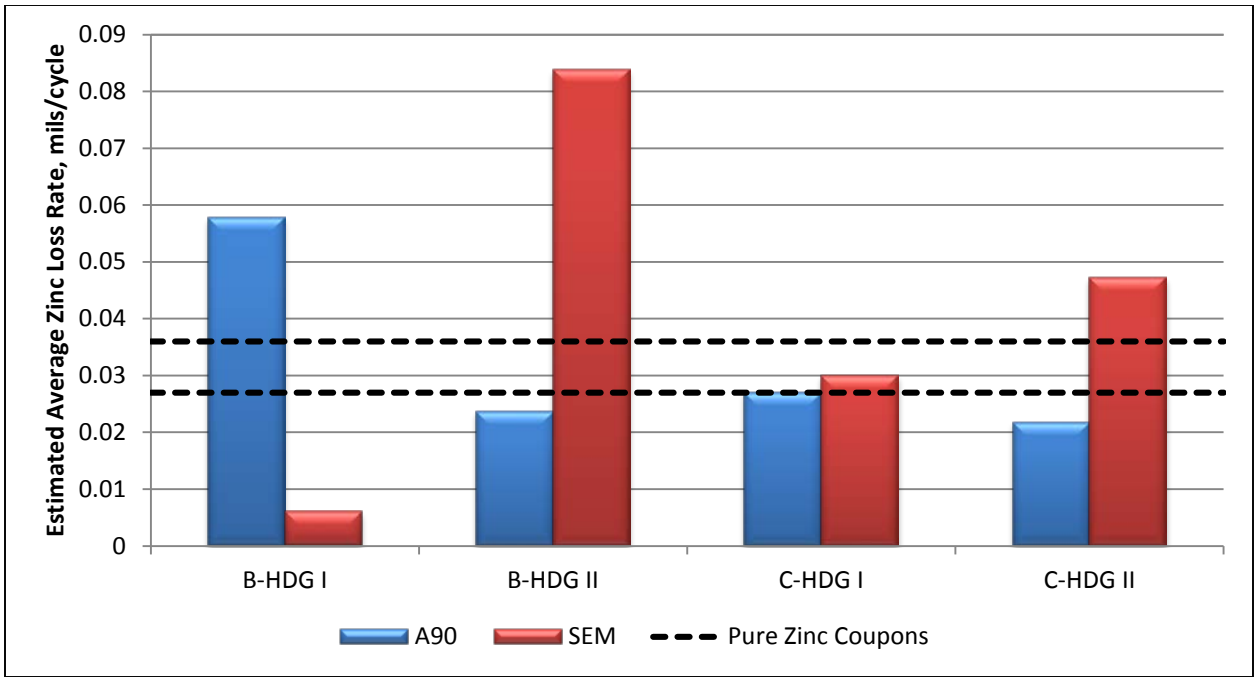

Figure 53: Estimated Average Zinc Loss Rate as a Function of Measurement Method

Corrosion Acceleration

Figure 54 presents a chart developed by American Galvanizers Association to predict the time to first maintenance for a given thickness of zinc in any of five generic environments [13]. The criteria used for first maintenance is 5% surface rusting. The visible rusting data gathered over the 120-cycle period of GMW14872 testing presented in Figure 49 can be used in conjunction with the curves in Figure 54 to estimate an acceleration factor. Five percent rusting occurred on the C-HDG Type I sample (2 mils thick) between 60 and 90 cycles of testing and is predicted to occur at approximately 35 years in an industrial environment and 65 years in a rural environment. Five percent rusting occurred on the B-HDG Type I sample (3.5 mils thick) between 90 and 120 cycles of testing and is predicted to occur at approximately 65 years in an industrial environment. More detailed data is necessary to establish correlations between the cyclic corrosion test and specific natural environments, however the observations suggest a trend exists.

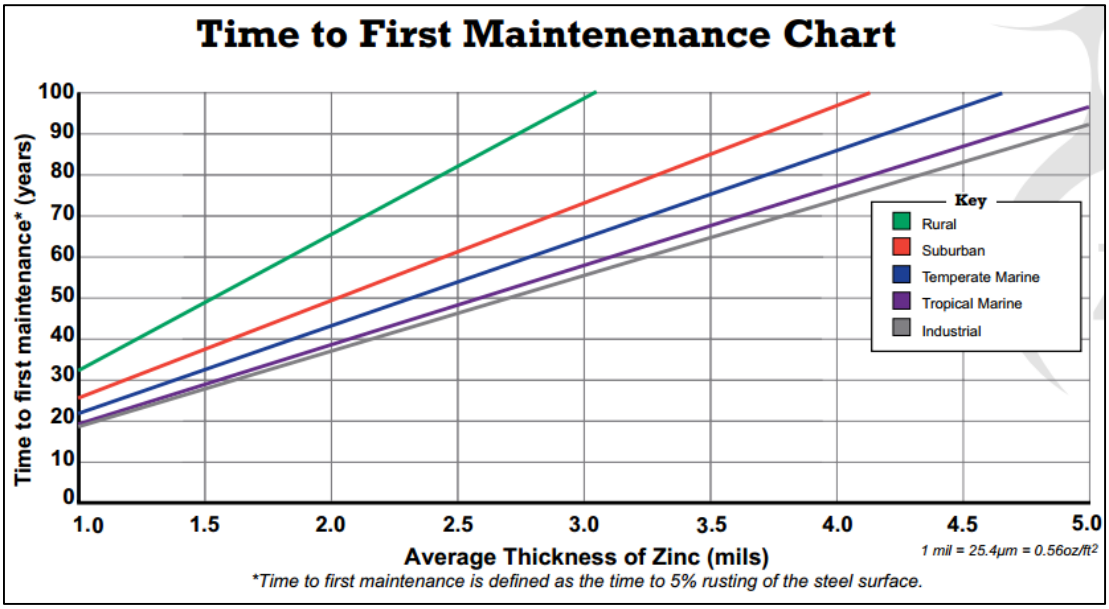

Figure 54: Time to First Maintenance Prediction (American Galvanizers Association [13])

Conclusions

The following conclusions are made based on the results of this study:

- The test results demonstrate a clear benefit of increased galvanized coating thickness for corrosion resistance, regardless of the galvanizing process.

- Crevices such as the splice area and areas under fasteners present the most significant corrosion problem for a guardrail.

    - The splice interface of B-HDG and C-HDG exhibited measurable pitting which was comparable for the two processes. An order of magnitude increase in pit depth was observed for the thinner (Type I) coating for both galvanizing processes.

    - The difference in the coupon data versus that of the 1-meter samples demonstrates the importance of testing with full-scale test pieces which incorporate realistic configuration details such as crevices.

- The test results do not clearly demonstrate the superiority of one hot dip galvanizing process over the other. However, they do demonstrate different characteristics of batch hot dip and continuous hot dip galvanizing.

    - Bold-faced surfaces of the B-HDG (Type I and Type II) and C-HDG Type II samples did not exhibit substrate corrosion (i.e., section loss) after 120-cycles in GMW14872.

        - B-HDG (Type I and Type II) samples exhibited rust staining, possibly due to corrosion of the iron in the intermetallic layers.

        - C-HDG I samples exhibited substrate corrosion after 120-cycles in GMW14872. A direct comparison to B-HDG Type I is not applicable due to the significant difference in thickness.

    - Guardrail edges of C-HDG samples, despite being uncoated, corroded at similar rates and to similar severities as edges on the B-HDG samples.

        - Edges of Type I samples exhibited more steel corrosion than the edges of Type II samples, regardless of galvanizing process.

- Non-destructive thickness testing was not an effective means of evaluating galvanized coating loss in the accelerated test.

Recommendations

The following recommendations are made based on the results of this study:

- Corroborate these laboratory data with observations of guardrails exposed in a service environment. Service exposure data would help confirm:
    - Relative performance of Type I and Type II guardrails
    - Relative performance of B-HDG and C-HDG guardrails
    - Relative magnitude of corrosion in crevices versus boldly exposed surfaces
- Establish a relationship between accelerated corrosion tests and highway environment corrosivity. Such a relationship would help specifiers develop guidelines for guardrail material selection. The guidelines would need to consider the environmental corrosivity, desired service life, and material performance.
- Evaluate the effectiveness of alternative treatments to mitigate crevice corrosion in the splice joint. In addition to the corrosion benefits, the cost effectiveness and manufacturability of alternatives should be considered. Alternatives may include a dielectric coating, double-dip coating of zinc on these junctions, thermal spray of additional zinc, or insertion of a sheet of zinc.

References

[1] General Motors Worldwide Engineering Standards, "GMW14872 Cyclic Corrosion Laboratory Test," March 2010.

[2] American Association of State Highway and Transportation Officials designation: M 180-12 - "Corrugated sheet steel beams for Highway Guardrail"

[3] "Comparison of Methods Used to Produce Hot-Dipped Galvanized W-Beam Guardrail," R. Till and C. Davis, January 1998, Michigan Department of Transportation Research Project No. R-1357.

[4] "Accelerated Corrosion Tests in the Automotive Industry: A Comparison of the Performance Towards Cosmetic Corrosion," N. LeBozec, N. Blandin and D. Thierry, 2008, Materials and Corrosion, 59, No. 11, 889-894

[5] Cramer, S. D., & Covino, B. S. (2005). ASM Handbook, Volume 13B, Corrosion: Materials. Materials Park: ASM International.

[6] Knotkova, D., Kreislova, K., & Dean, S. W. (2010). International Atmospheric Exposure Program: Summary of Results. Bay Shore: ASTM International.

[7] Repp, J., Ault, J. P., & Handsy, I. C. (2009). Evaluation Of Army Materials Of Manufacture In The Hawaiian Islands – Lessons Learned. 2009 DoD Corrosion Conference, (pp. 1-12). Washington, D.C.

[8] Terrence R. Giles, Michelle Lerminez and Sabrinia Smith, "Examination of the Effects of Test Piece Spacing in ASTM B117-97 Neutral SaltSpray and General Motors 9540P" 2003 SAE World Congress, SAE International.

[9] American Galvanizers Association, "The HDG Coating," http://www.galvanizeit.org/hot-dip-galvanizing/what-is-hot-dip-galvanizing-hdg/the-hdg-coating

[10] American Galvanizers Association, 2004, "Hot-Dip Galvanizing for Corrosion Prevention—A Guide to Specifying and Inspecting Hot-Dip Galvanized Reinforcing Steel," http://www.galvanizedrebar.com/Documents/Publication/Specifiers%20Guide%20To%20Rebar%200504.pdf, Page 12.

[11] GalvInfo Center, 2011, "The Spangle on Hot-Dip Galvanized Steel Sheet, http://galvinfo.com/ginotes/GalvInfoNote_2_6.pdf.

[12] Singh, A.K, Jha, G., and Chakrabarti, S., 2003, "Spangle Formation on Hot-Dip Galvanized Stele Sheet and its Effects on Corrosion-Resistant Properties," NACE Corrosion Journal, Vol. 59, No. 2, Page 194.

[13] American Galvanizers Association, 2010, “General Hot-Dip Galvanizing vs. Continuous Sheet Galvanizing”, http://www.galvanizeit.org/uploads/publications/Hot-Dip_Galvanizing_vs_Continuous_Sheet_Galvanizing.pdf

Appendix A- SEM/EDX Baseline Analysis

ISO 17025

Testing Cert. #2797. 02

SCANNING ELECTRON MICROSCOPY (SEM)
LABORATORY ANALYSIS REPORT
26 Aug 2014

JOB NUMBER P0EMR948
PO NUMBER NJ-126

for

Rich Gianforcaro
Elzly Technology Corporation

Prepared by:

Lori LaVanier
Auger/SEM Specialist
(Tel. 952-641-1242; llavanier@eag.com)

Reviewed by:

Juergen Scherer, Ph.D.
Specialist
(Tel. 952-641-1241; jscherer@eag.com)

SEM ANALYSIS REPORT

Requester: Rich Gianforcaro
Job Number: P0EMR948
Analysis Date: 26 Aug 2014

Purpose

To measure layer thickness and identify elemental composition of layers on polished cross-sections of galvanized steel samples **B-HDG I, B-HDG II, C-HDG I and C-HDG II.**

Results and Interpretations

SEM images were taken to document the EDX analysis locations and also used for measurement overlays of layer thicknesses. Weight percentages were calculated for all spectra and are summarized in the Excel table. Note that Au/Pd and Pt (materials used to coat the sample for conductivity) were excluded from the calculations.

Two locations an each sample were imaged for layer thickness estimations, and also analyzed for composition. Back scattered electron (BSE) images were taken to show contrast related to atomic number (with heavier elements showing brighter contrast).

Note that EDX analysis of the Gamma layer on samples B-HDG I and B-HDG II likely contains signal from the adjacent layers since this layer is less than 2um thick.

SEM/EDS Instrument Conditions

Instrument: Hitachi Variable Pressure SEM Model S-3400N
Electron Beam Conditions: 20kV, 0º sample tilt

The samples were coated previously with Au/Pd at EAG-NJ for SEM. Samples B-HDG I and B-HDG II were coated with Pt at EAG-MN for additional conductivity for best imaging.

Unless specifically stated otherwise elsewhere in this report the uncertainty of dimensional SEM measurements is about ±10% (providing an estimated level of confidence of 95% using a coverage factor k = 2). Uncertainty estimates are calculated in accordance with the ISO "Guide to the Expression of Uncertainty in Measurement".

EDS should be considered a "semi-quantitative" analysis technique. Concentrations provided can typically be reproduced for major constituents of homogeneous samples to better than ±10%. However, the concentrations provided could have a "bias" when compared to certified reference materials (e.g. NIST standard reference materials). This "bias" could be corrected by calibrating the sensitivity factors against such certified reference materials (if available).

After reviewing this report, you may assess our services using an electronic service evaluation form. This can be done by clicking on the link below, or by pasting it into your internet browser. Your comments and suggestions allow us to determine how to better serve you in the future.
http://www.eaglabs.com/main-survey.html?job=P0EMR948

This analysis report should not be reproduced except in full, without the written approval of EAG.

08-26-2014

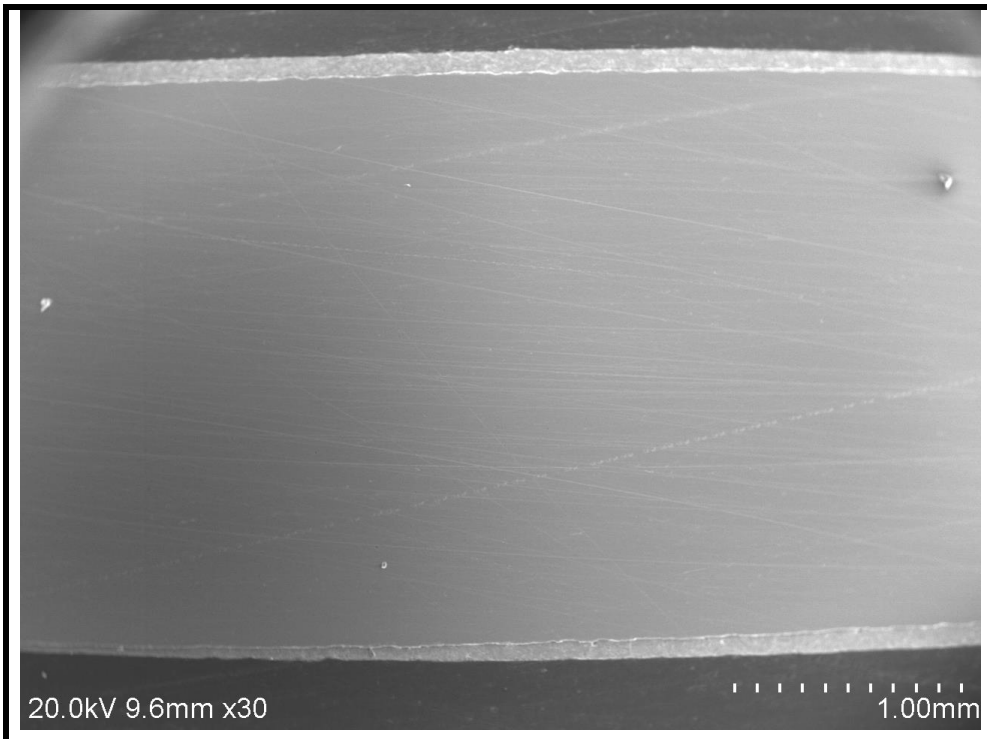

Figure 1

Mag = 30X

Voltage = 20kV

Comment:

C-HDG I
Pre-exposure

Au/Pd coated

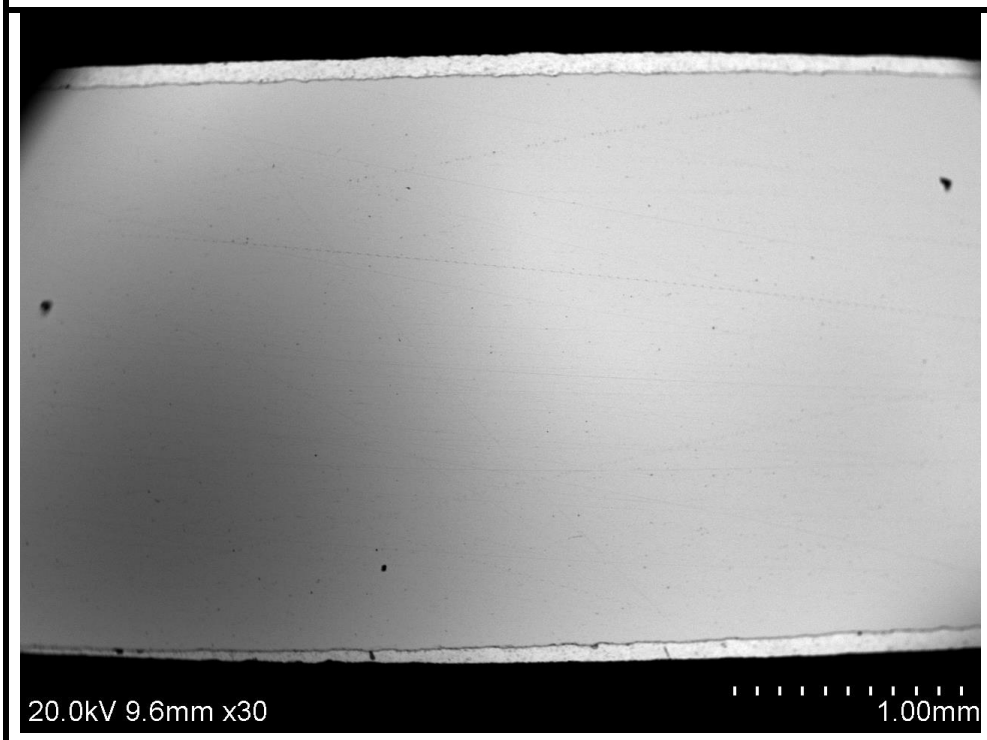

Figure 2

Mag = 30X

Voltage = 20kV

Comment:

C-HDG I
Pre-exposure

BSE image

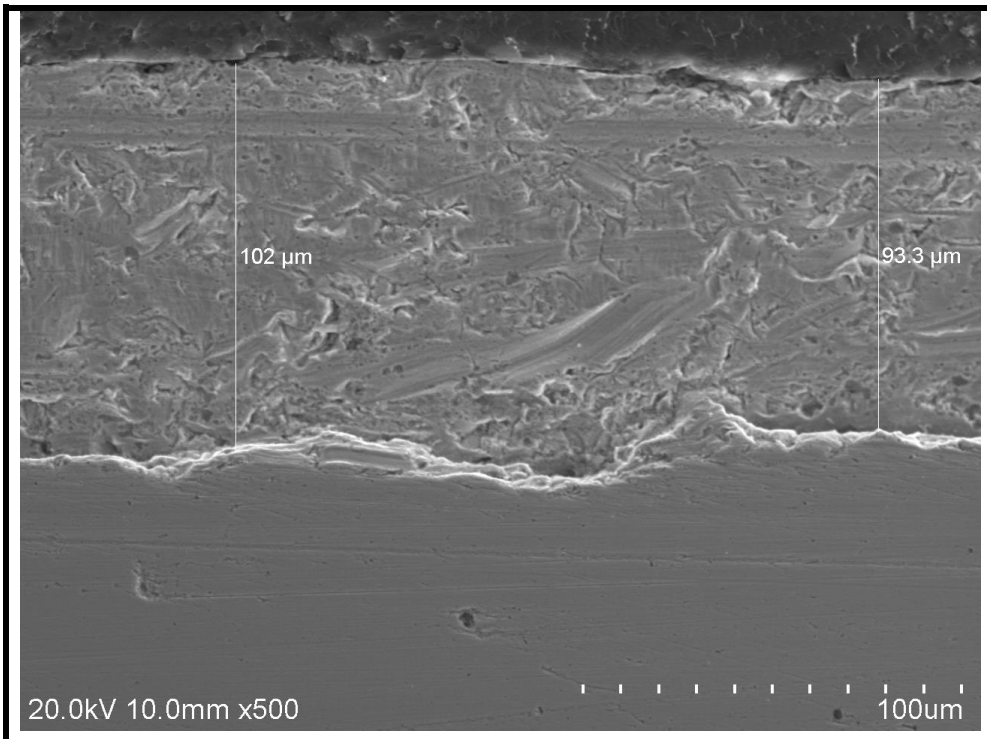

Figure 3

Mag = 500X

Voltage = 20kV

Comment:

C-HDG I
Pre-exposure

Location 1

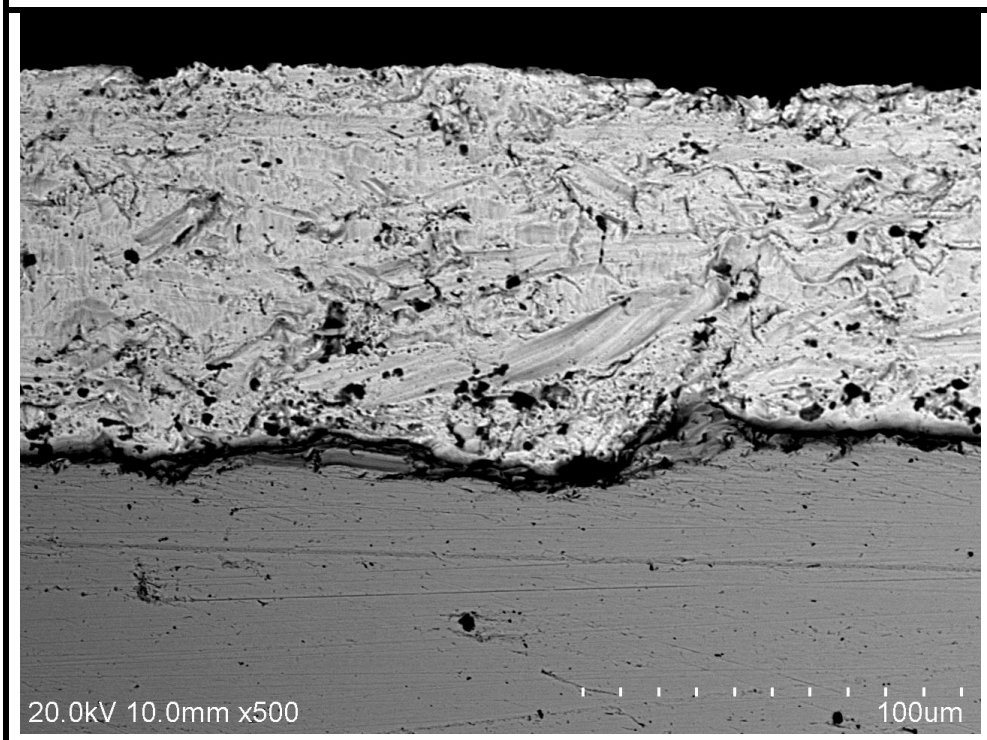

Figure 4

Mag = 500X

Voltage = 20kV

Comment:

C-HDG I
Pre-exposure

Location 1
BSE image

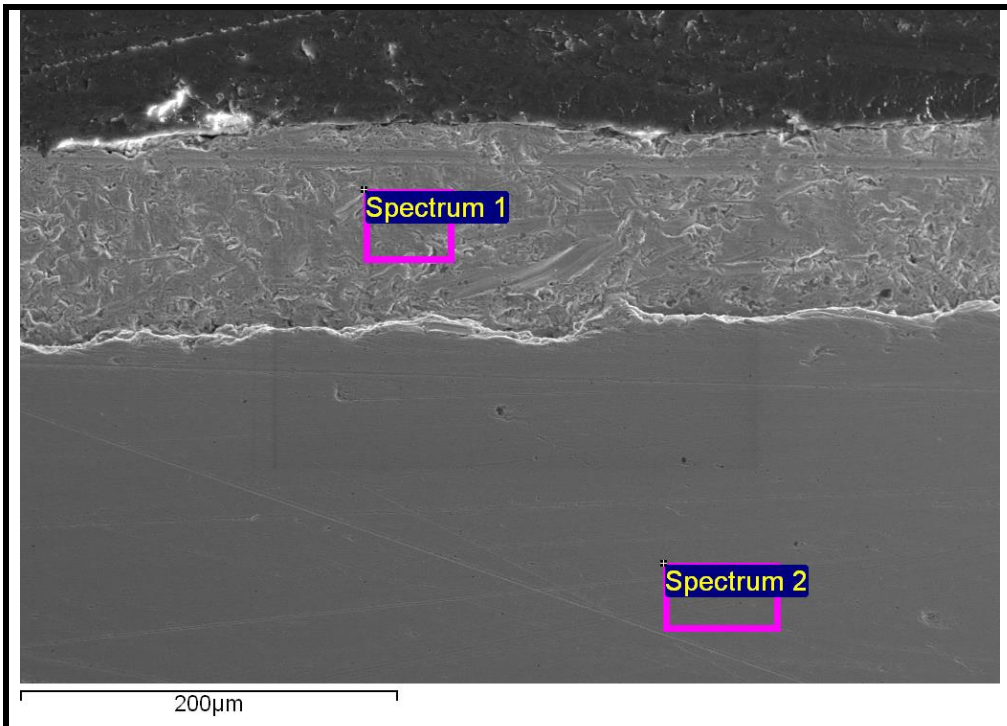

Figure 5

Mag = 250X

Voltage = 20kV

Comment:

C-HDG I
Pre-exposure

Location 1

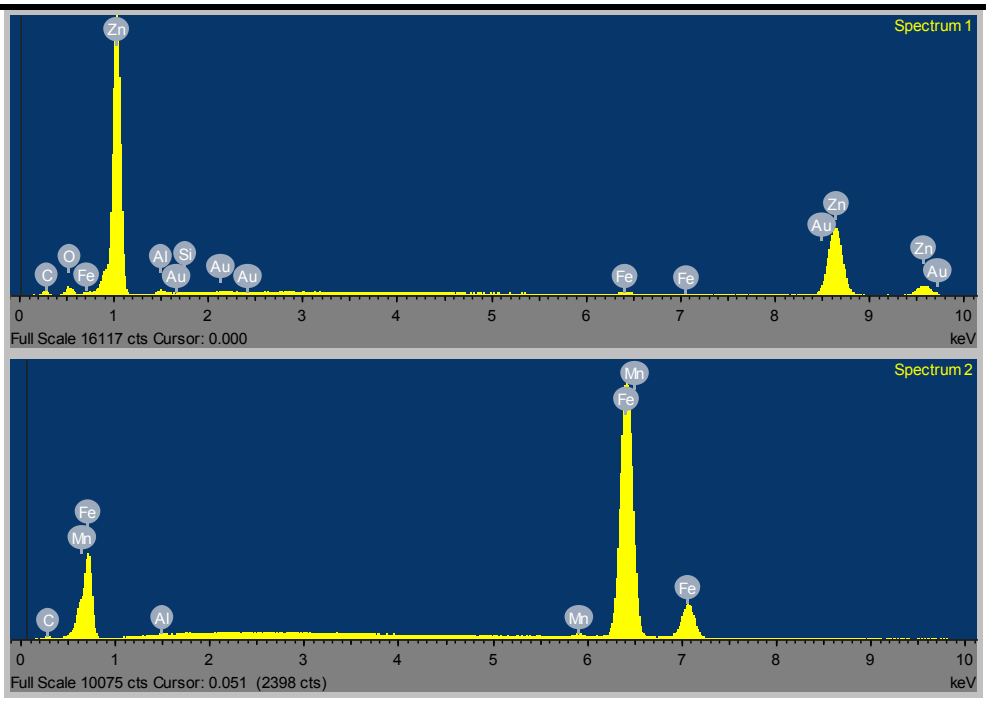

Figure 6

Voltage = 20kV

Comment:

C-HDG I
Pre-exposure

Location 1

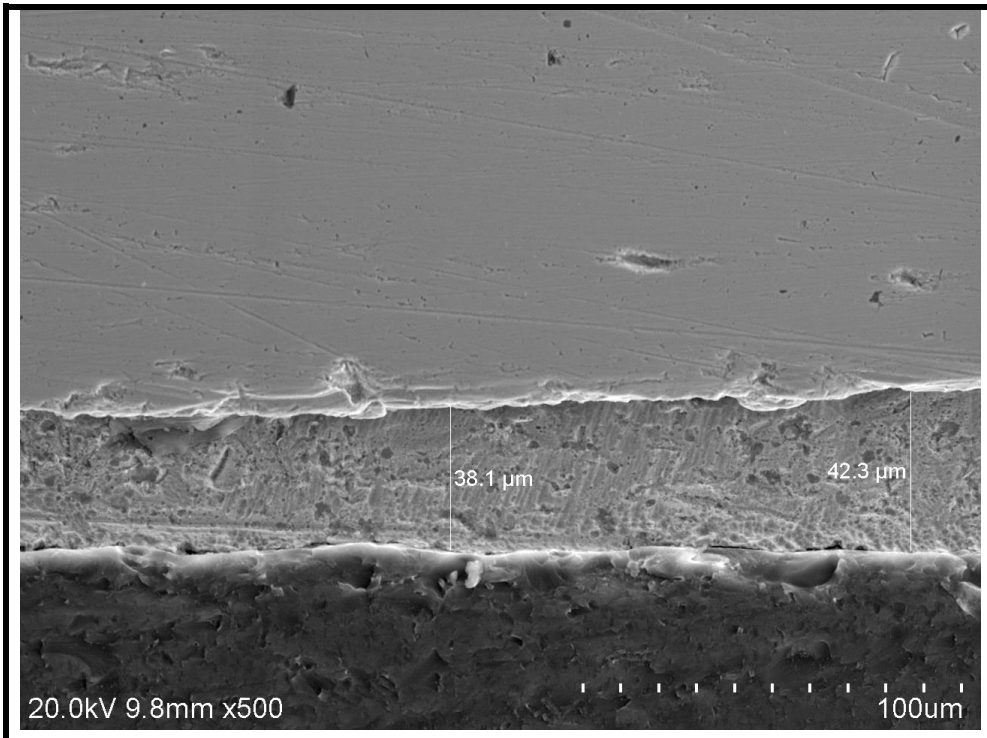

Figure 7

Mag = 500X

Voltage = 20kV

Comment:

C-HDG I
Pre-exposure

Location 2

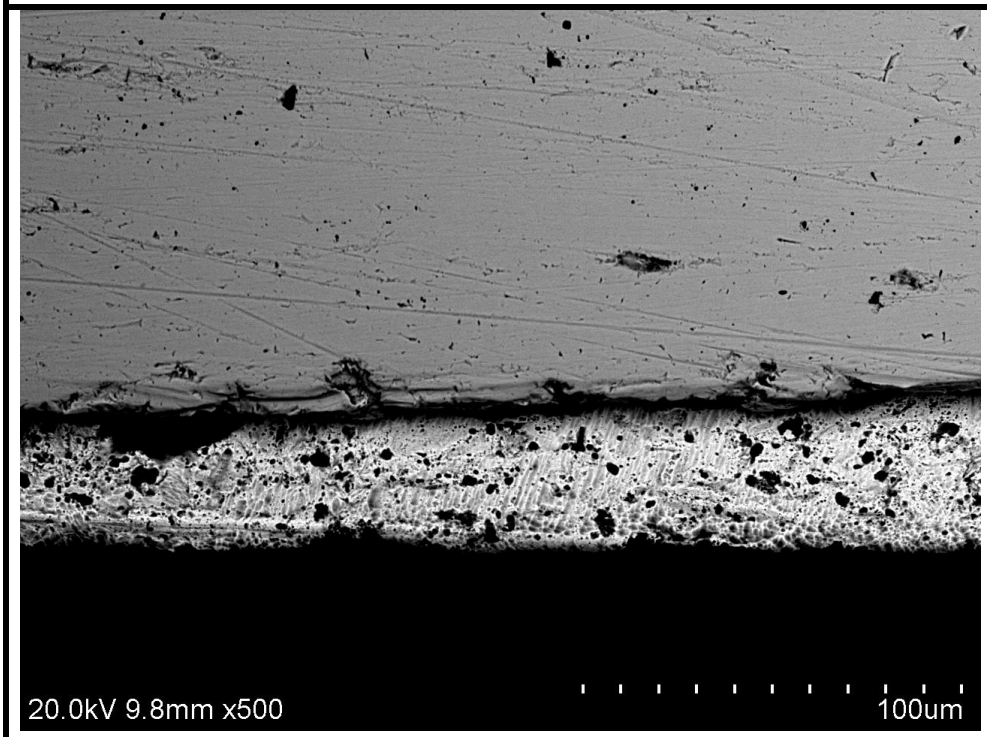

Figure 8

Mag = 500X

Voltage = 20kV

Comment:

C-HDG I
Pre-exposure

Location 2

BSE image

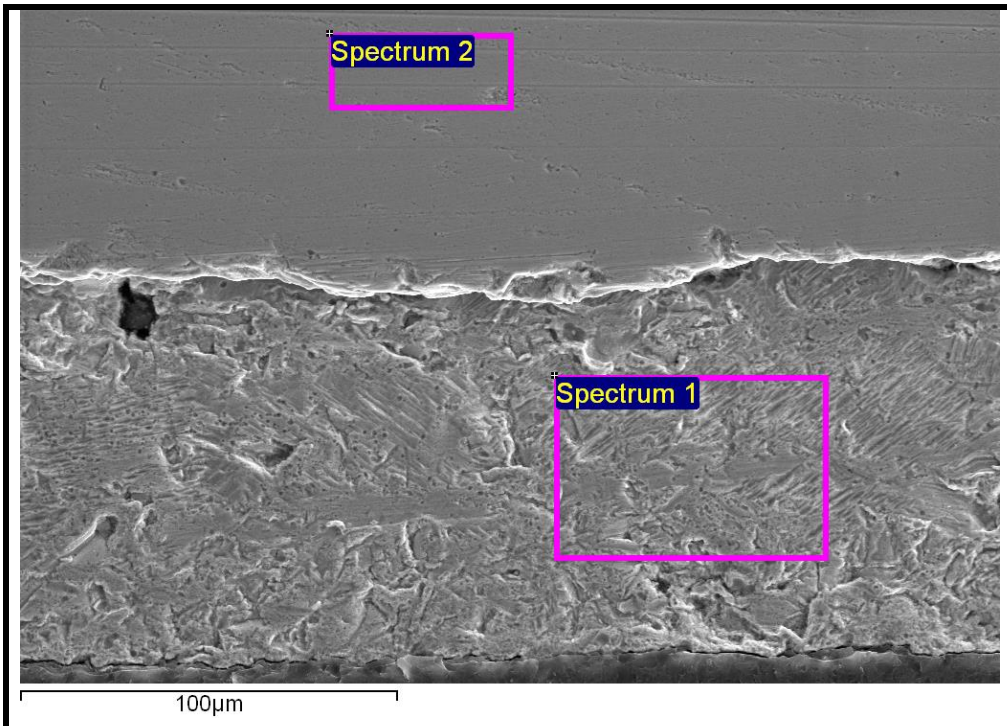

Figure 9

Mag = 500X

Voltage = 20kV

Comment:

C-HDG I
Pre-exposure

Location 3

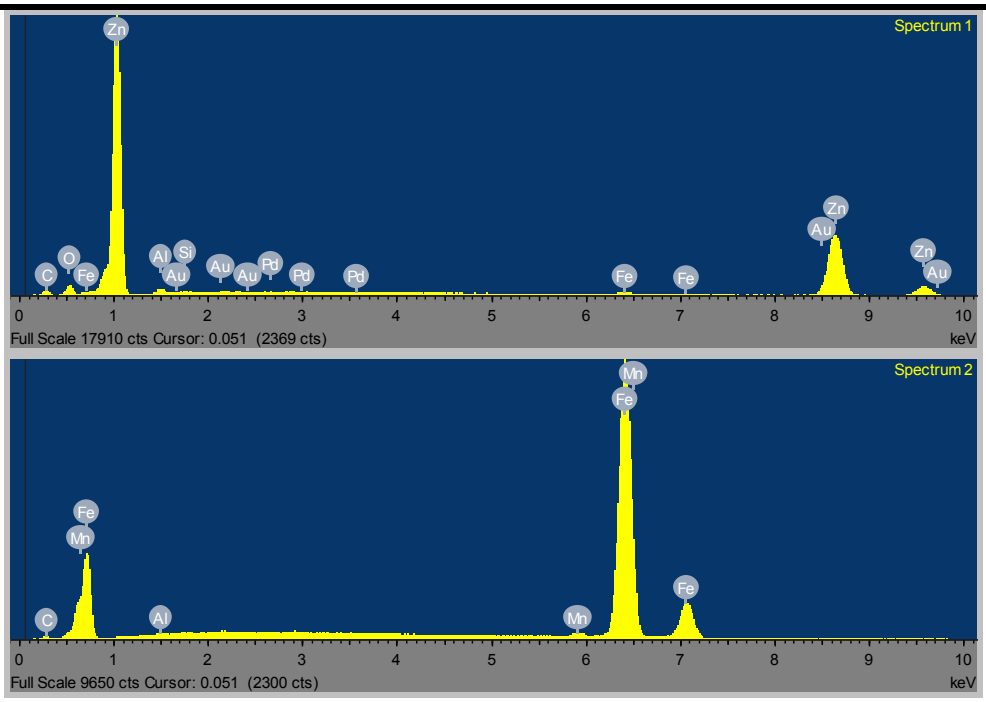

Figure 10

Voltage = 20kV

Comment:

C-HDG I
Pre-exposure

Location 3

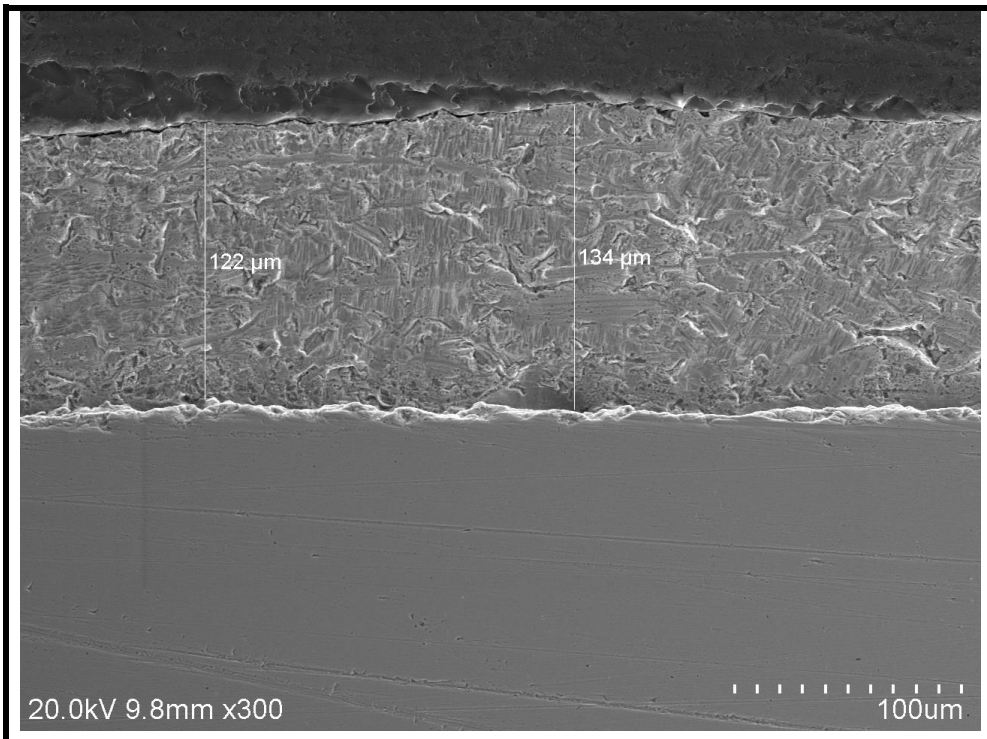

Figure 11

Mag = 300X

Voltage = 20kV

Comment:

C-HDG II
Pre-exposure

Location 1

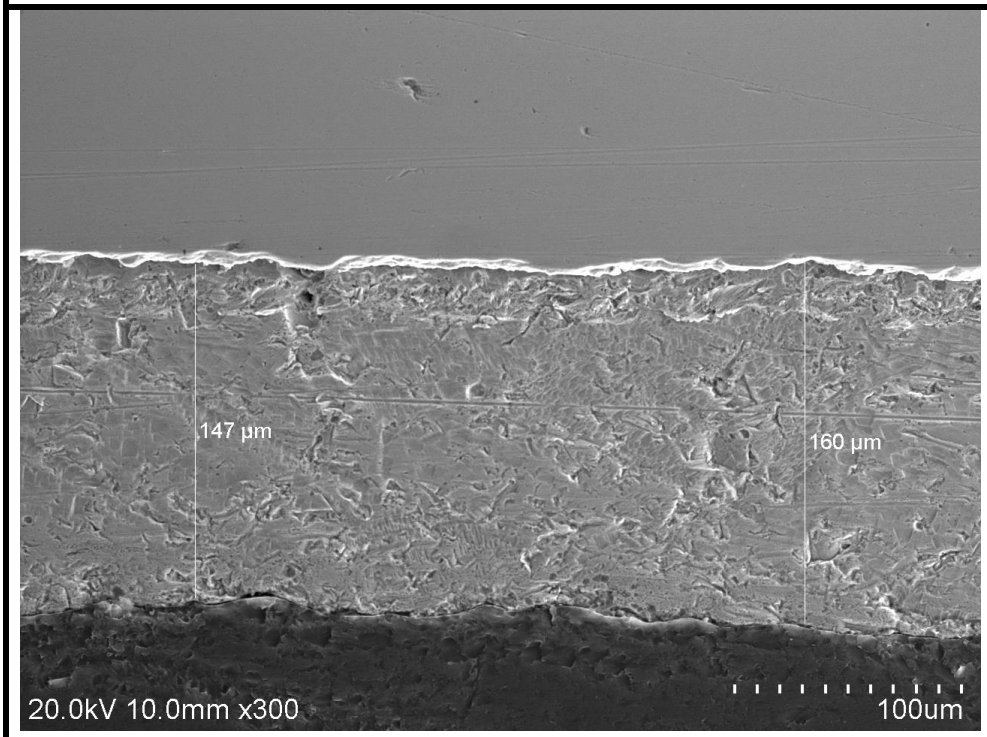

Figure 12

Mag = 300X

Voltage = 20kV

Comment:

C-HDG II
Pre-exposure

Location 2

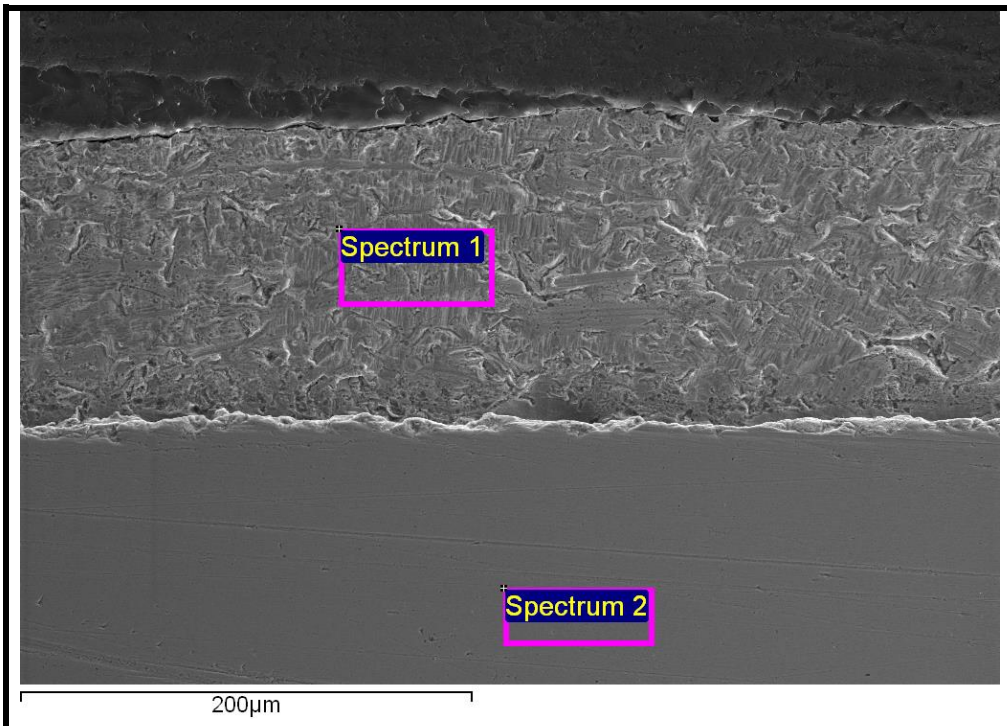

Figure 13

Mag = 300X

Voltage = 20kV

Comment:

C-HDG II
Pre-exposure

Location 1

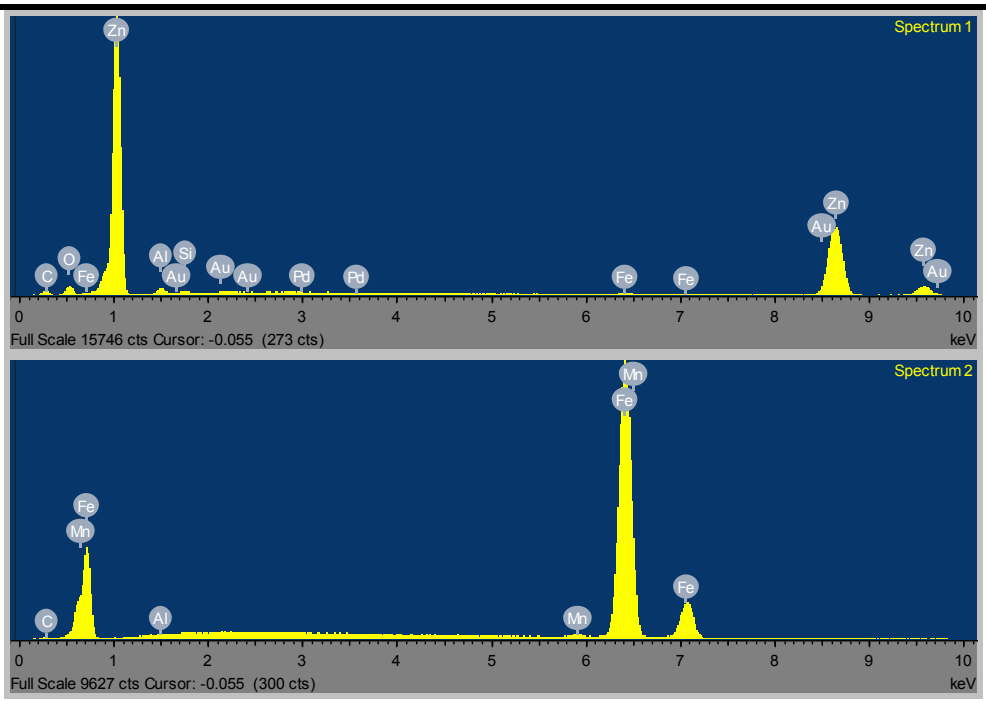

Figure 14

Voltage = 20kV

Comment:

C-HDG II
Pre-exposure

Location 1

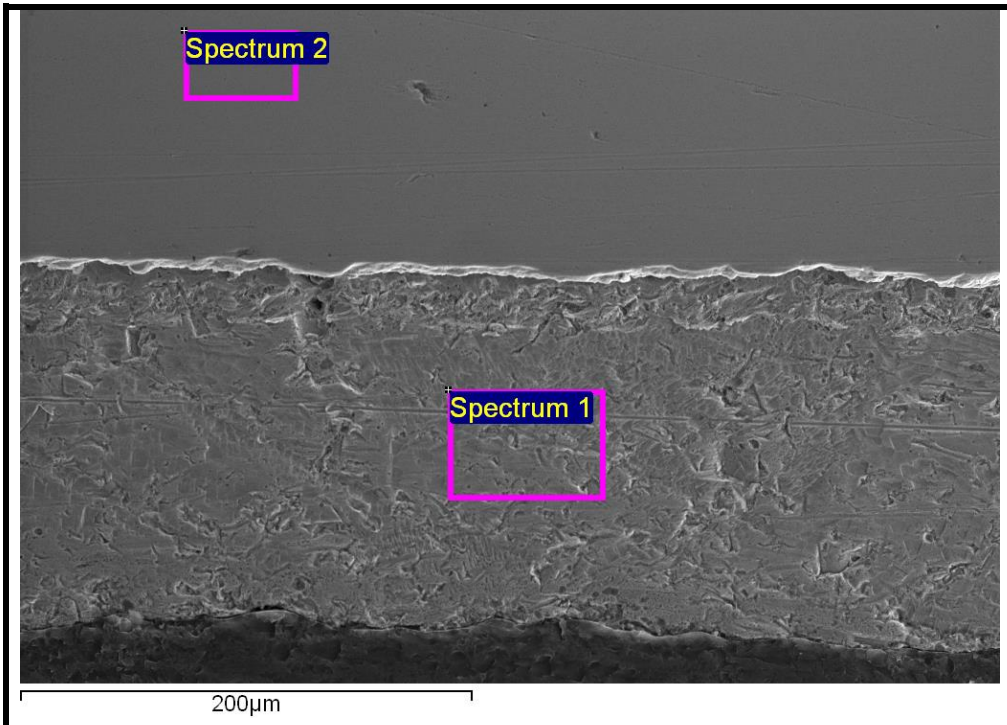

Figure 15

Mag = 300X

Voltage = 20kV

Comment:

C-HDG II
Pre-exposure

Location 2

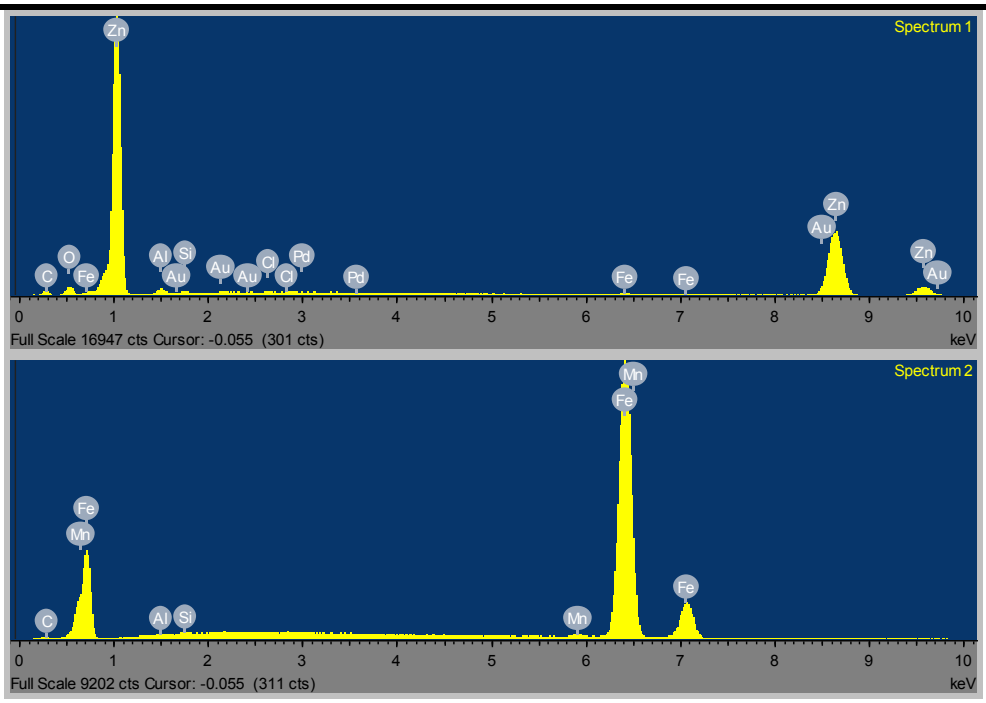

Figure 16

Voltage = 20kV

Comment:

C-HDG II
Pre-exposure

Location 2

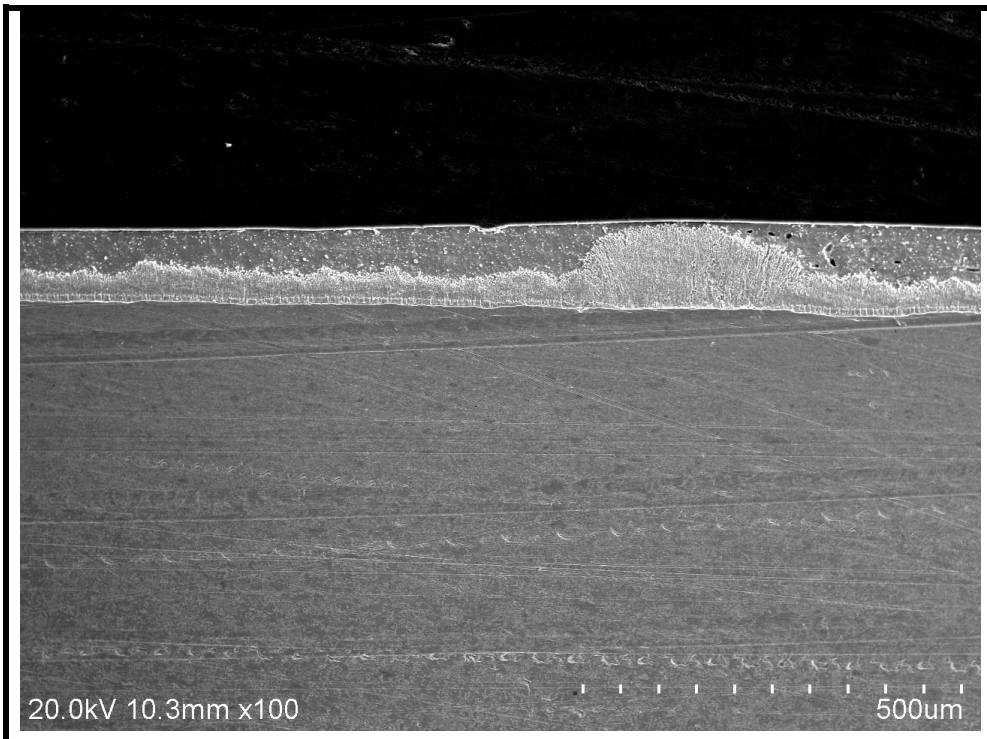

Figure 17

Mag = 100X

Voltage = 20kV

Comment:

B-HDG I
Pre-exposure

Pt coated at EAG-MN

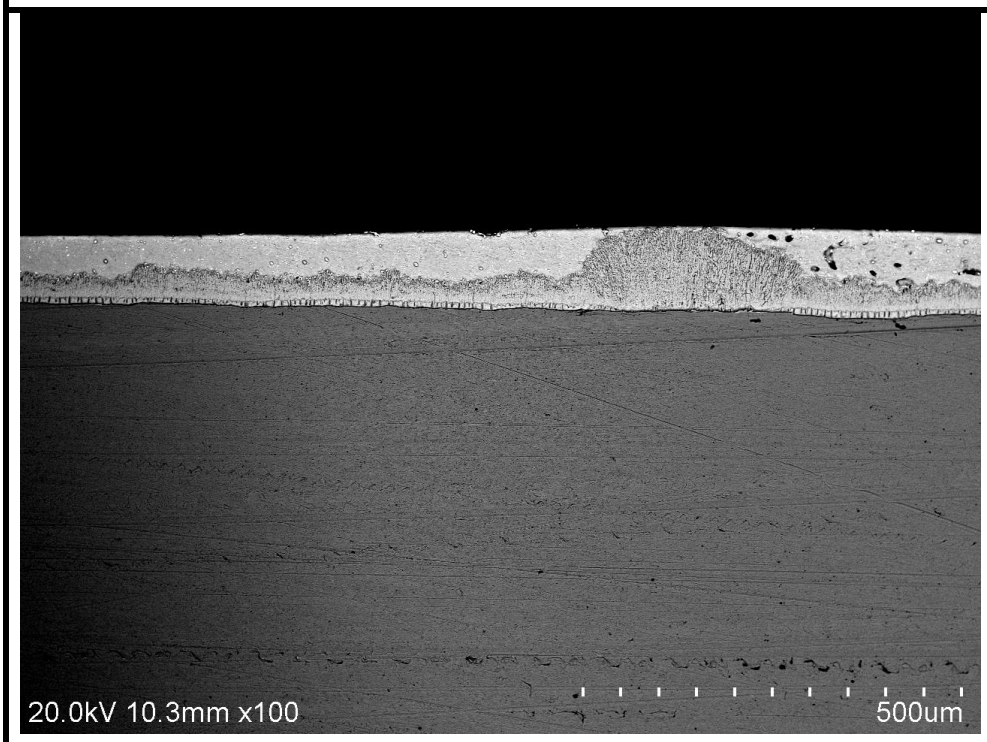

Figure 18

Mag = 100X

Voltage = 20kV

Comment:

B-HDG I
Pre-exposure

BSE image

Pt coated at EAG-MN

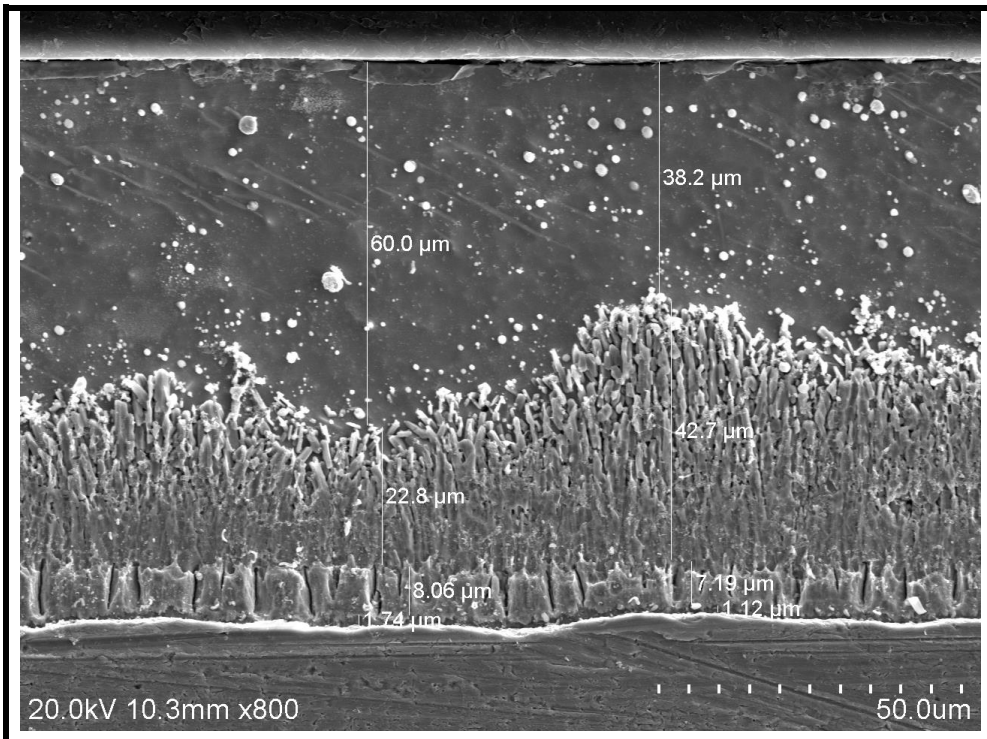

Figure 19

Mag = 800X

Voltage = 20kV

Comment:

B-HDG I
Pre-exposure

Pt coated at EAG-MN

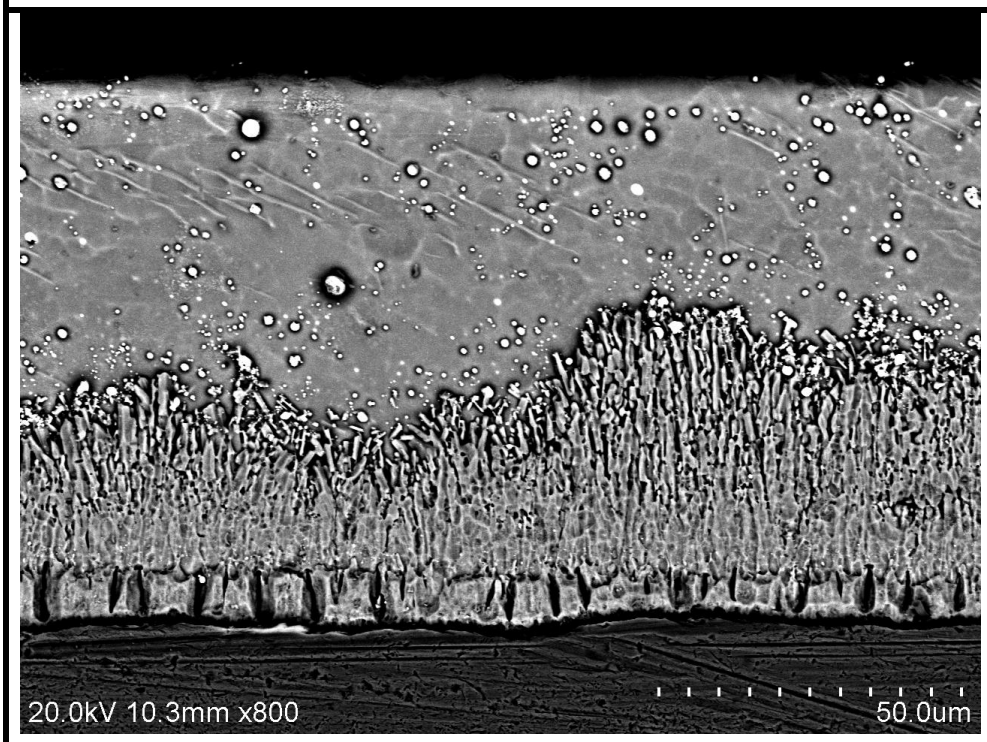

Figure 20

Mag = 800X

Voltage = 20kV

Comment:

B-HDG I
Pre-exposure

BSE image

Pt coated at EAG-MN

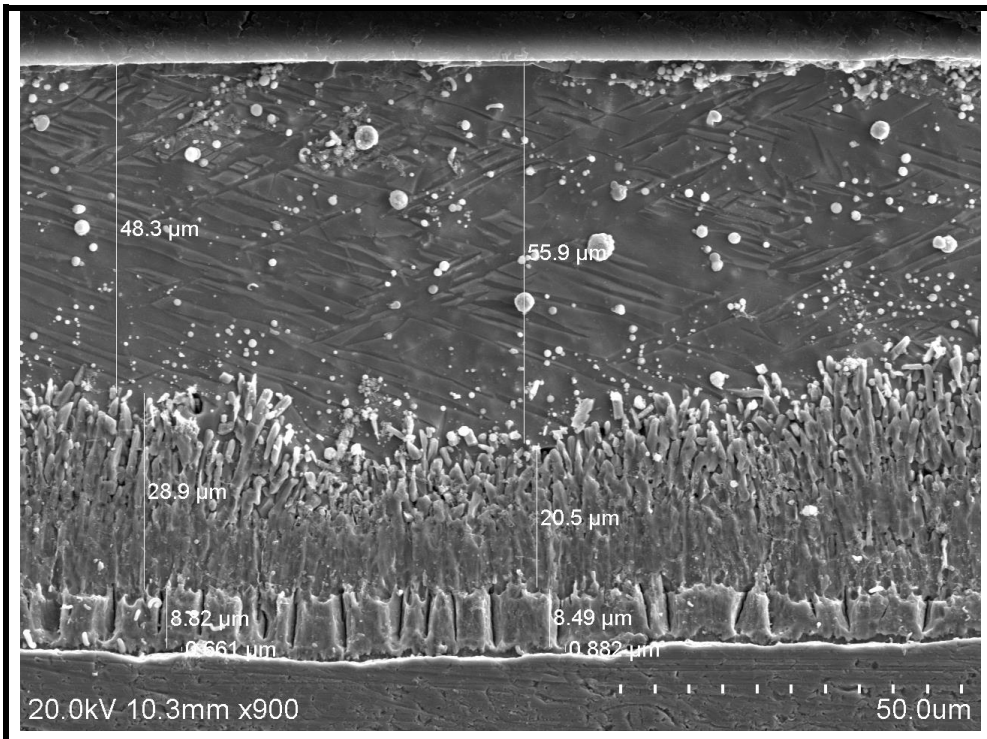

Figure 21

Mag = 900X

Voltage = 20kV

Comment:

B-HDG I
Pre-exposure

Second Location

Pt coated at EAG-MN

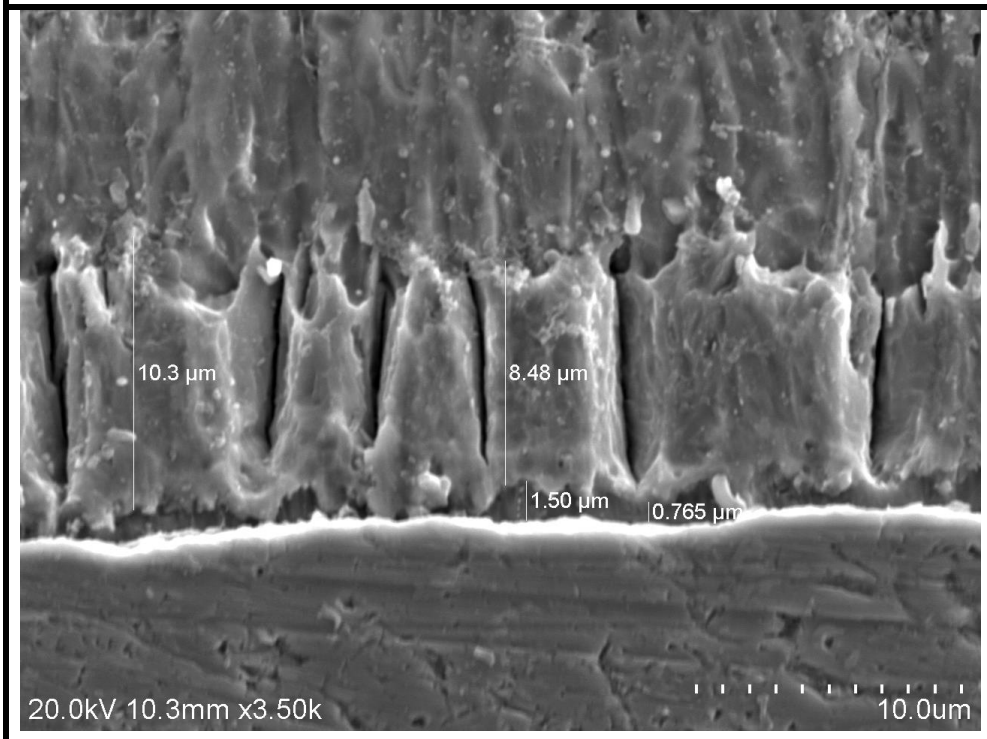

Figure 22

Mag = 3500X

Voltage = 20kV

Comment:

B-HDG I
Pre-exposure

Second Location
Higher Magnification of Gamma

Pt coated at EAG-MN

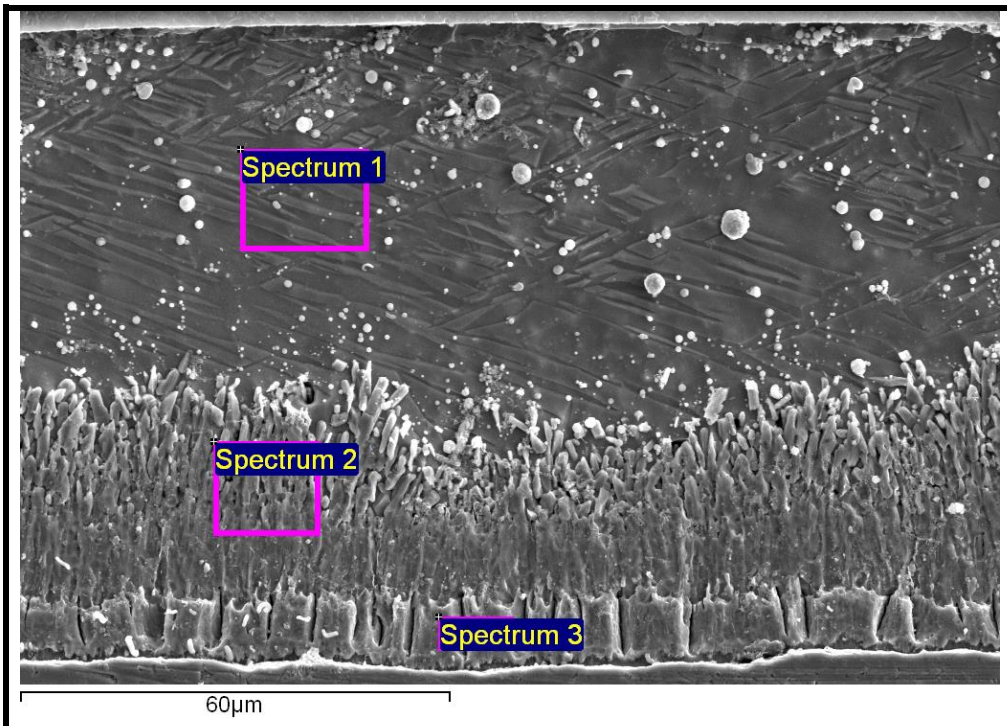

Figure 23

Mag = 950X

Voltage = 20kV

Comment:

B-HDG I
Pre-exposure

Pt coated at EAG-MN

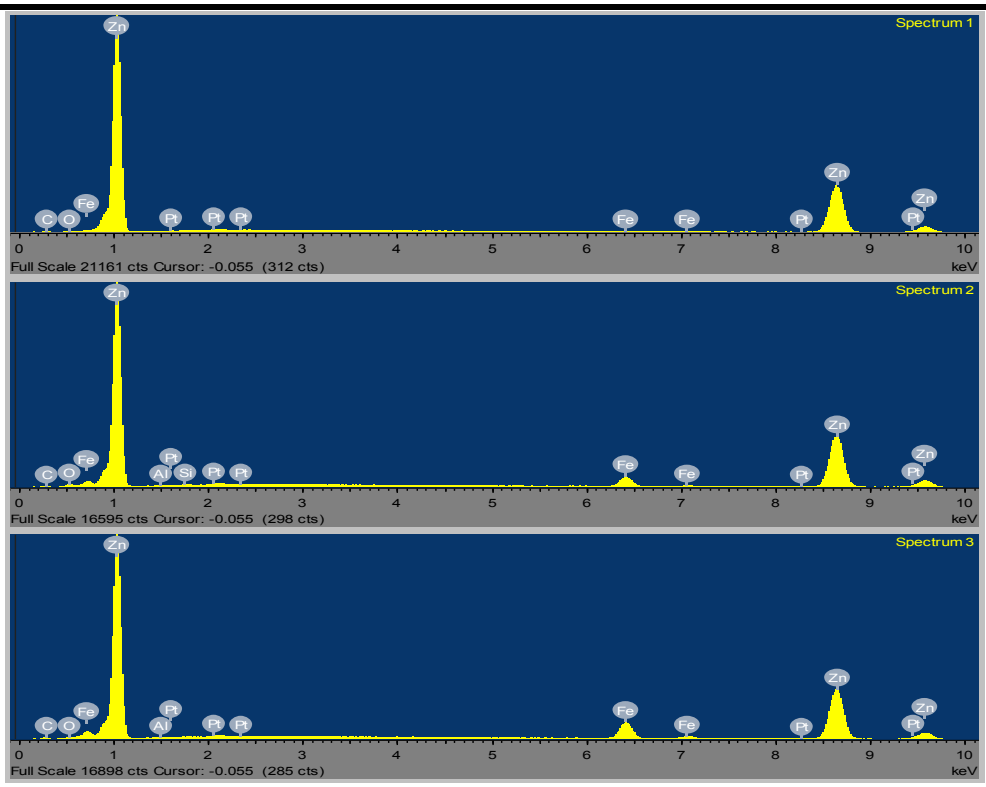

Figure 24

Voltage = 20kV

Comment:

B-HDG I
Pre-exposure

Pt coated at EAG-MN

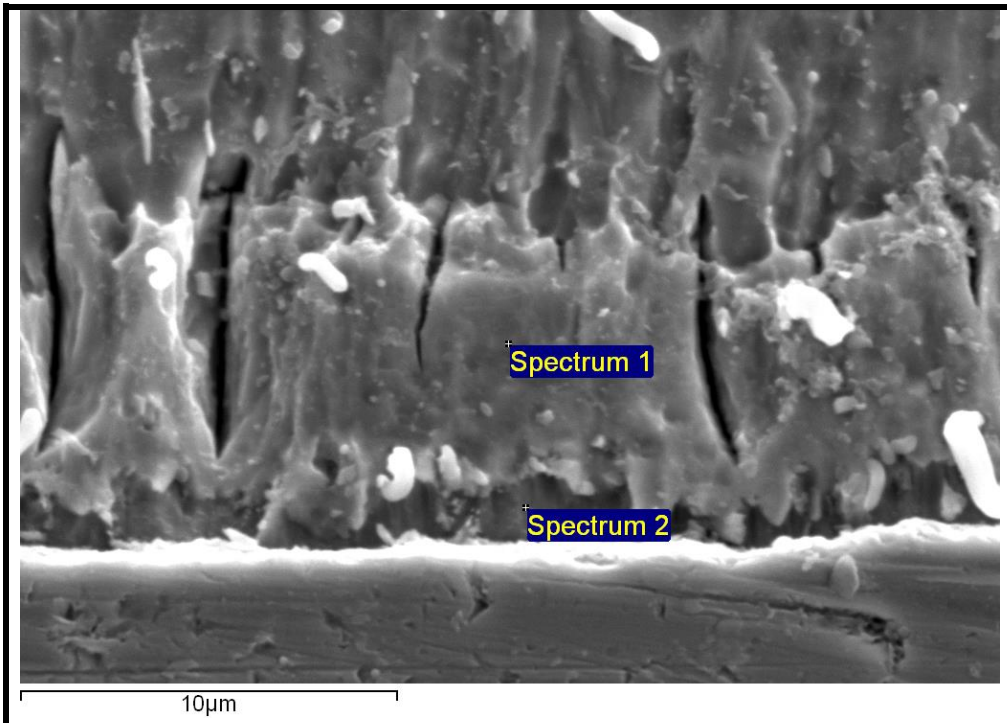

Figure 25

Mag = 5000X

Voltage = 20kV

Comment:

B-HDG I
Pre-exposure

Pt coated at EAG-MN

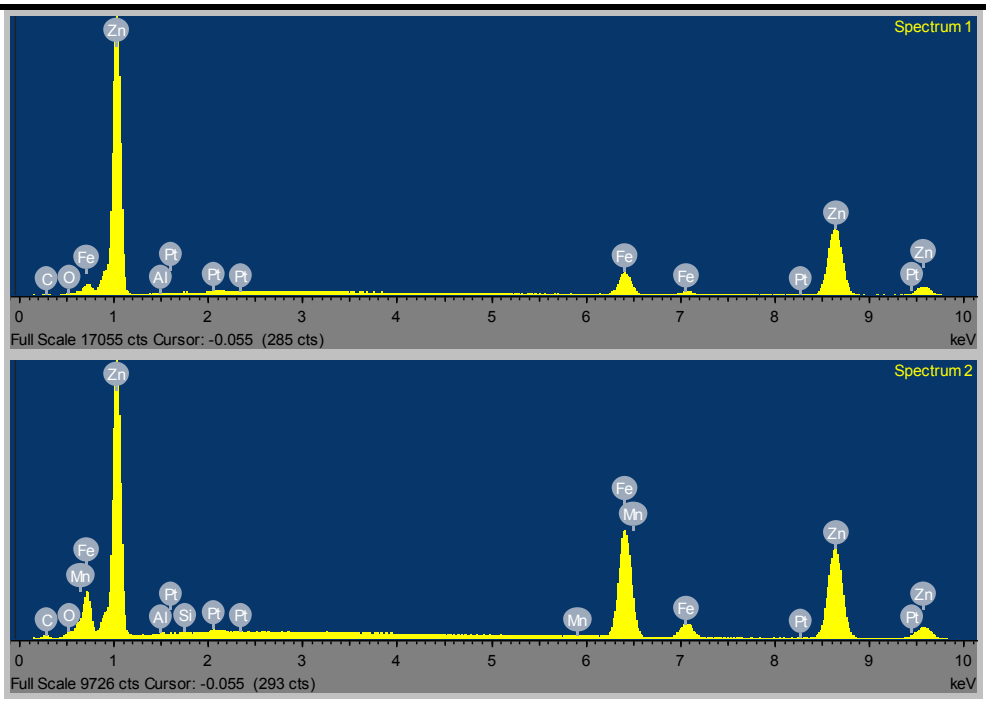

Figure 26

Voltage = 20kV

Comment:

B-HDG I
Pre-exposure

*note that Gamma region may contain signal from adjacent regions

Pt coated at EAG-MN

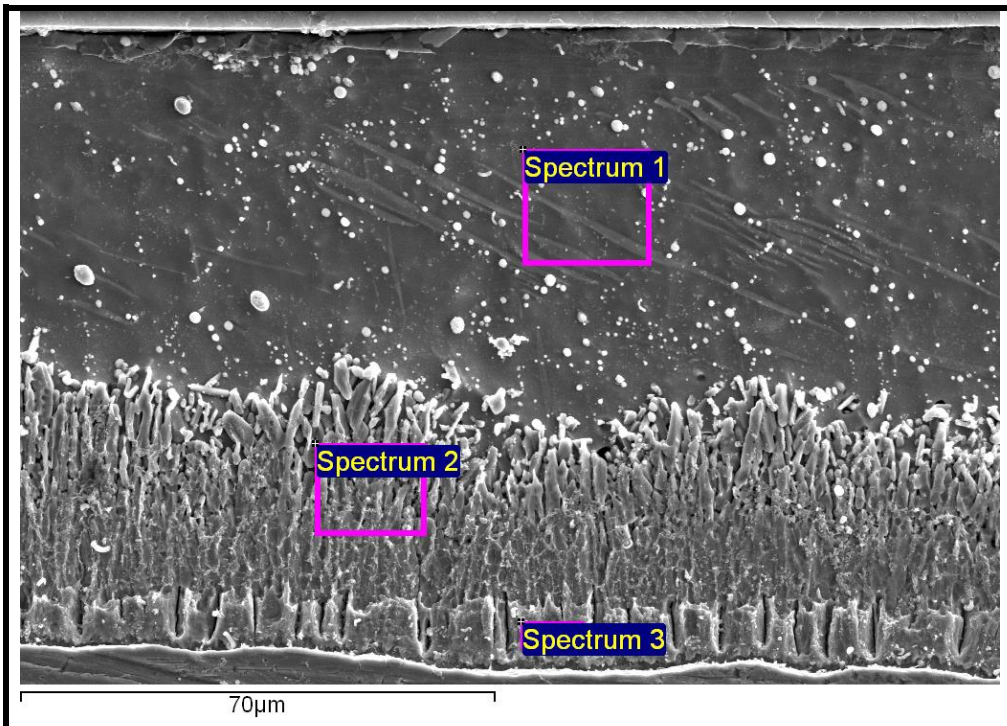

Figure 27

Mag = 900X

Voltage = 20kV

Comment:

B-HDG I
Pre-exposure

Location 2

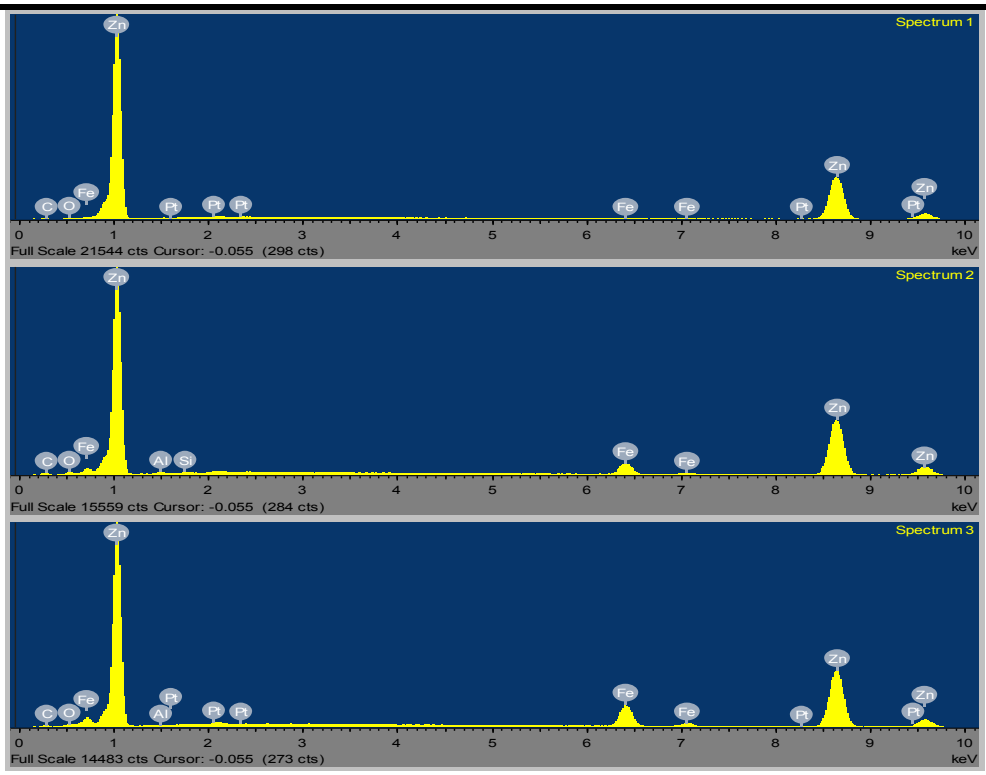

Figure 28

Voltage = 20kV

Comment:

B-HDG I
Pre-exposure

Location 2

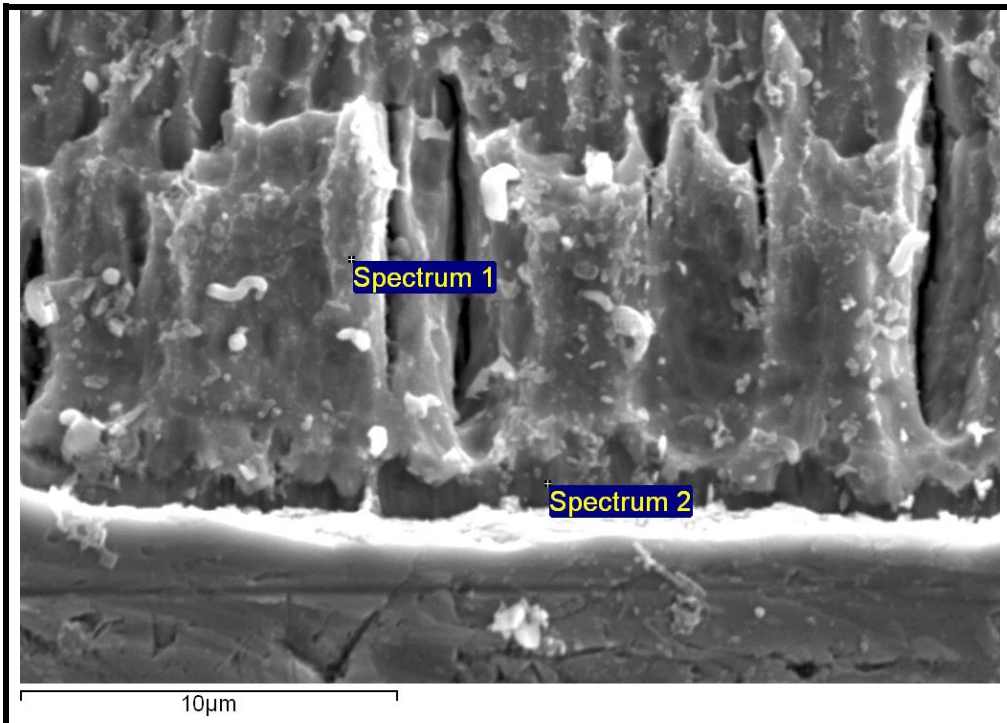

Figure 29

Mag = 5000X

Voltage = 20kV

Comment:

B-HDG I
Pre-exposure

Location 2

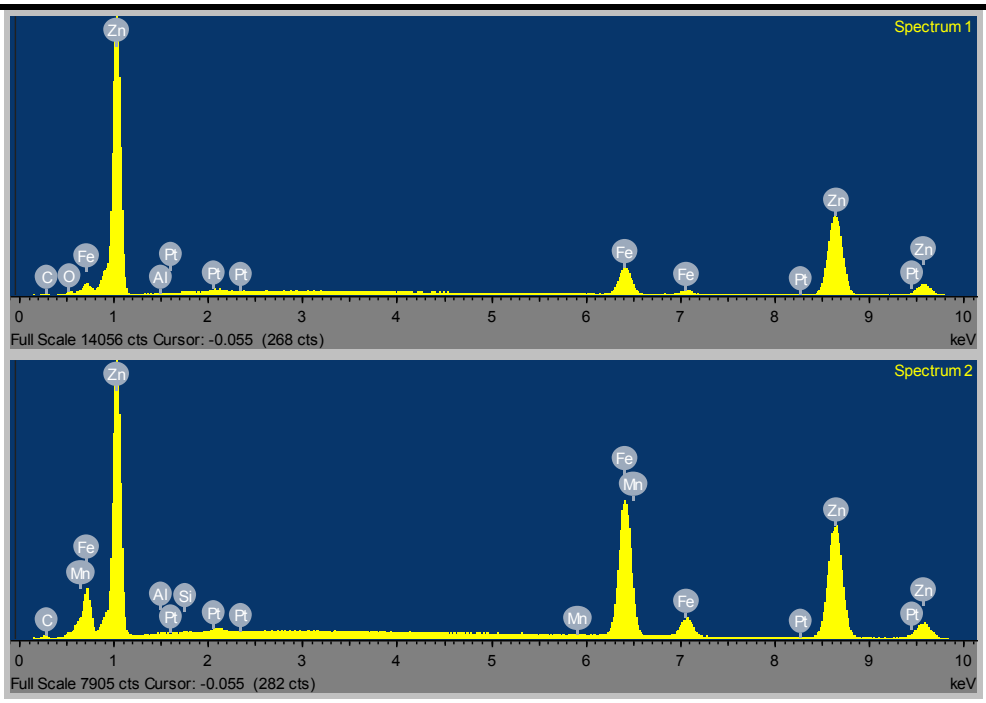

Figure 30

Voltage = 20kV

Comment:

B-HDG I
Pre-exposure

Location 2

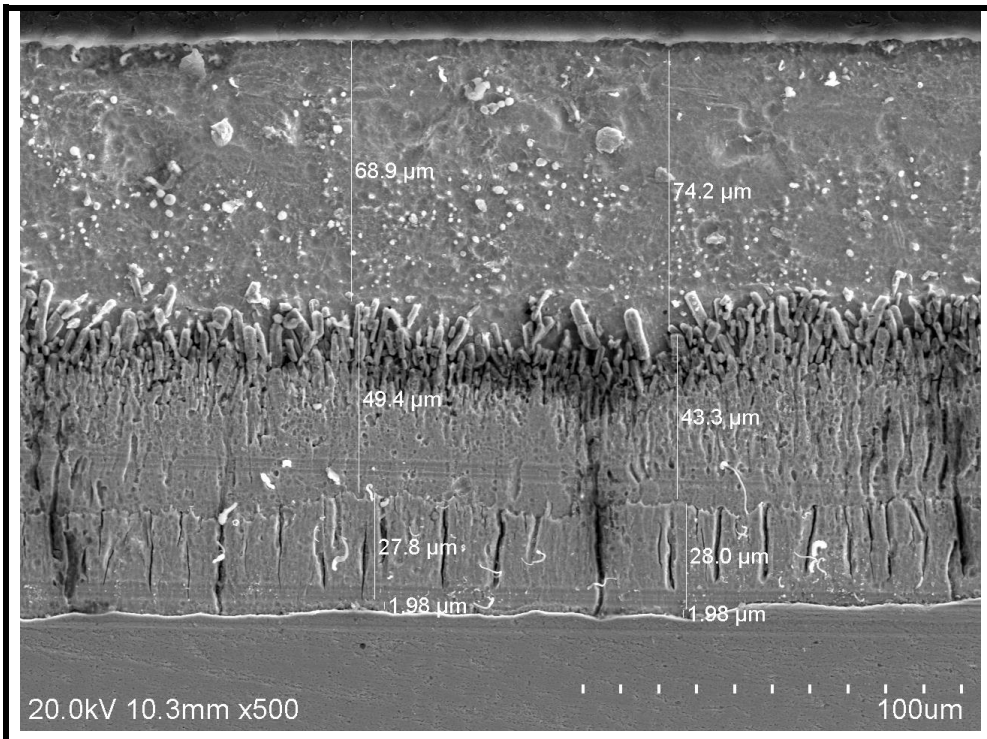

Figure 31

Mag = 500X

Voltage = 20kV

Comment:

B-HDG II
Pre-exposure

Location 1

Pt coated at EAG-MN

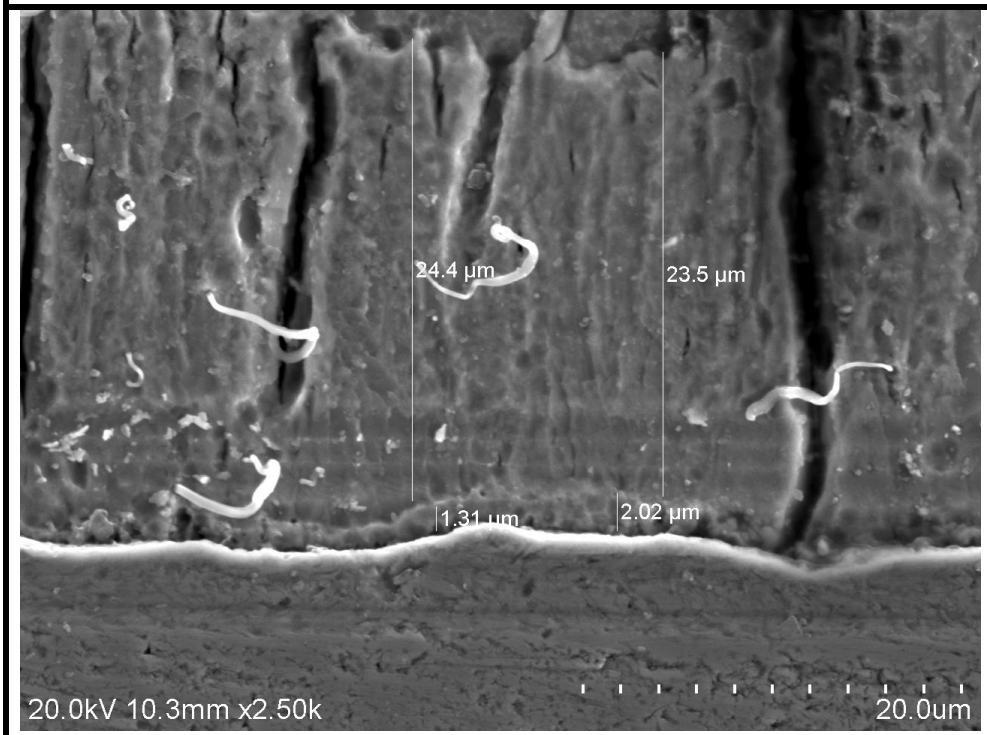

Figure 32

Mag = 2500X

Voltage = 20kV

Comment:

B-HDG II
Pre-exposure

Location 1

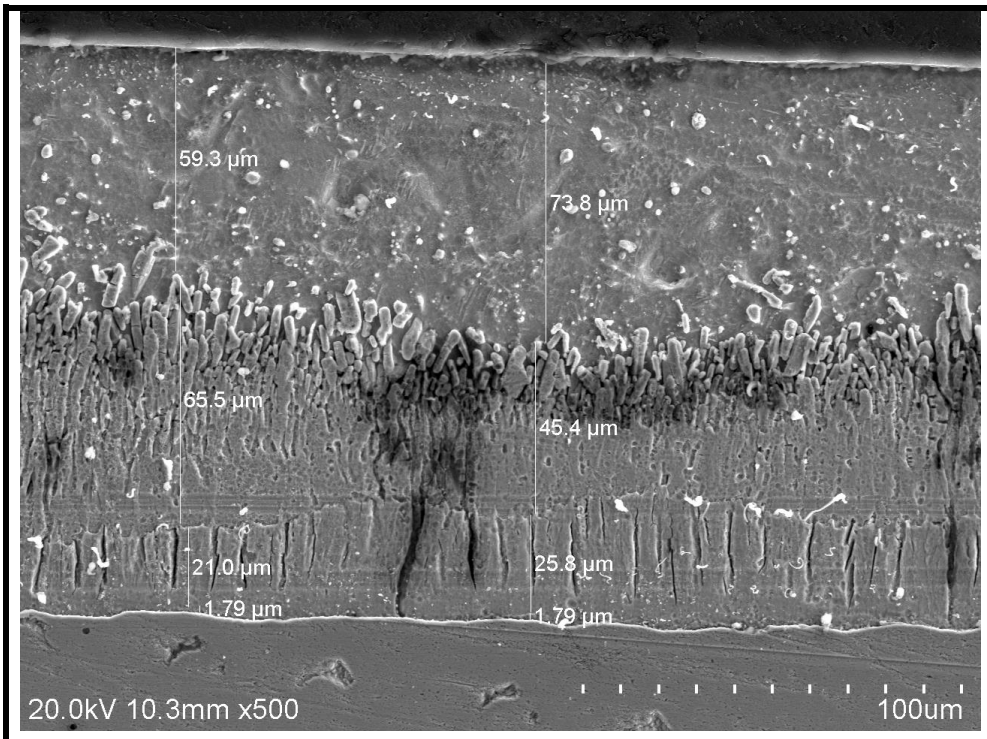

Figure 33

Mag = 500X

Voltage = 20kV

Comment:

B-HDG II
Pre-exposure

Location 2

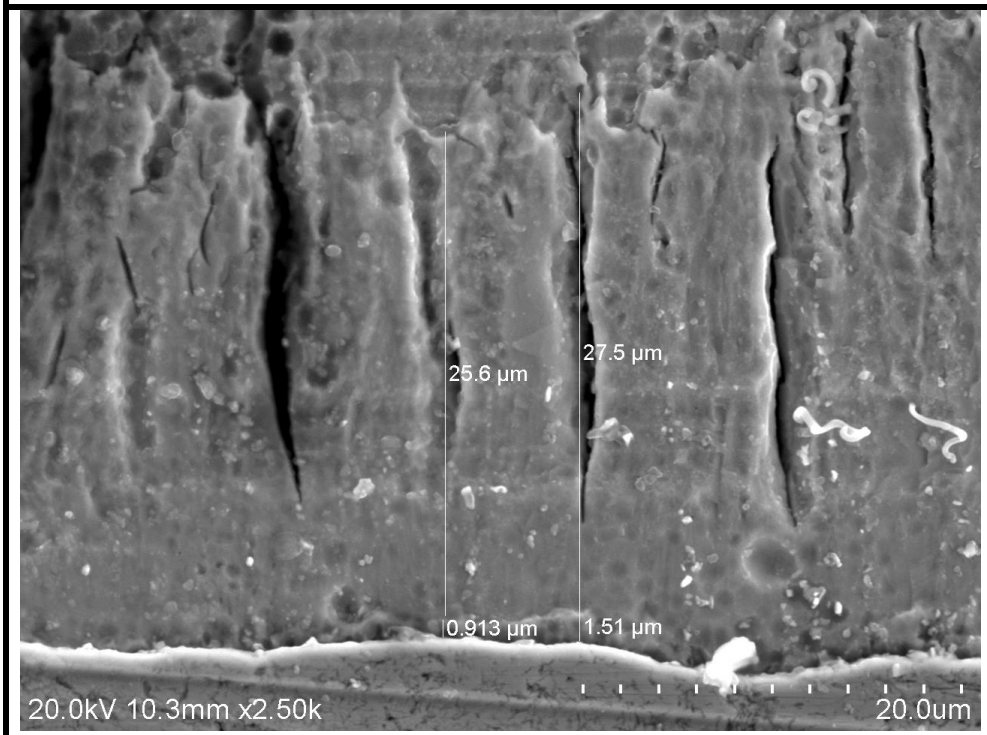

Figure 34

Mag = 2500X

Voltage = 20kV

Comment:

B-HDG II
Pre-exposure

Location 2

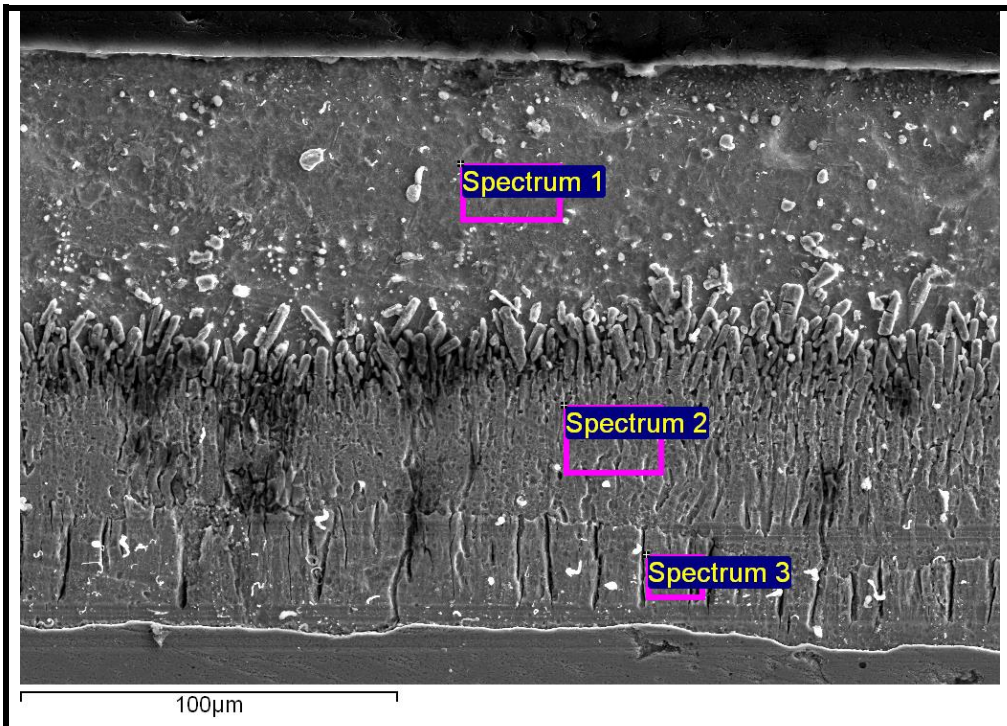

Figure 35

Mag = 500X

Voltage = 20kV

Comment:

B-HDG II
Pre-exposure

Location 1

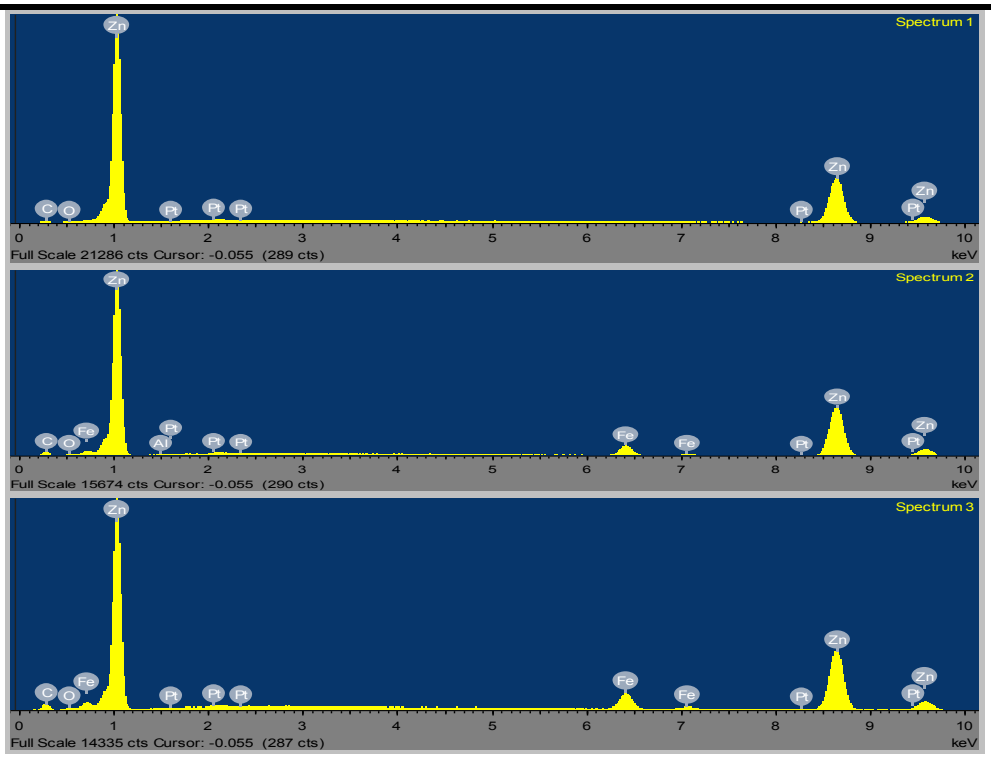

Figure 36

Voltage = 20kV

Comment:

B-HDG II
Pre-exposure

Location 1

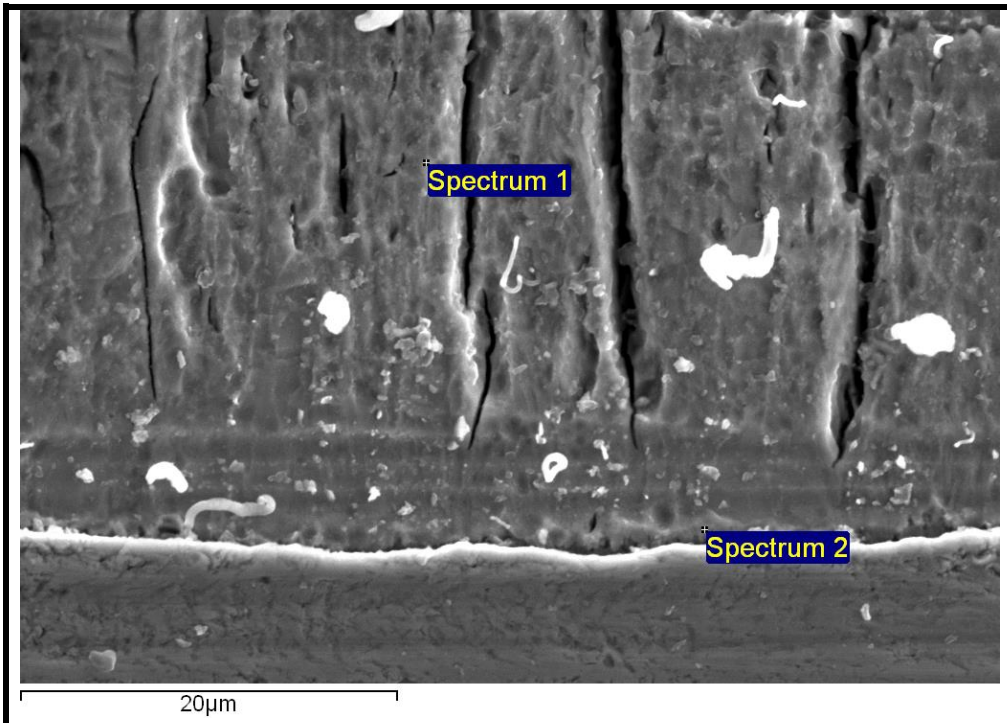

Figure 37

Mag = 2500X

Voltage = 20kV

Comment:

B-HDG II
Pre-exposure

Location 1

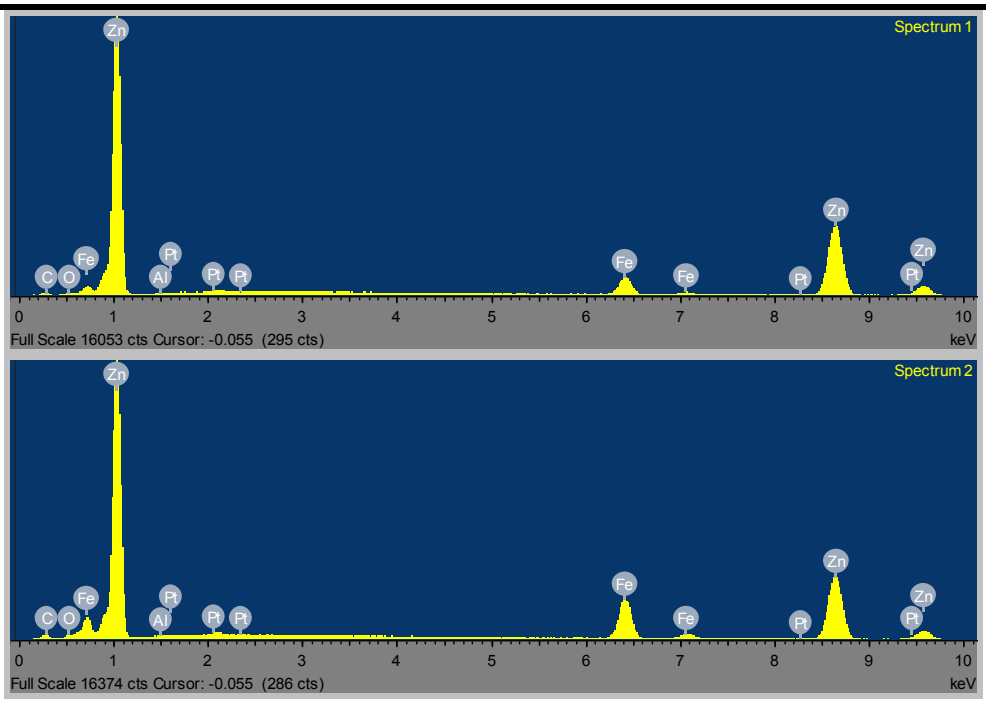

Figure 38

Voltage = 20kV

Comment:

B-HDG II
Pre-exposure

Location 1

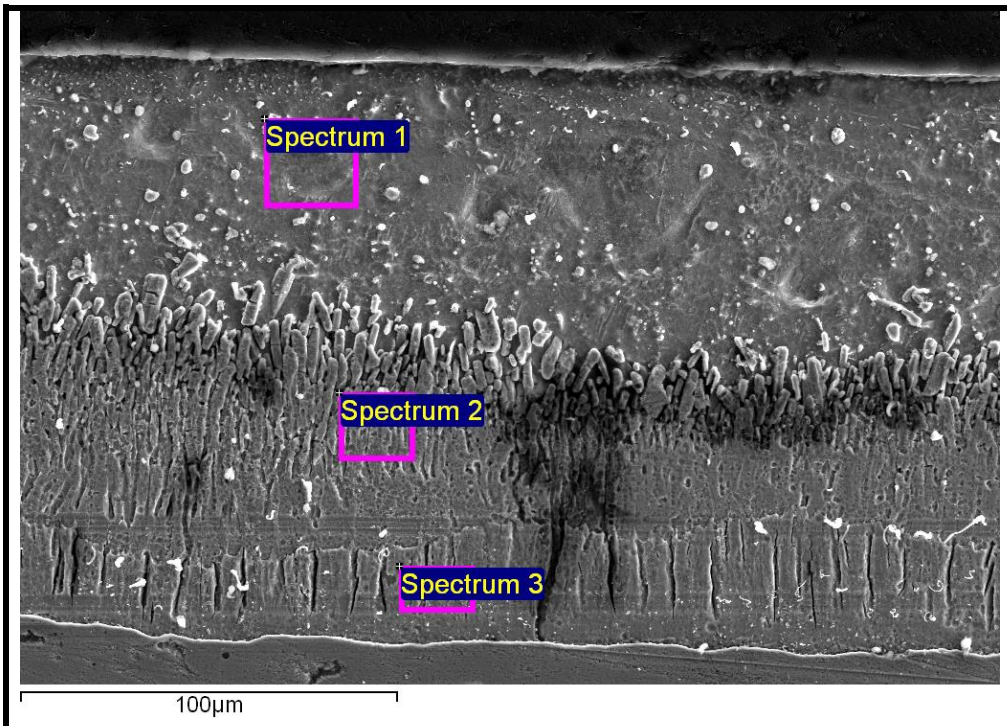

Figure 39

Mag = 500X

Voltage = 20kV

Comment:

B-HDG II
Pre-exposure

Location 2

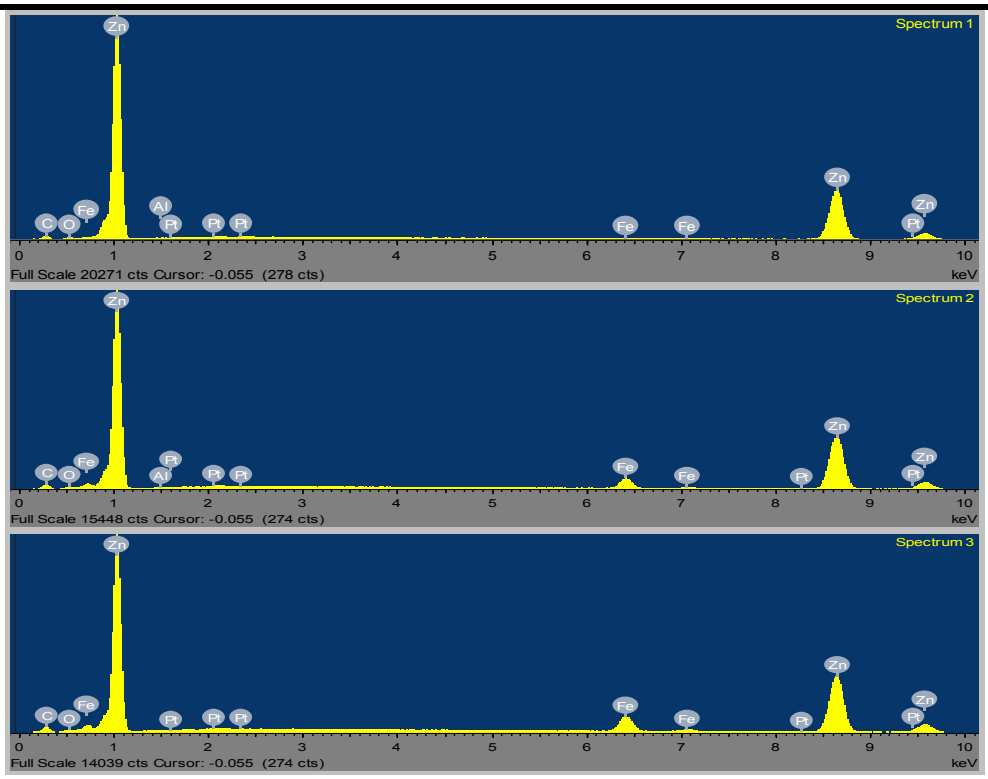

Figure 40

Voltage = 20kV

Comment:

B-HDG II
Pre-exposure

Location 2

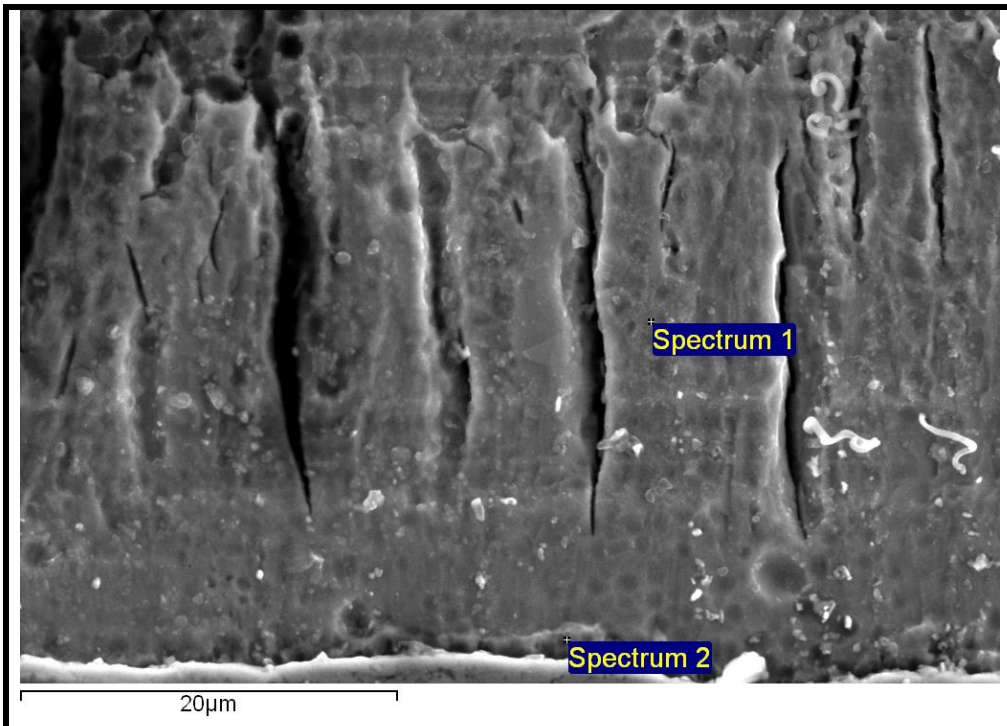

Figure 41

Mag = 2500X

Voltage = 20kV

Comment:

B-HDG II
Pre-exposure

Location 2

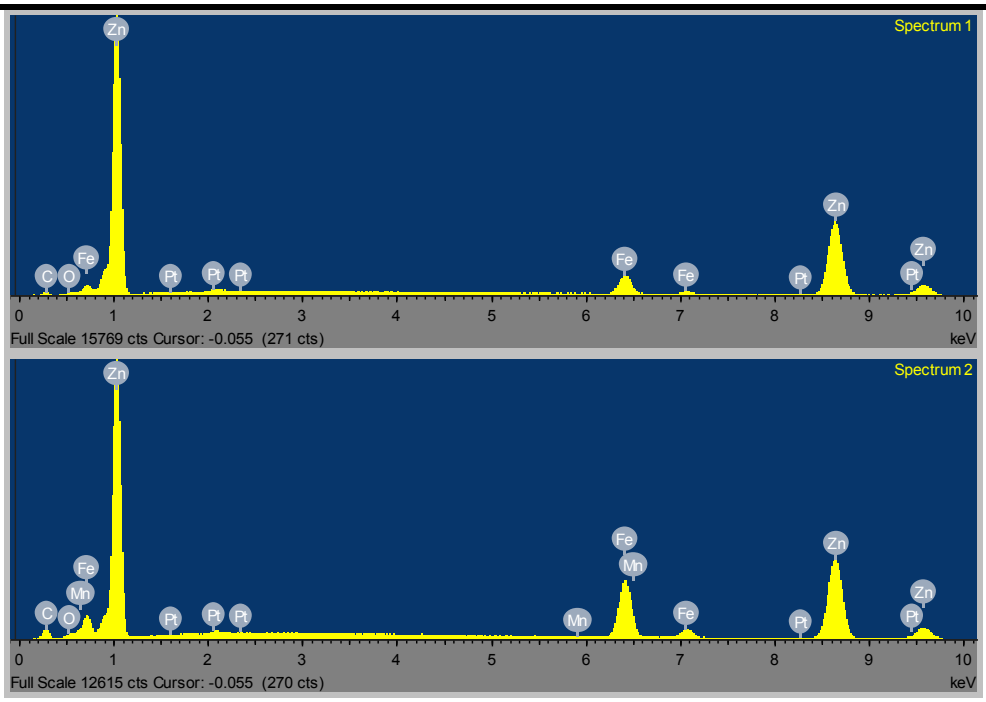

Figure 42

Voltage = 20kV

Comment:

B-HDG II
Pre-exposure

Location 2

EAG-MN **P0EMR948** **All results in weight%**

	C	O	Al	Si	Mn	Fe	Zn
C-HDG I Figure 5							
Zinc	10.3	4.5	1.0	0.2	…	0.8	83.3
Substrate	3.7	…	0.2	…	0.8	95.3	…
C-HDG I Figure 9							
Zinc	12.7	5.6	1.2	0.4	…	1.0	79.2
Substrate	3.8	…	0.2	…	0.9	95.1	…
C-HDG II Figure 13							
Zinc	11.5	5.1	1.3	0.5	…	0.8	80.7
Substrate	3.2	…	0.2	…	0.8	95.8	…
C-HDG II Figure 15							
Zinc	12.3	5.3	1.3	0.4	…	0.6	80.2
Substrate	3.3	…	0.2	0.1	0.9	95.5	…
B-HDG I Figure 23							
Eta	5.5	0.9	…	…	…	0.2	93.4
Zeta	5.7	1.8	0.2	0.3	…	6.0	86.1
Delta	5.8	1.4	0.2	…	…	10.2	82.5
B-HDG I Figure 25							
Delta	3.8	1.1	0.1	…	…	10.3	84.7
Gamma	4.9	1.6	0.2	0.2	0.2	28.8	64.2
B-HDG I Figure 27							
Eta	5.7	0.9	…	…	…	0.2	93.2
Zeta	7.0	2.0	0.4	0.2	…	6.0	84.3
Delta	5.5	1.8	0.1	…	…	11.6	81.0
B-HDG I Figure 29							
Delta	4.5	1.5	0.3	…	…	10.3	83.5
Gamma	4.1	…	0.1	0.2	0.2	30.2	65.2
B-HDG II Figure 35							
Eta	8.8	0.8	…	…	…	…	90.4
Zeta	13.1	1.4	0.2	…	…	5.6	79.9
Delta	13.8	1.3	…	…	…	7.6	77.3
B-HDG II Figure 37							
Delta	8.6	1.1	0.1	…	…	7.4	82.8
Gamma	11.1	1.8	0.1	…	…	16.5	70.4
B-HDG II Figure 39							
Eta	12.7	1.1	0.1	…	…	0.2	85.9
Zeta	14.6	1.8	0.3	…	…	5.3	78.0
Delta	13.7	1.3	…	…	…	7.8	77.1
B-HDG II Figure 41							
Delta	7.6	1.0	…	…	…	8.1	83.4
Gamma	13.2	1.3	…	…	0.2	18.1	67.2

Page 24 / 24

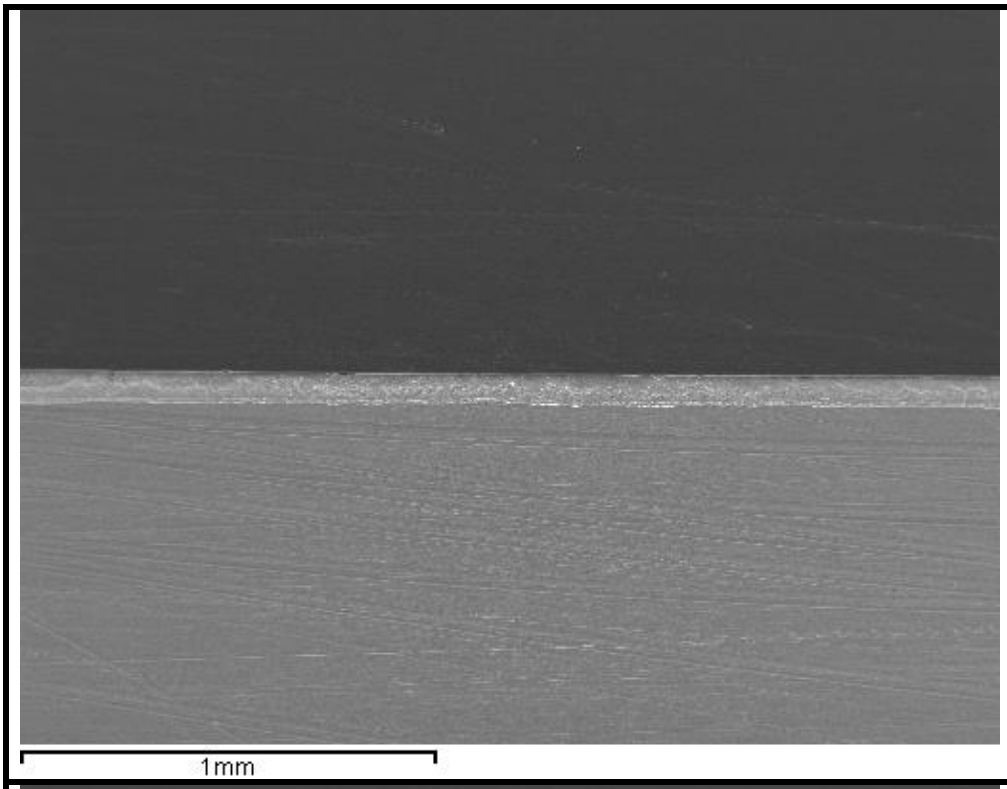

Figure 1

Mag = X50

Voltage = 20kV

Comment:
B-HDG I
Pre-exposure

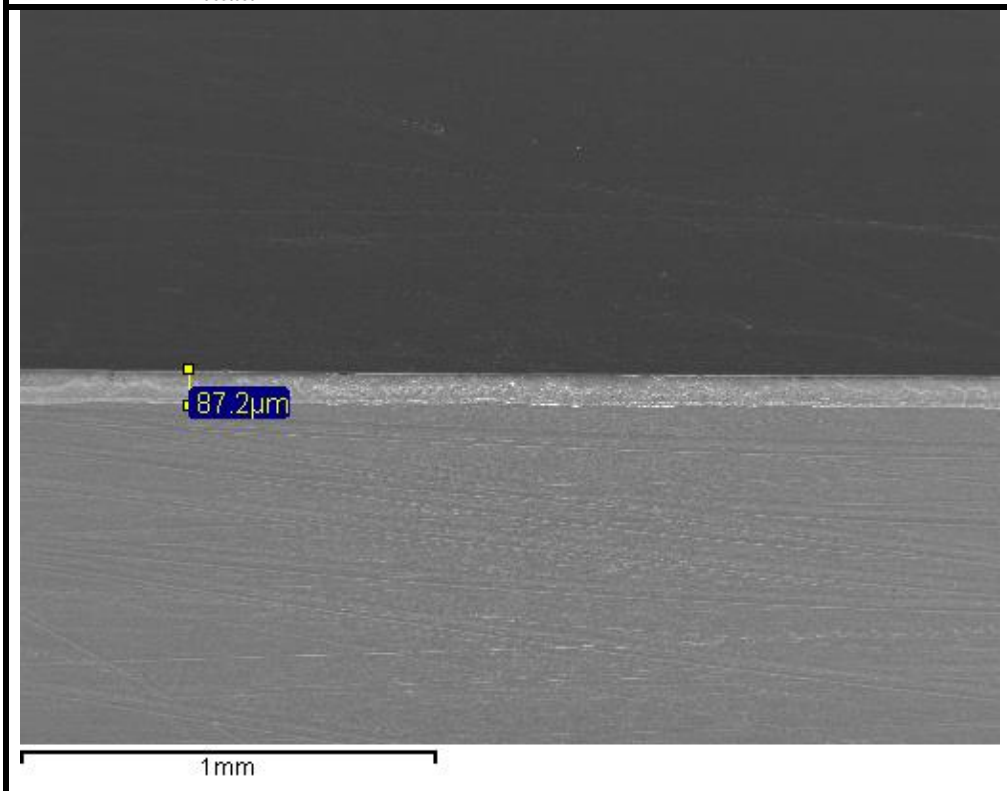

Figure 2

Mag = X50

Voltage = 20kV

Comment:
B-HDG I
Pre-exposure

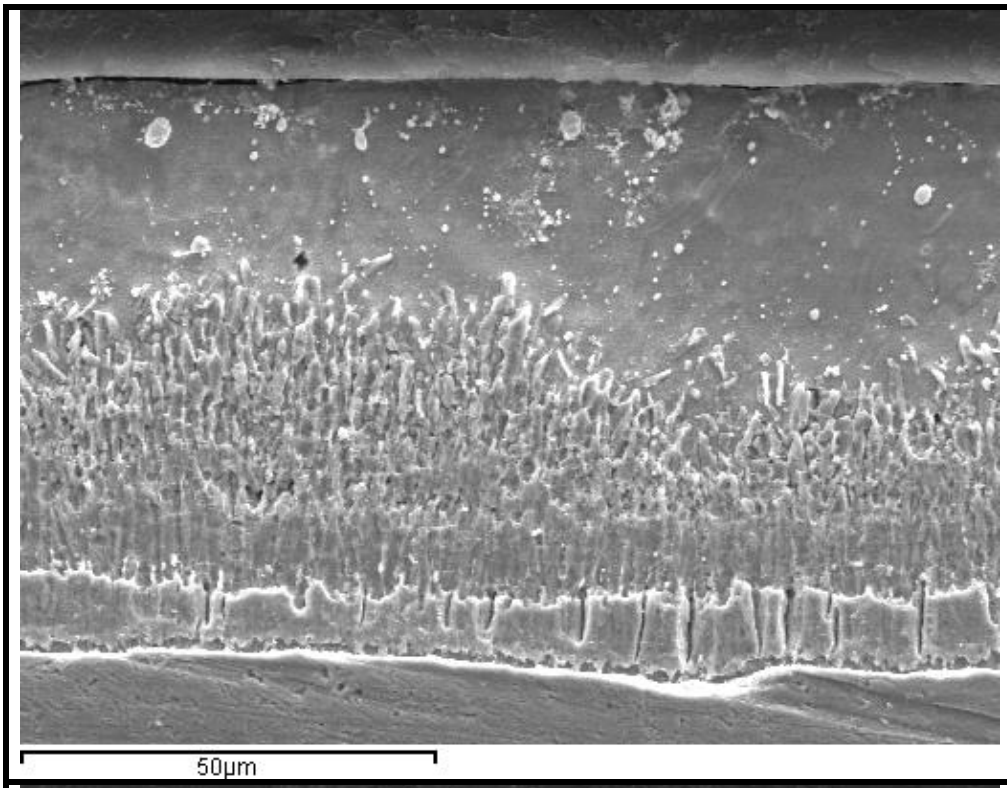

Figure 3

Mag = X1,000

Voltage = 20kV

Comment:
B-HDG I
Pre-exposure

Location 1

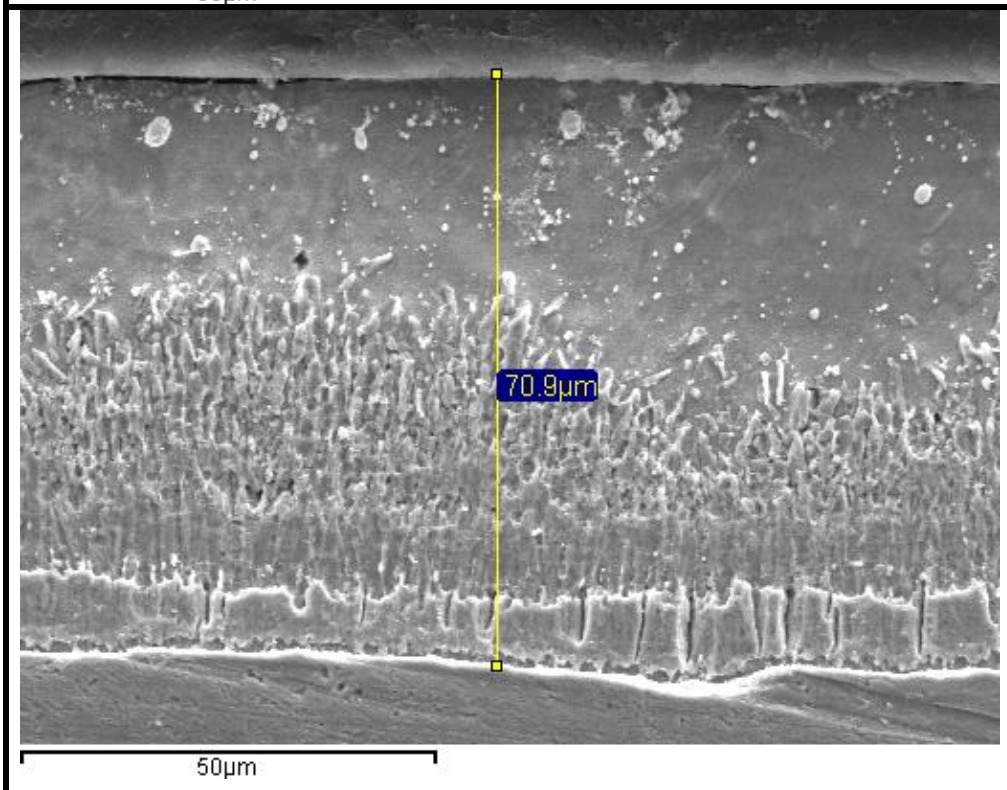

Figure 4

Mag = X1,000

Voltage = 20kV

Comment:
B-HDG I
Pre-exposure

Location 1

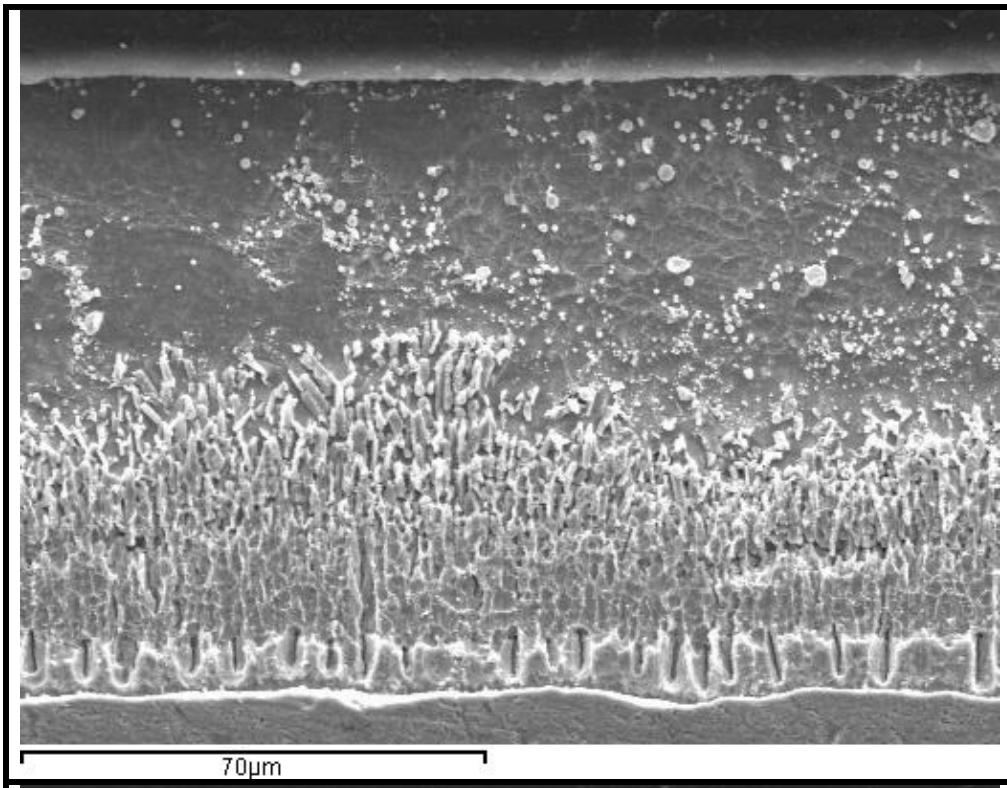

Figure 5

Mag = X800

Voltage = 20kV

Comment:
B-HDG I
Pre-exposure

Location 2

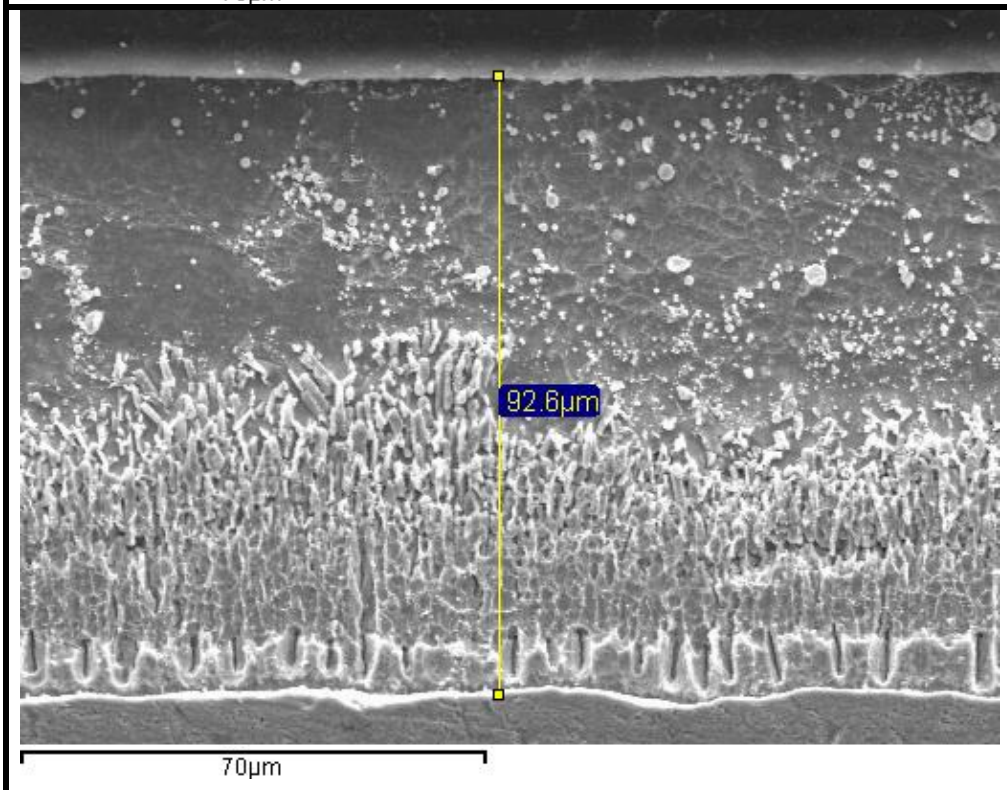

Figure 6

Mag = X800

Voltage = 20kV

Comment:
B-HDG I
Pre-exposure

Location 2

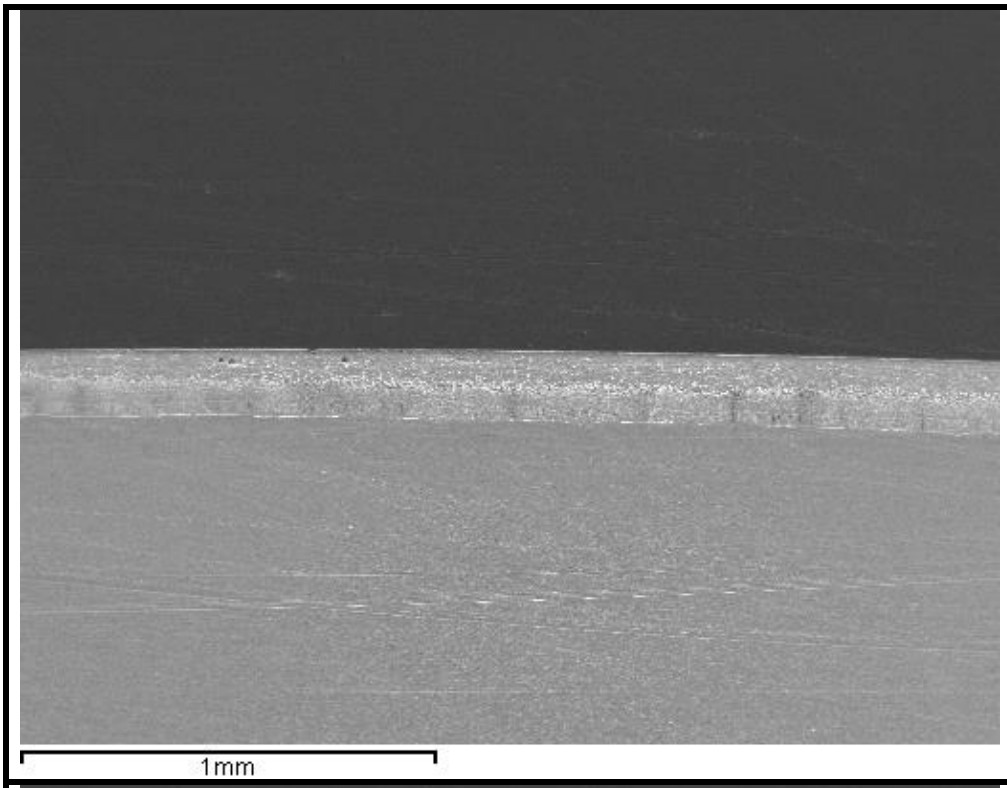

Figure 7

Mag = X50

Voltage = 20kV

Comment:
B-HDG II
Pre-exposure

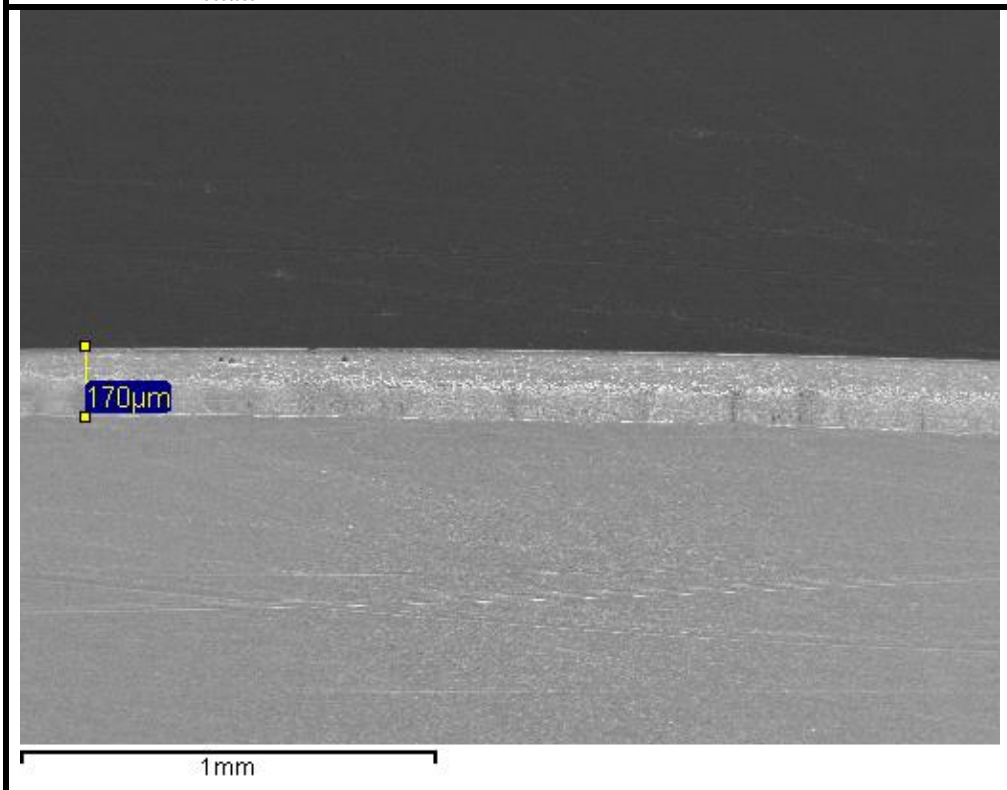

Figure 8

Mag = X50

Voltage = 20kV

Comment:
B-HDG II
Pre-exposure

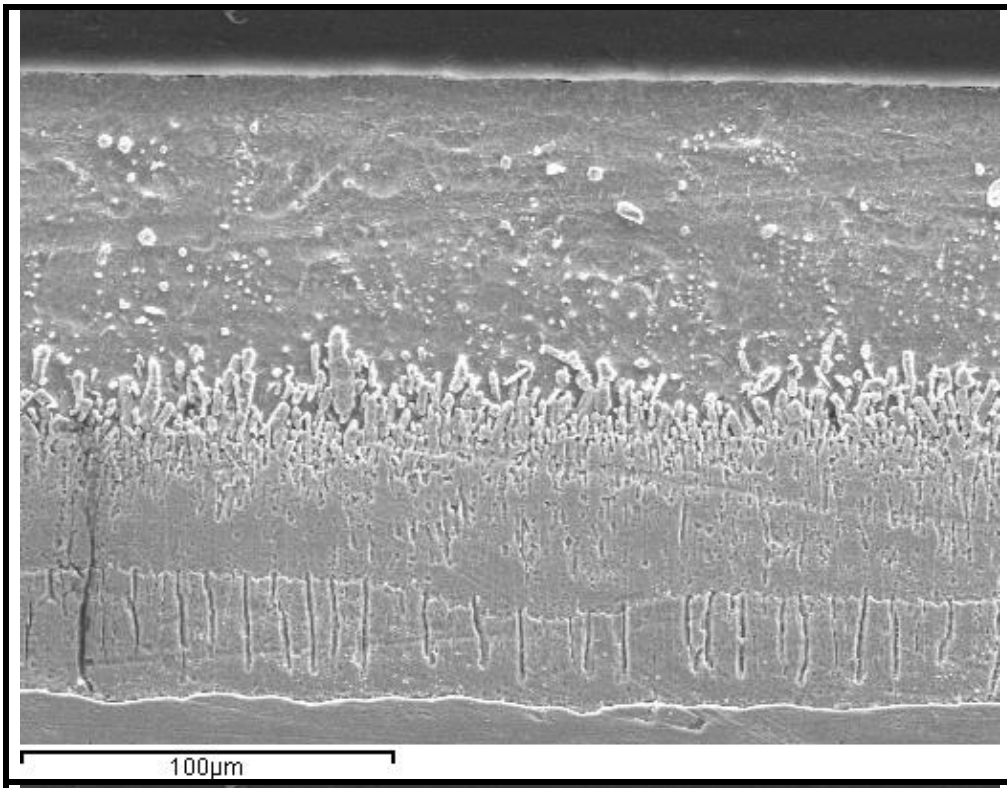

Figure 9

Mag = X450

Voltage = 20kV

Comment:
B-HDG II
Pre-exposure

location 1

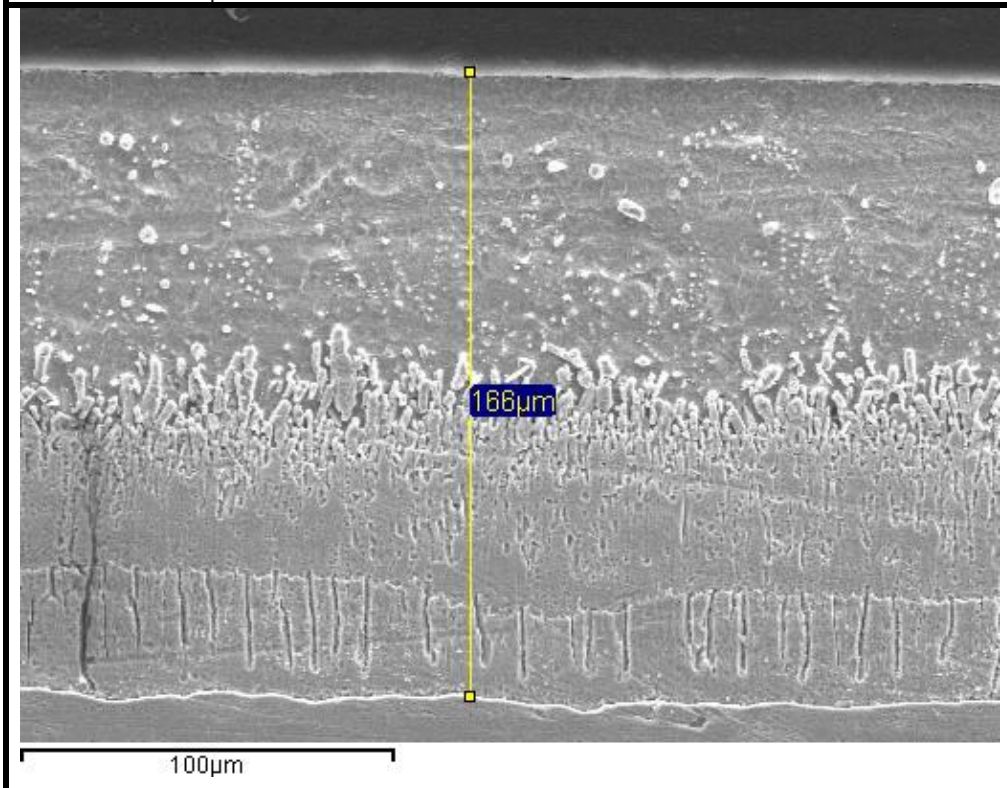

Figure 10

Mag = X450

Voltage = 20kV

Comment:
B-HDG II
Pre-exposure

location 1

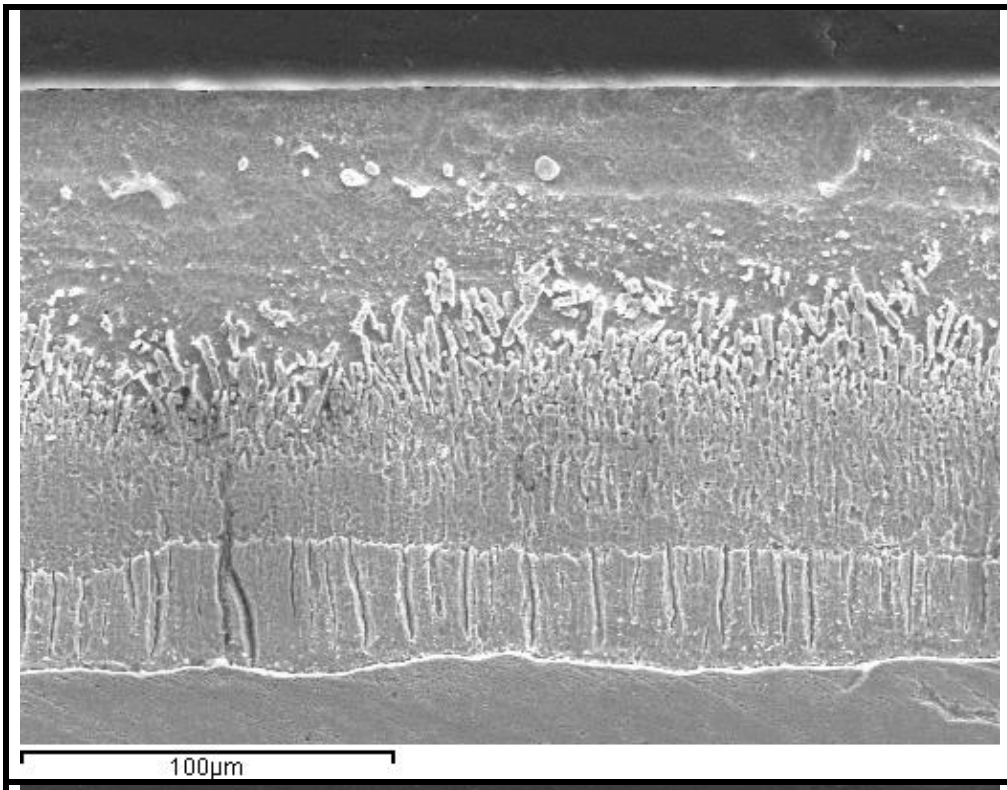

Figure 11

Mag = X450

Voltage = 20kV

Comment:
B-HDG II
Pre-exposure

location 2

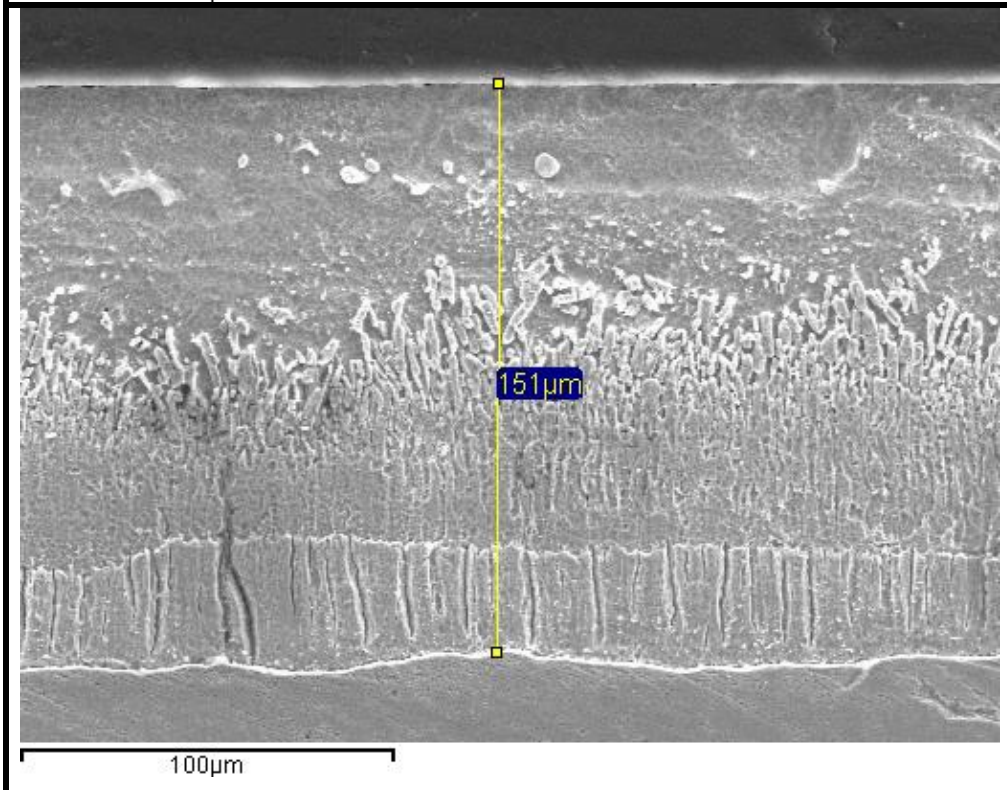

Figure 12

Mag = X450

Voltage = 20kV

Comment:
B-HDG II
Pre-exposure

location 2

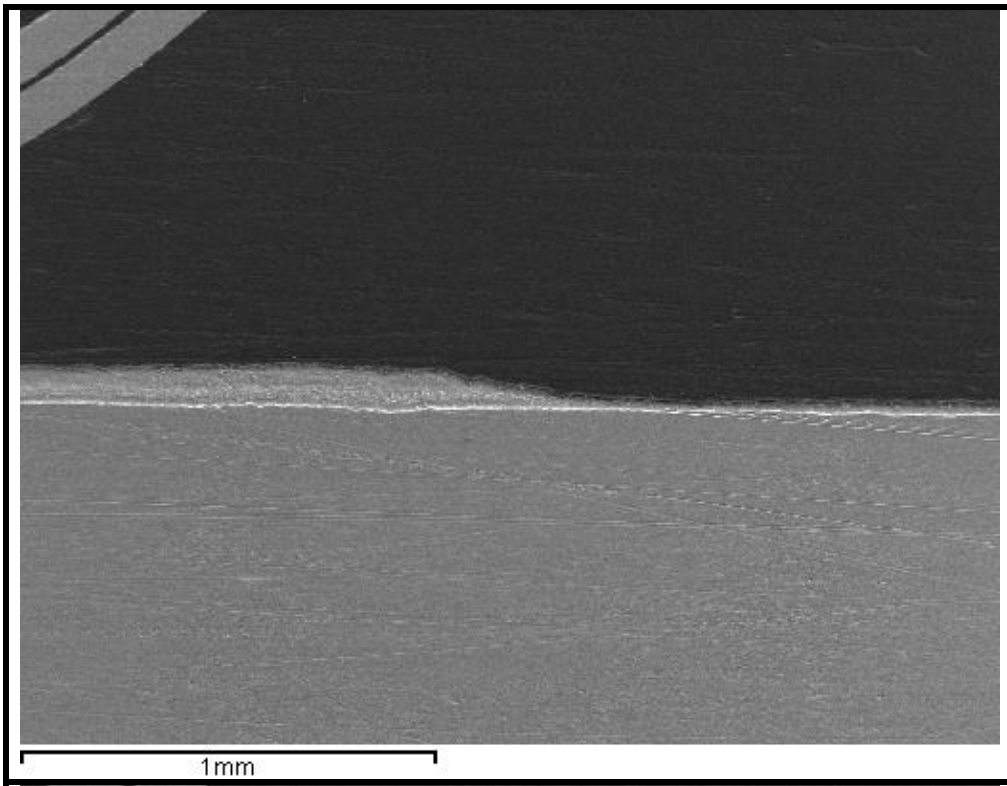

Figure 13

Mag = X50

Voltage = 20kV

Comment:
B-HDG I
60-Cycles

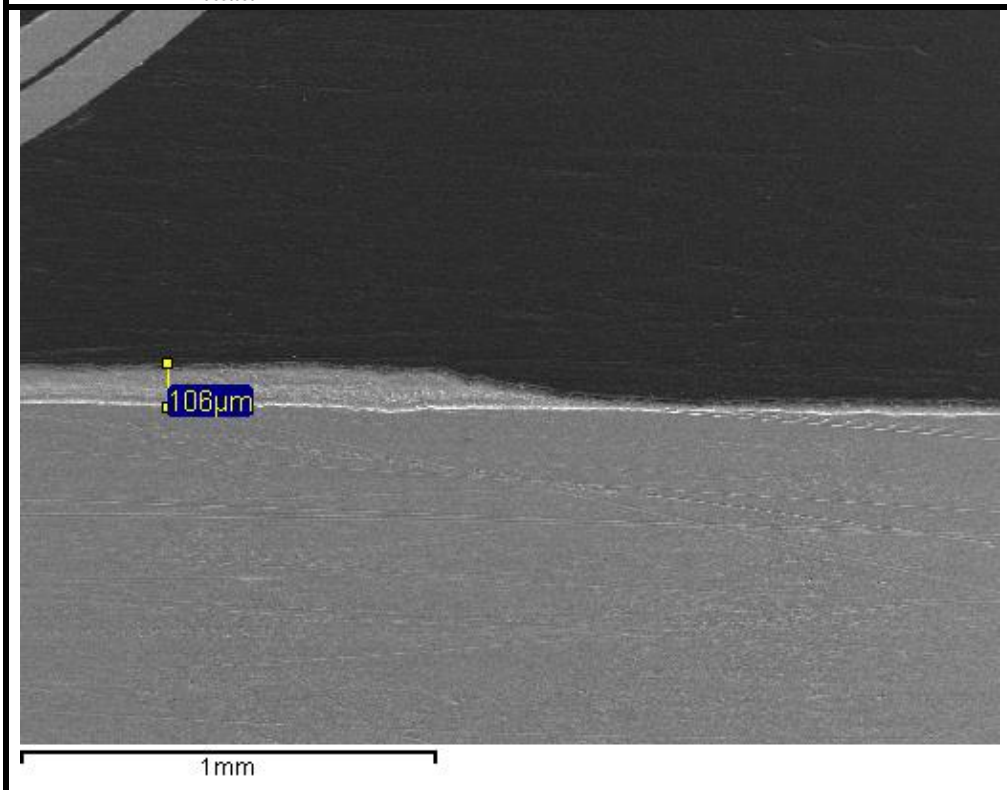

Figure 14

Mag = X50

Voltage = 20kV

Comment:
B-HDG I
60-Cycles

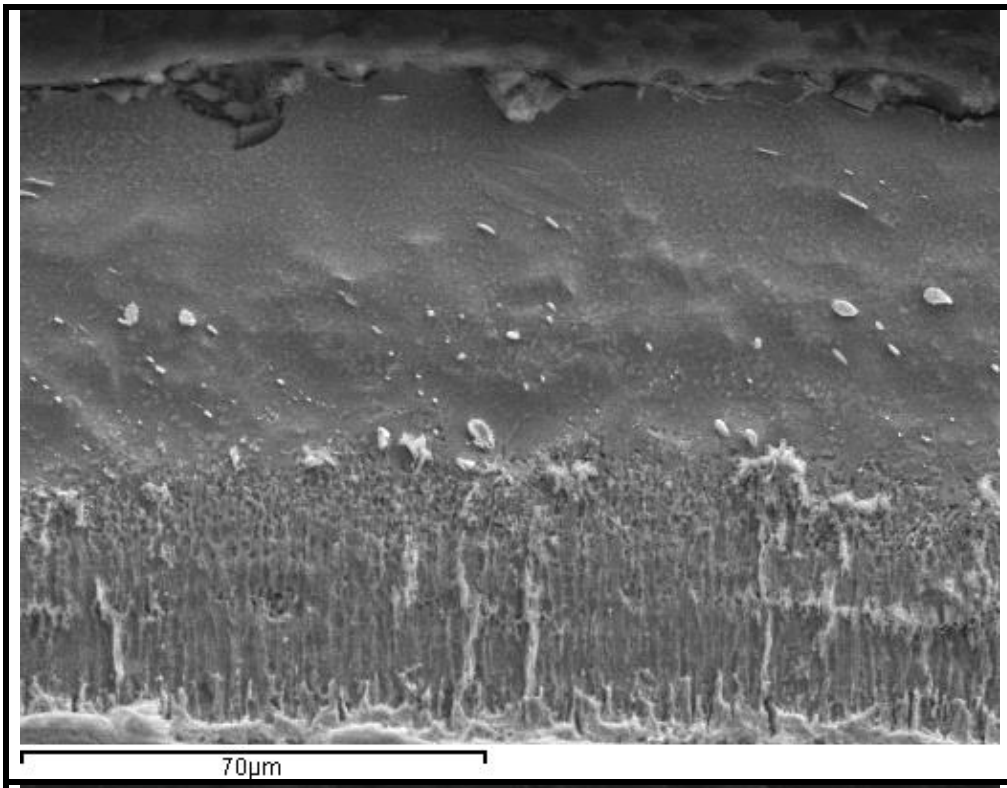

Figure 15

Mag = X800

Voltage = 20kV

Comment:
B-HDG I
60-Cycles

Location 1

corresponds to the left side of the area in Figure 13

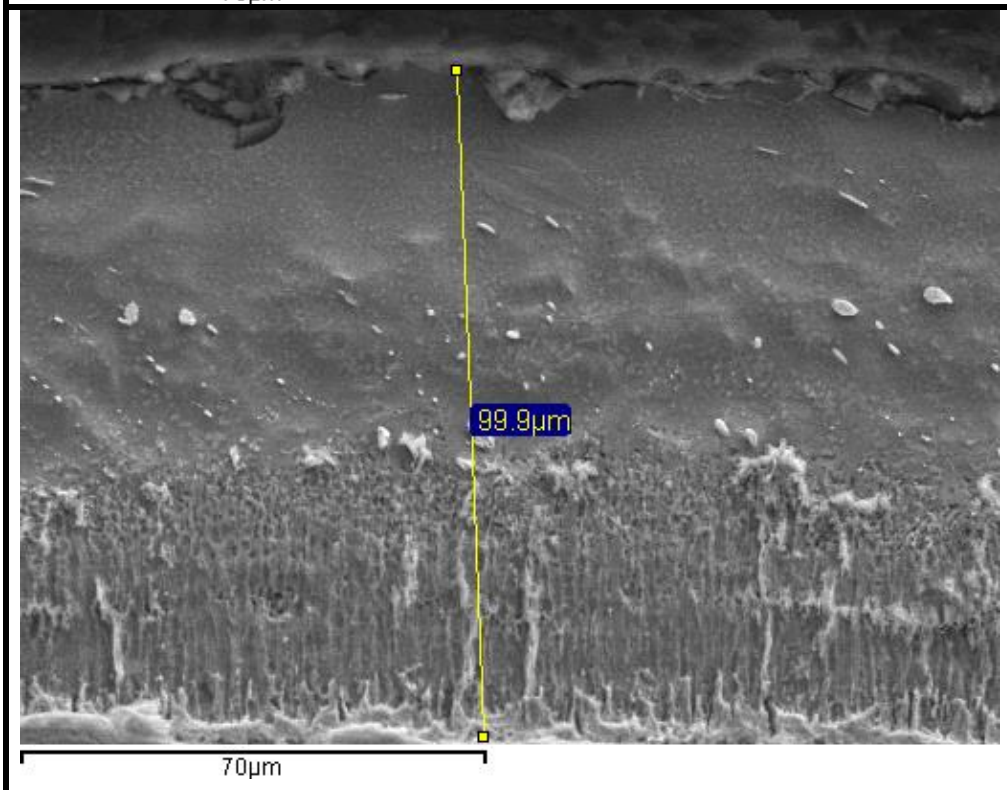

Figure 16

Mag = X800

Voltage = 20kV

Comment:
B-HDG I
60-Cycles

Location 1

corresponds to the left side of the area in Figure 13

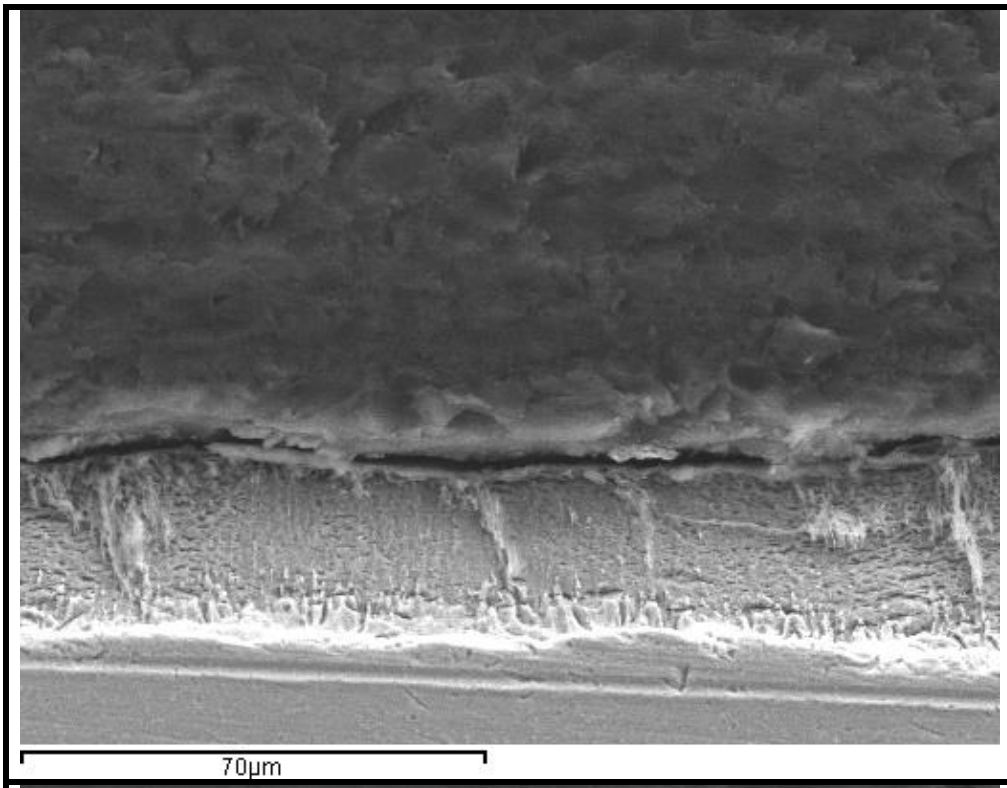

Figure 17

Mag = X800

Voltage = 20kV

Comment:
B-HDG I
60-Cycles

Location 2

corresponds to the right side of the area in Figure 13

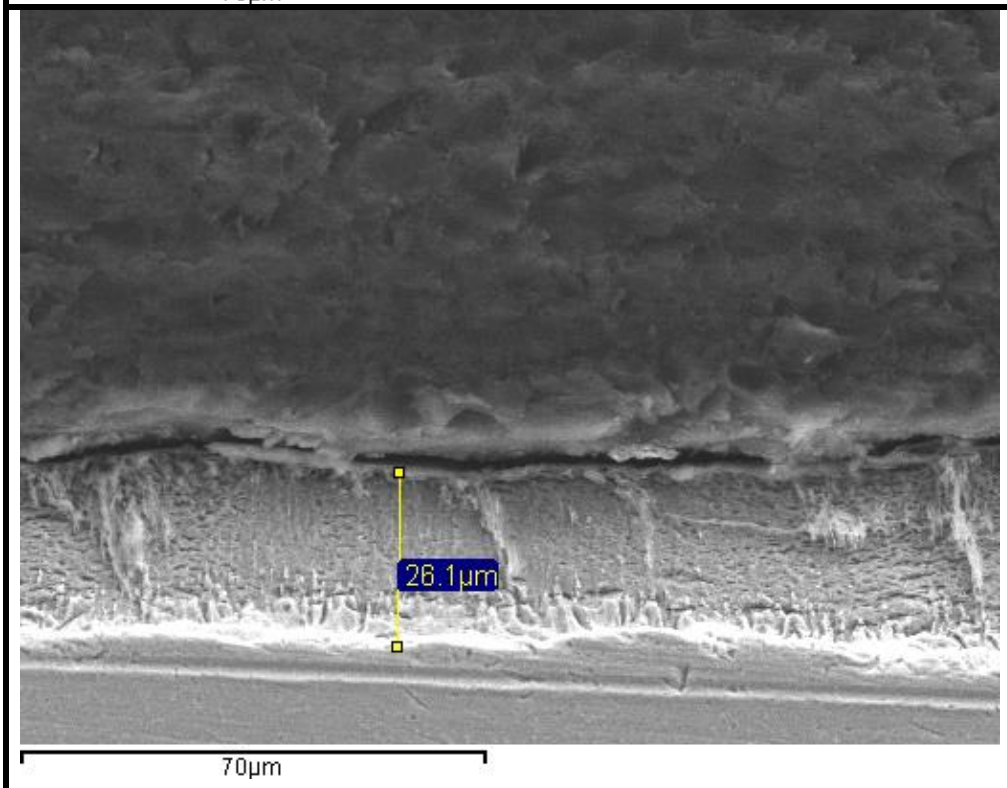

Figure 18

Mag = X800

Voltage = 20kV

Comment:
B-HDG I
60-Cycles

Location 2

corresponds to the right side of the area in Figure 13

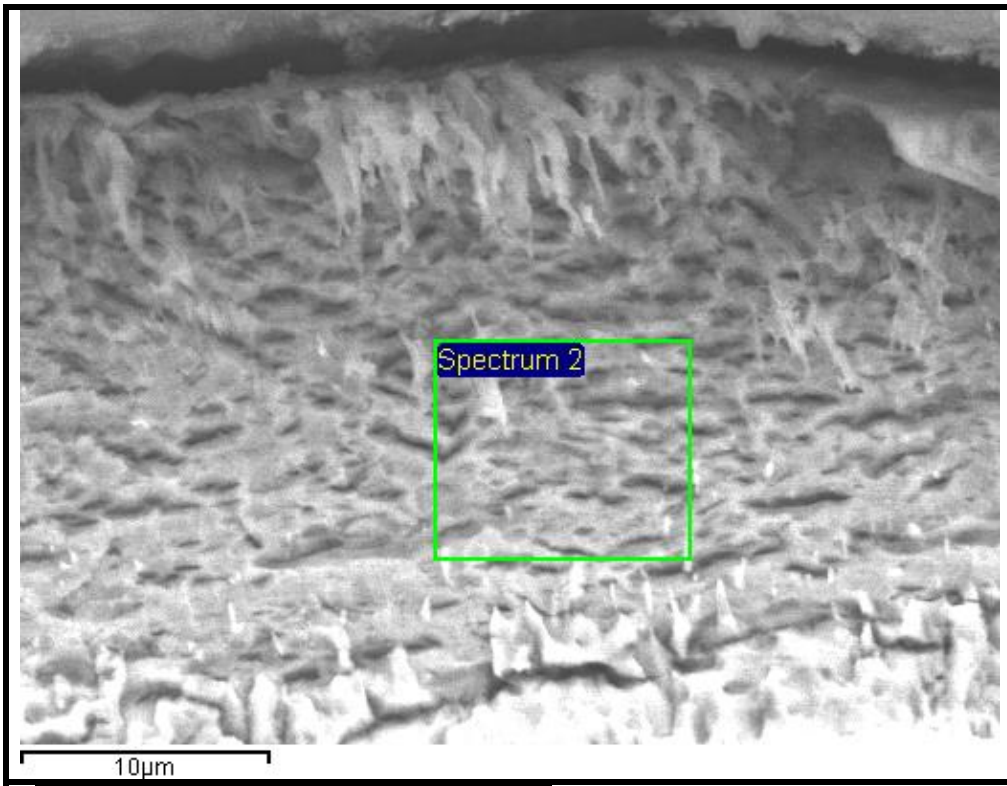

Figure 19

Mag = X3000

Voltage = 20kV

Comment:
B-HDG I
60-Cycles

Zoom in on
Location 2

Element	Weight%	Weight% Sigma	Atomic%
C	11.10	0.91	34.15
O	8.55	0.44	19.75
Fe	7.23	0.26	4.78
Zn	73.11	0.88	41.32
Totals	100.00		

Figure 20

Quant Results

Voltage = 20kV

Comment:
Semi-quantitative results calculated from stored reference spectra

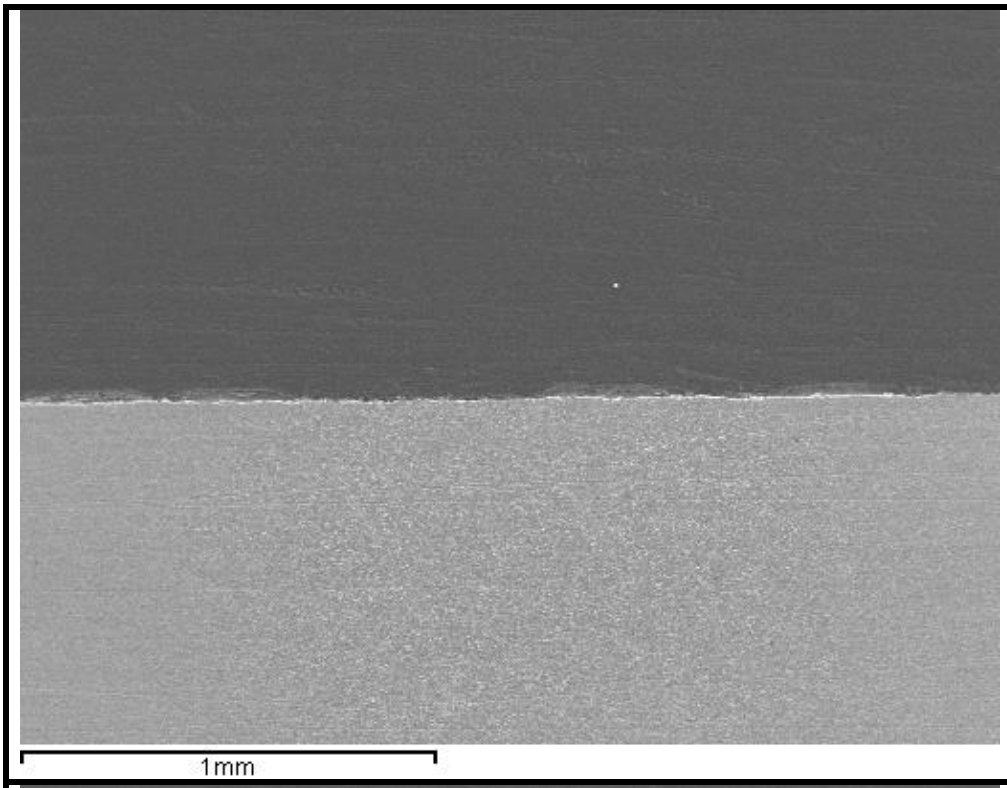

Figure 21

Mag = X50

Voltage = 20kV

Comment:
B-HDG II
60-Cycles

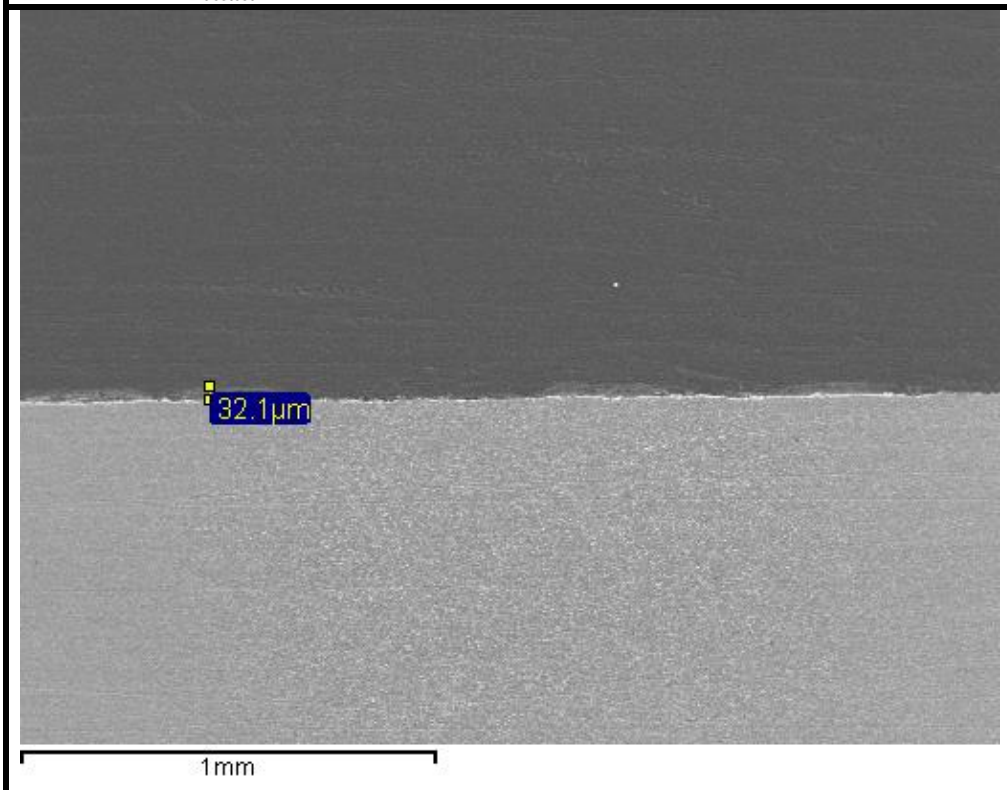

Figure 22

Mag = X50

Voltage = 20kV

Comment:
B-HDG II
60-Cycles

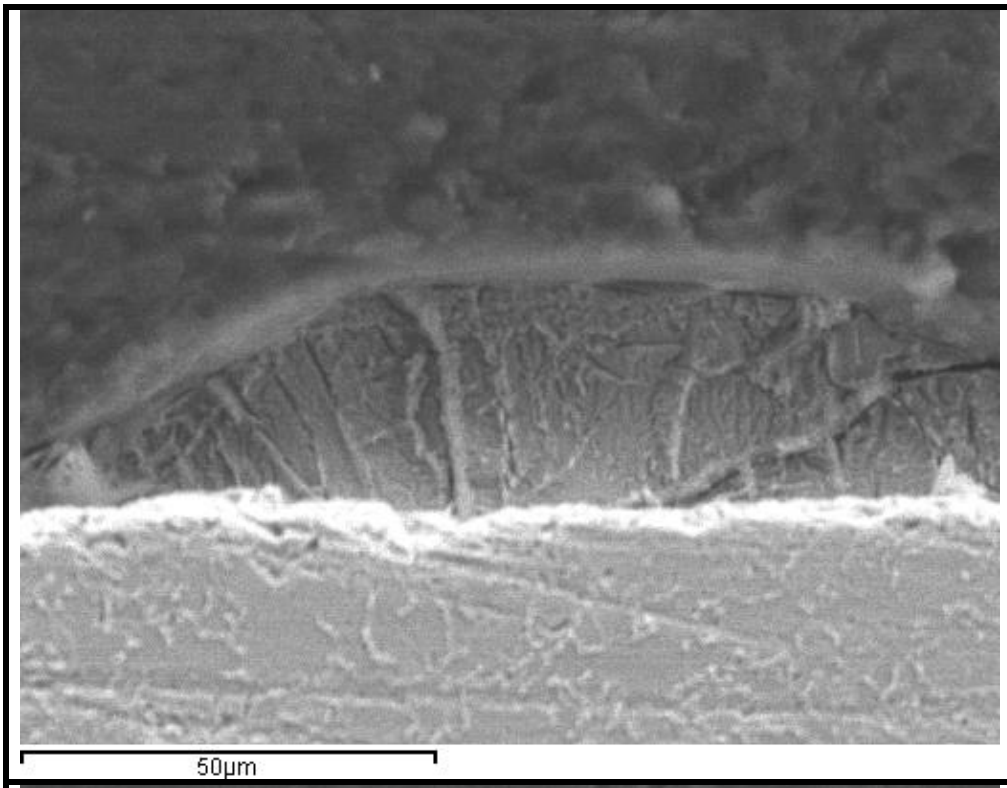

Figure 23

Mag = X1000

Voltage = 20kV

Comment:
B-HDG II
60-Cycles

Location 1

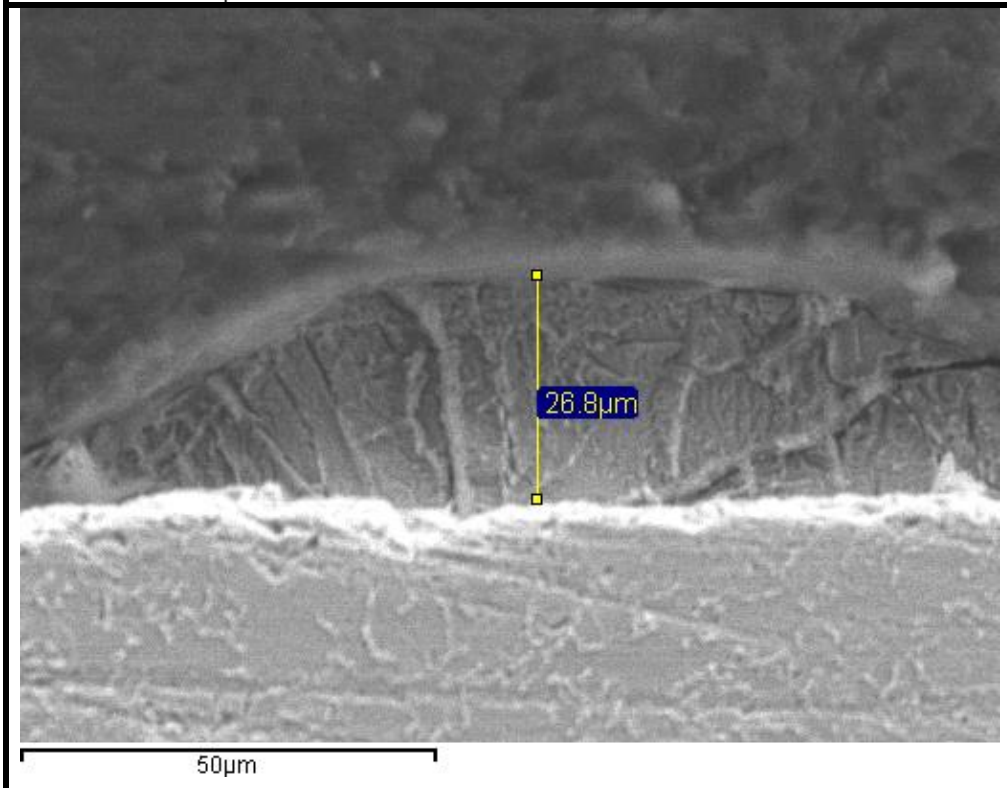

Figure 24

Mag = X1000

Voltage = 20kV

Comment:
B-HDG II
60-Cycles

Location 1

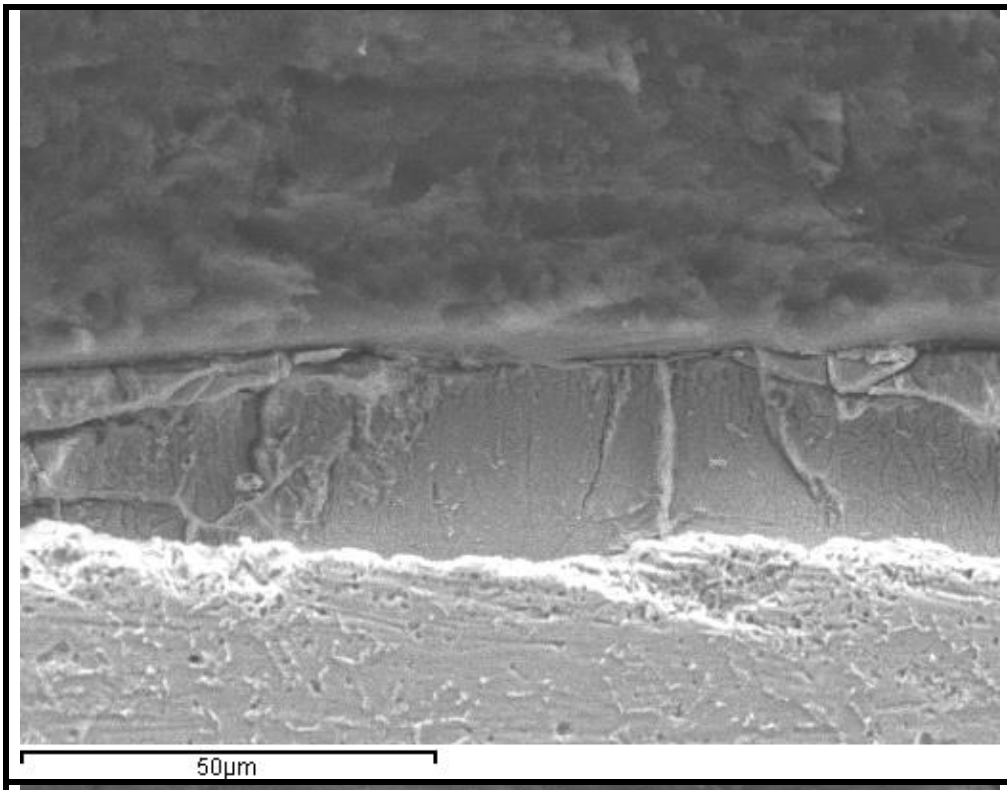

Figure 25

Mag = X1000

Voltage = 20kV

Comment:
B-HDG II
60-Cycles

Location 2

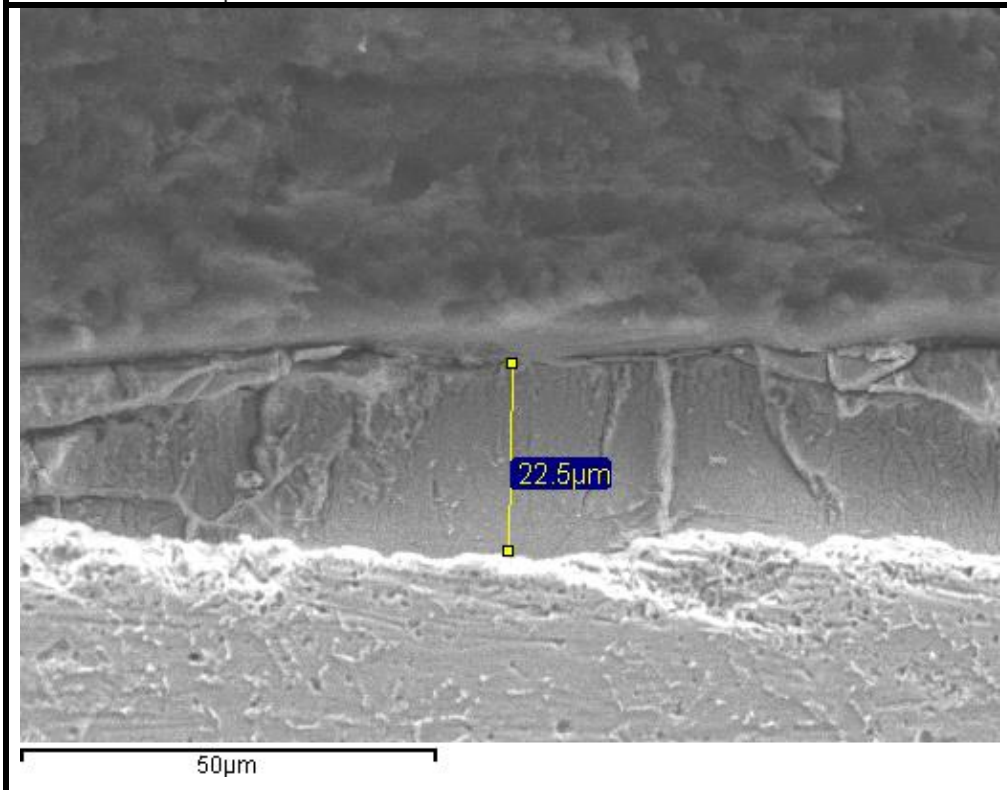

Figure 26

Mag = X1000

Voltage = 20kV

Comment:
B-HDG II
60-Cycles

Location 2

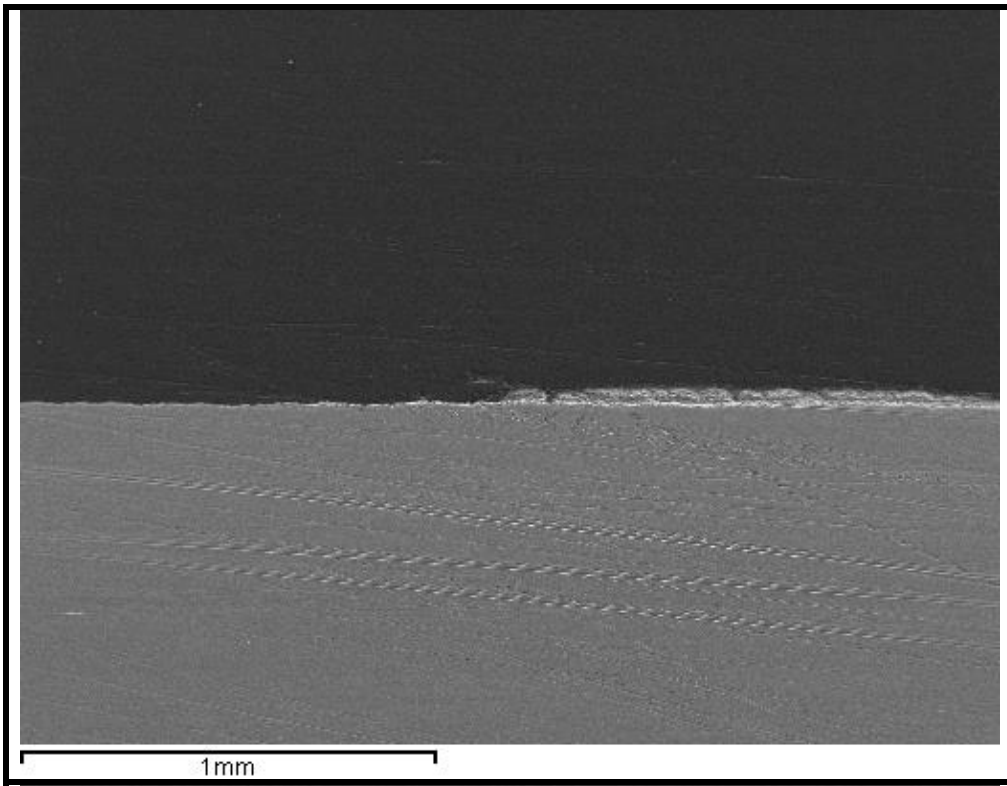

Figure 27

Mag = X50

Voltage = 20kV

Comment:
C-HDG I
60-Cycles

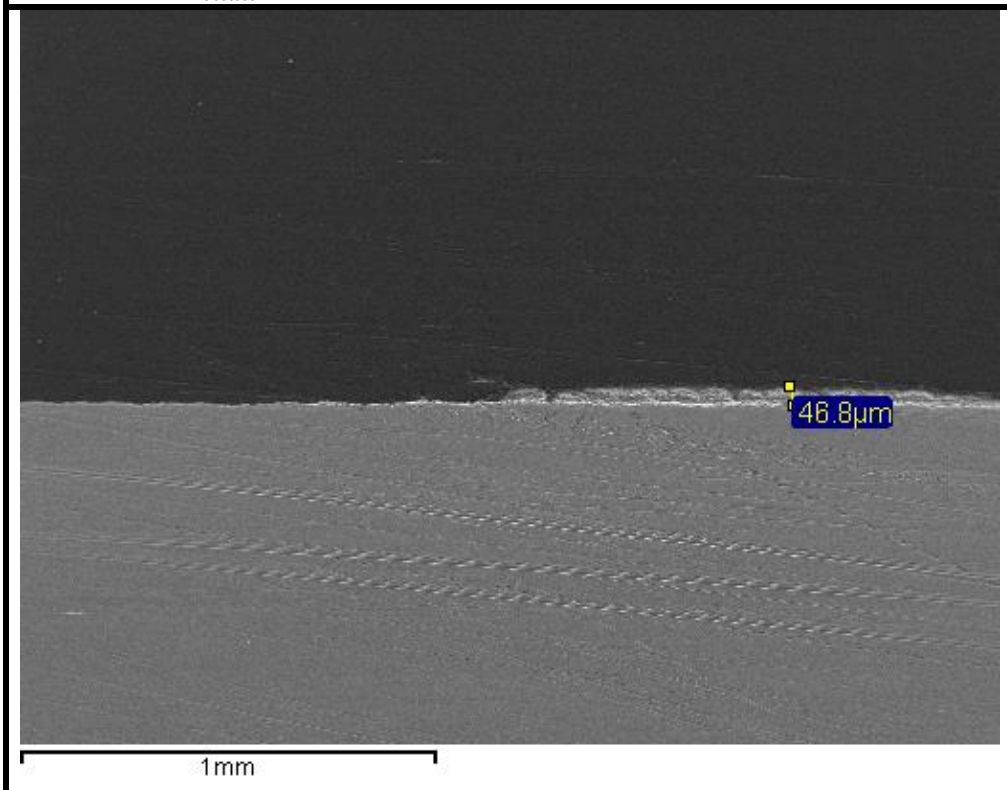

Figure 28

Mag = X

Voltage = 20kV

Comment:
C-HDG I
60-Cycles

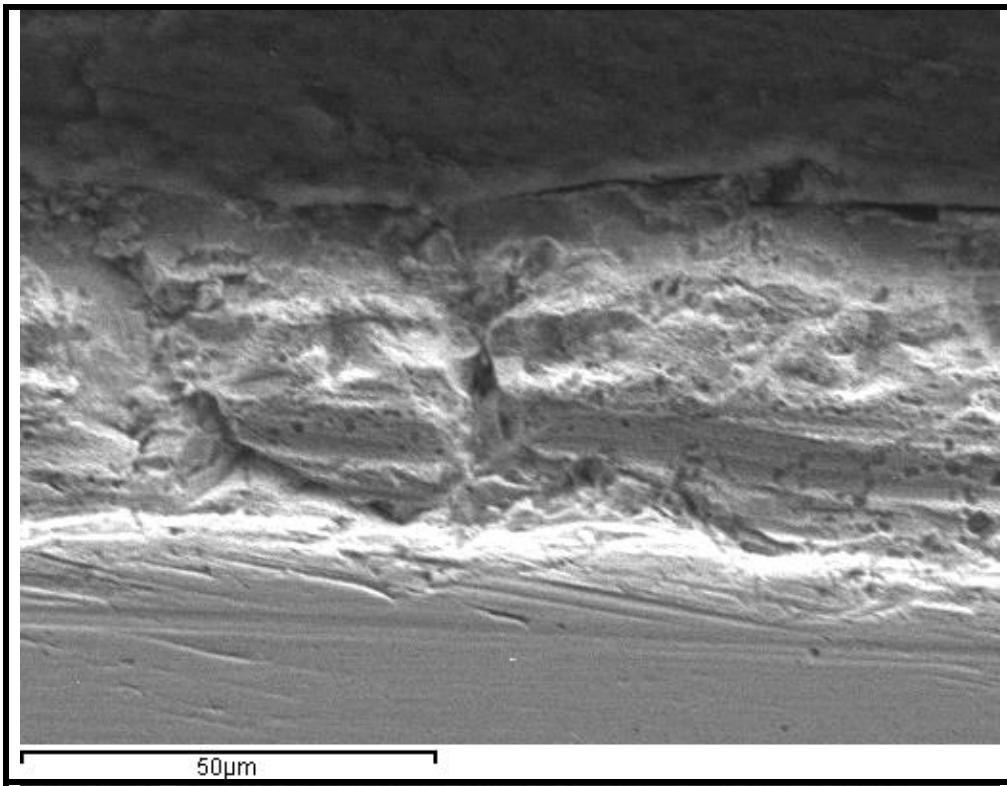

Figure 29

Mag = X1000

Voltage = 20kV

Comment:
C-HDG I
60-Cycles

Location 1

Zoom in on right side of Figure 28

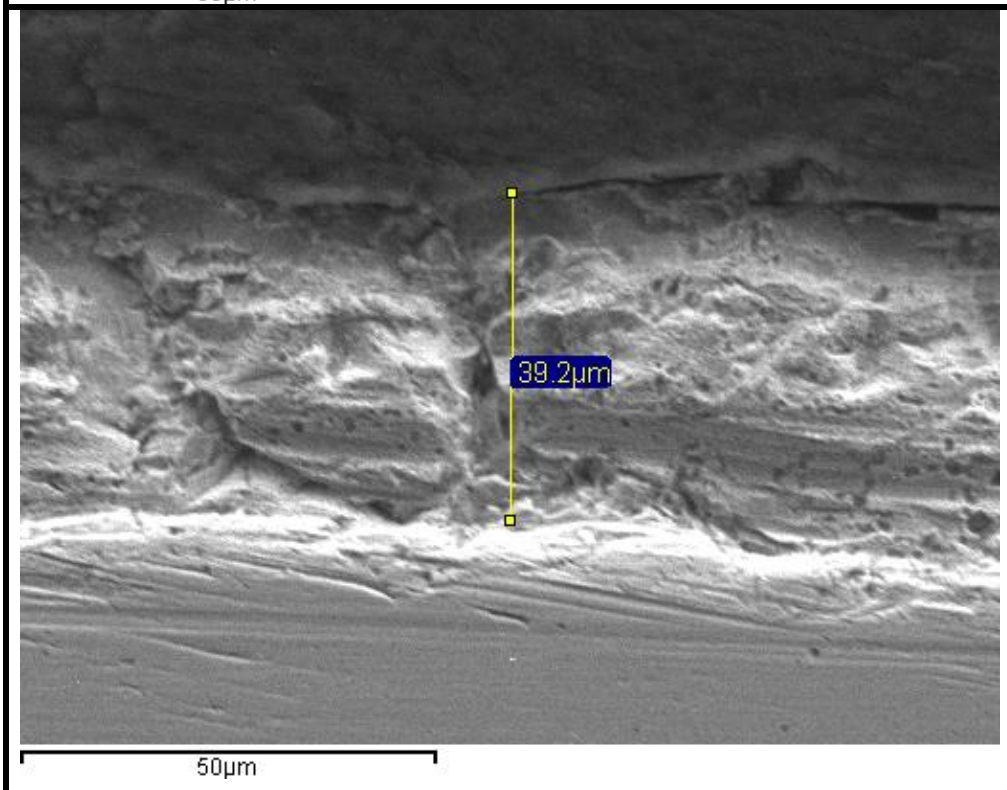

Figure 30

Mag = X

Voltage = 20kV

Comment:
C-HDG I
60-Cycles

Location 1

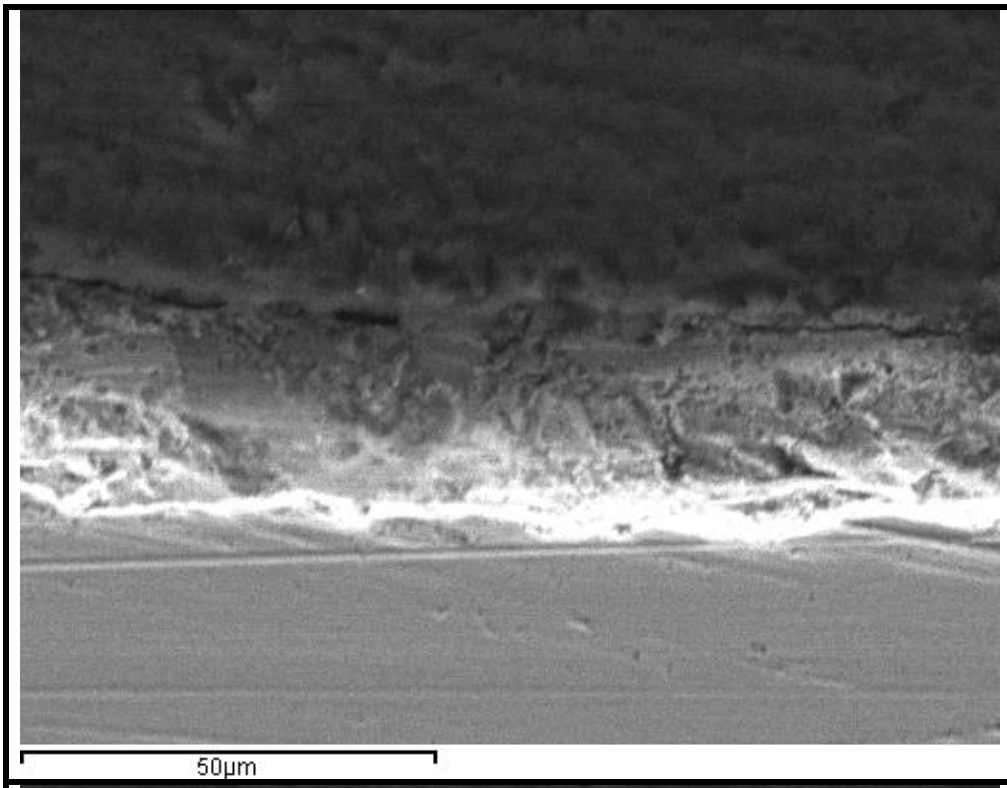

Figure 31

Mag = X1,000

Voltage = 20kV

Comment:
C-HDG I
60-Cycles

Location 2

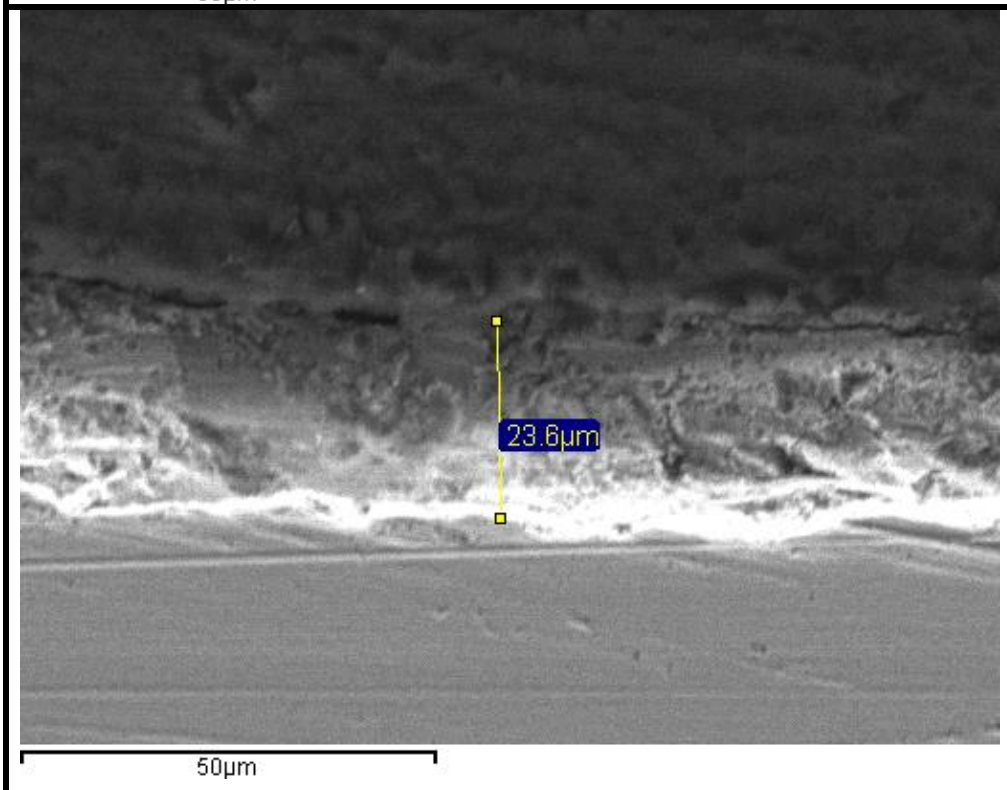

Figure 32

Mag = X1,000

Voltage = 20kV

Comment:
C-HDG I
60-Cycles

Location 2

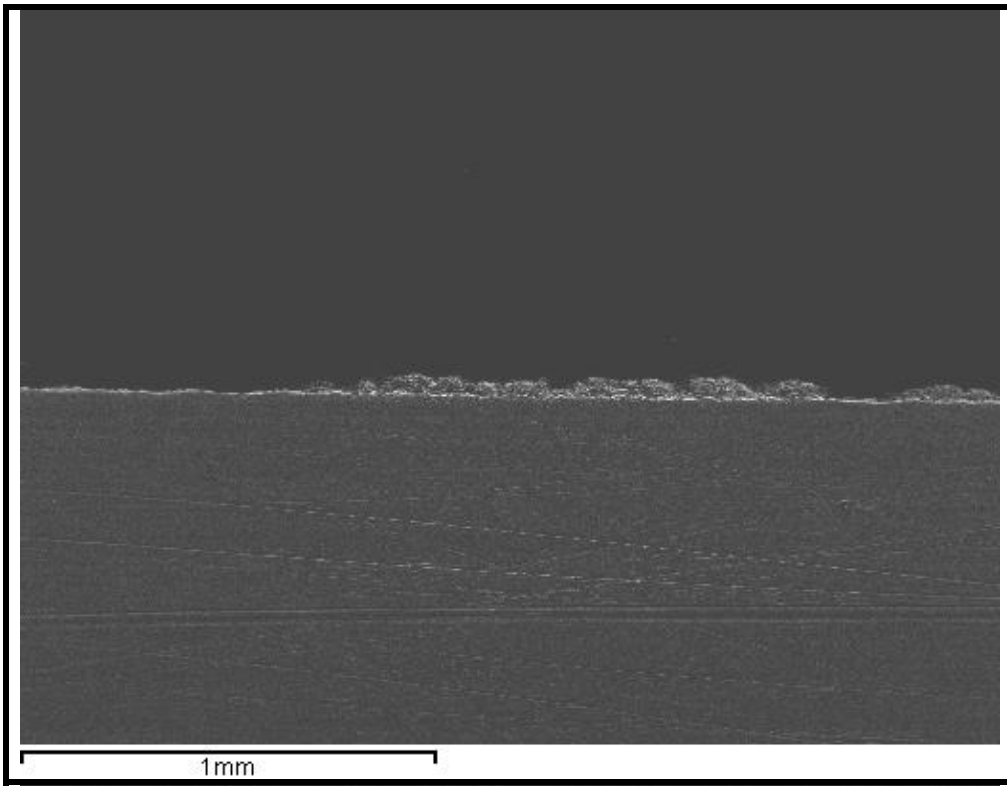

Figure 33

Mag = X50

Voltage = 20kV

Comment:
C-HDG II
60-Cycles

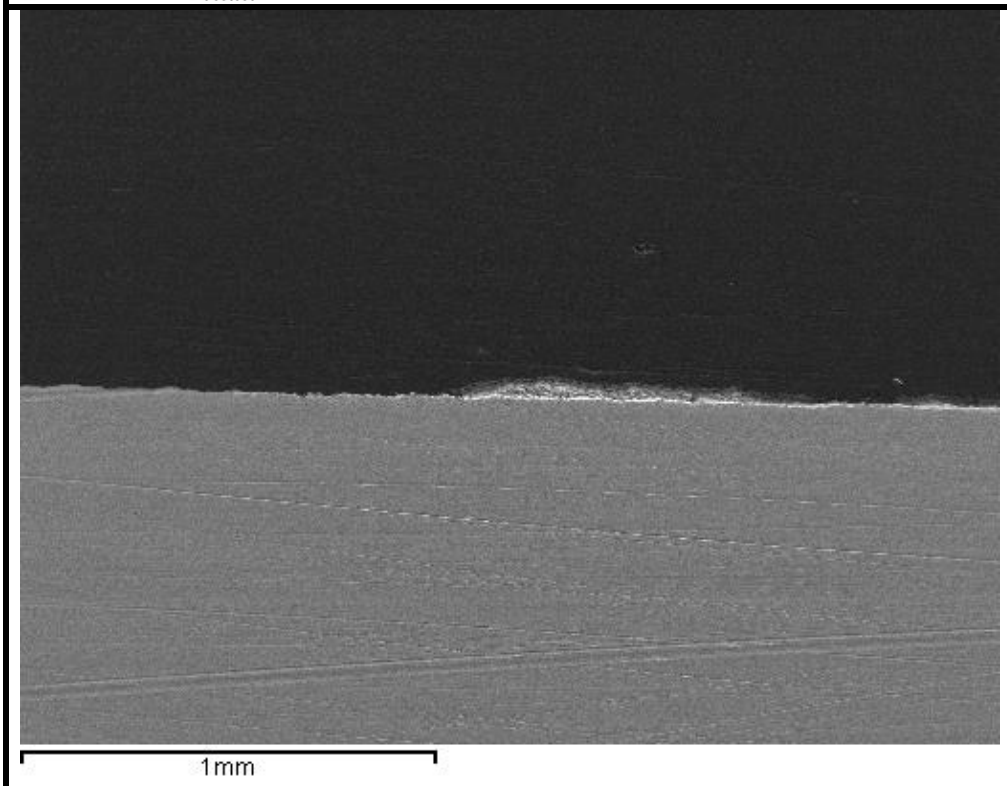

Figure 34

Mag = X50

Voltage = 20kV

Comment:
C-HDG II
60-Cycles

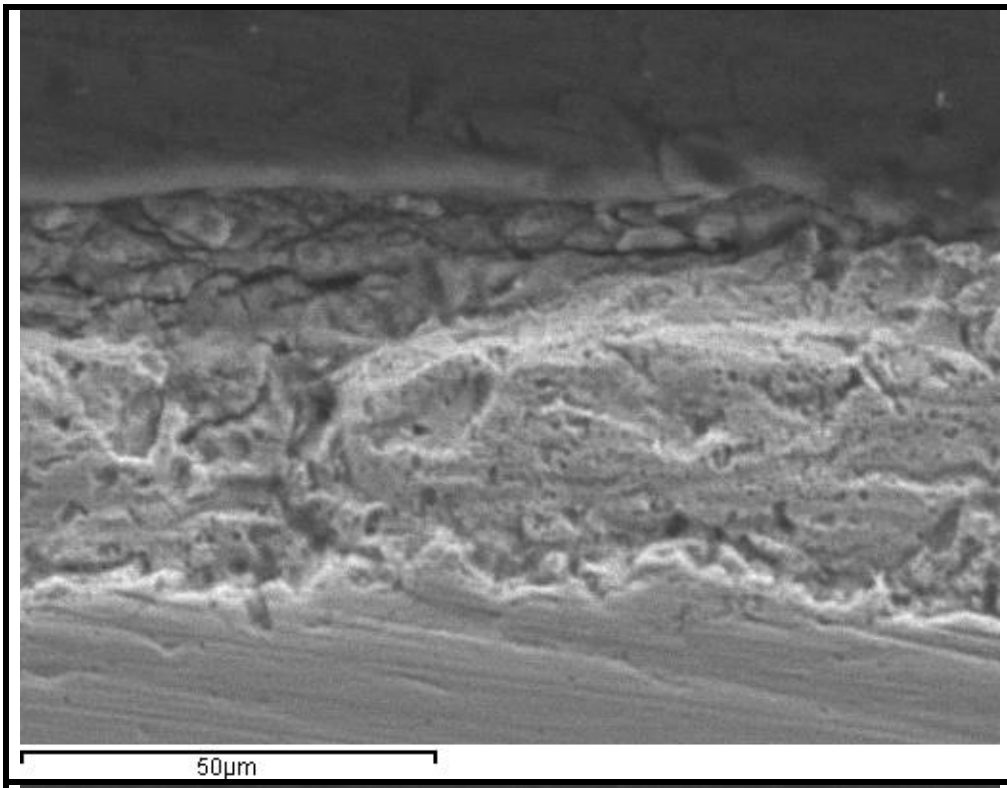

Figure 35

Mag = X1000

Voltage = 20kV

Comment:
C-HDG II
60-Cycles

Location 1
zoom in on the
area in Figure 27

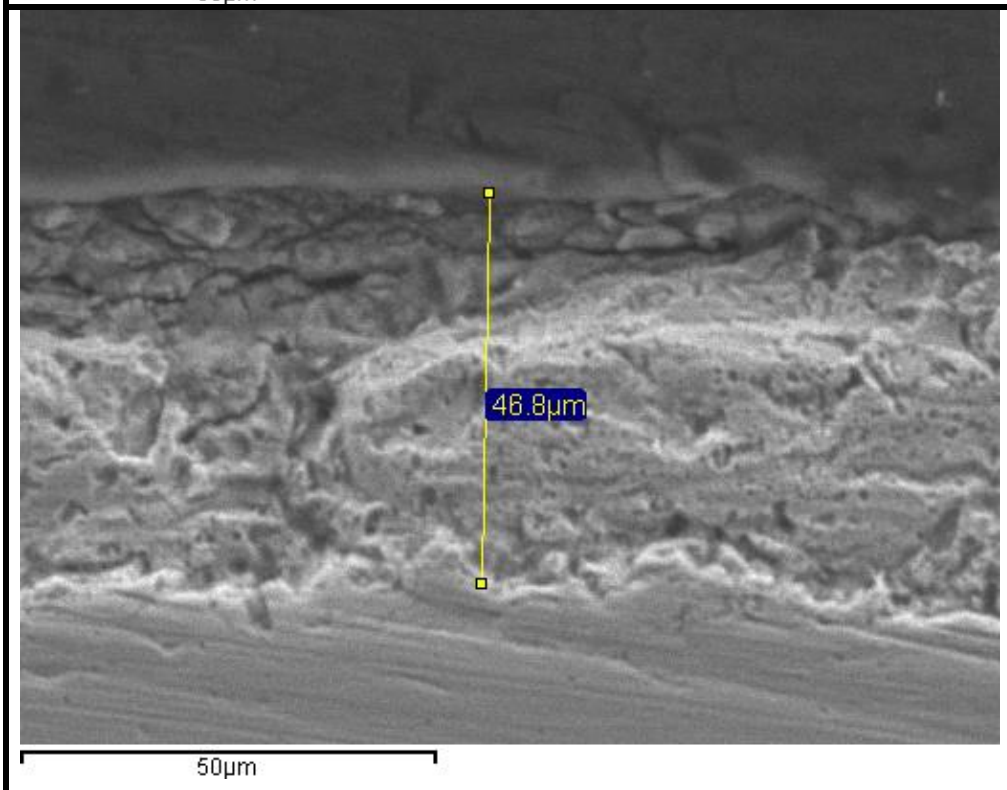

Figure 36

Mag = X1000

Voltage = 20kV

Comment:
C-HDG II
60-Cycles

Location 1
zoom in on the
area in Figure 27

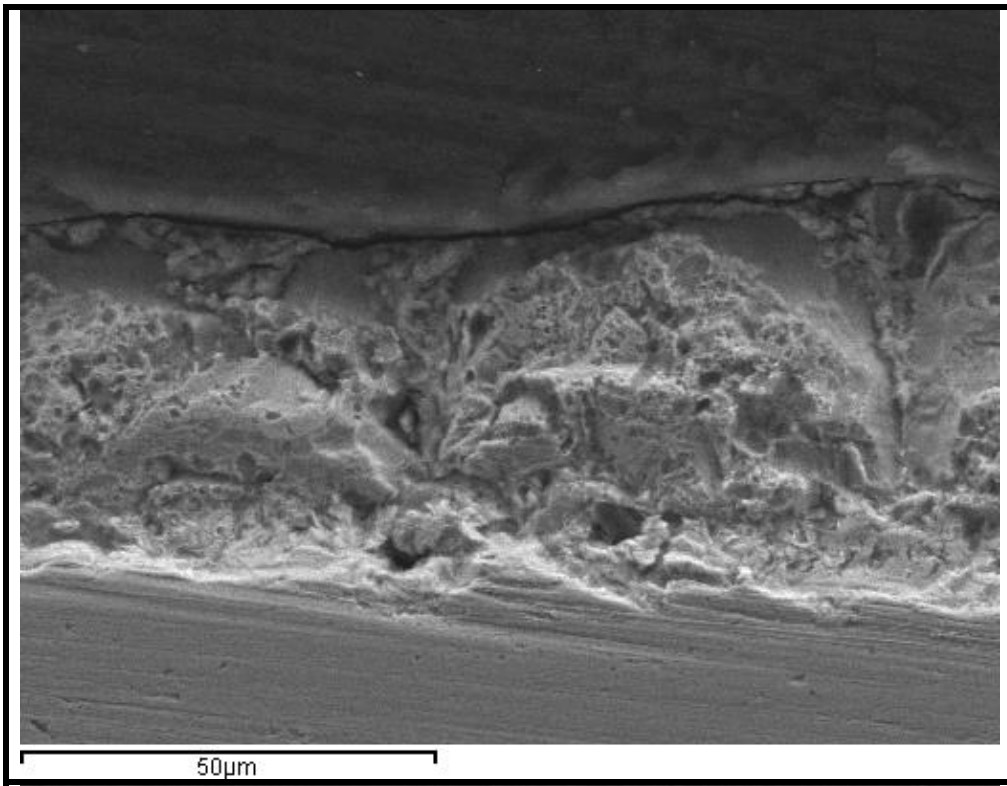

Figure 37

Mag = X1000

Voltage = 20kV

Comment:
C-HDG II
60-Cycles

Location 2
zoom in on the
area in Figure 28

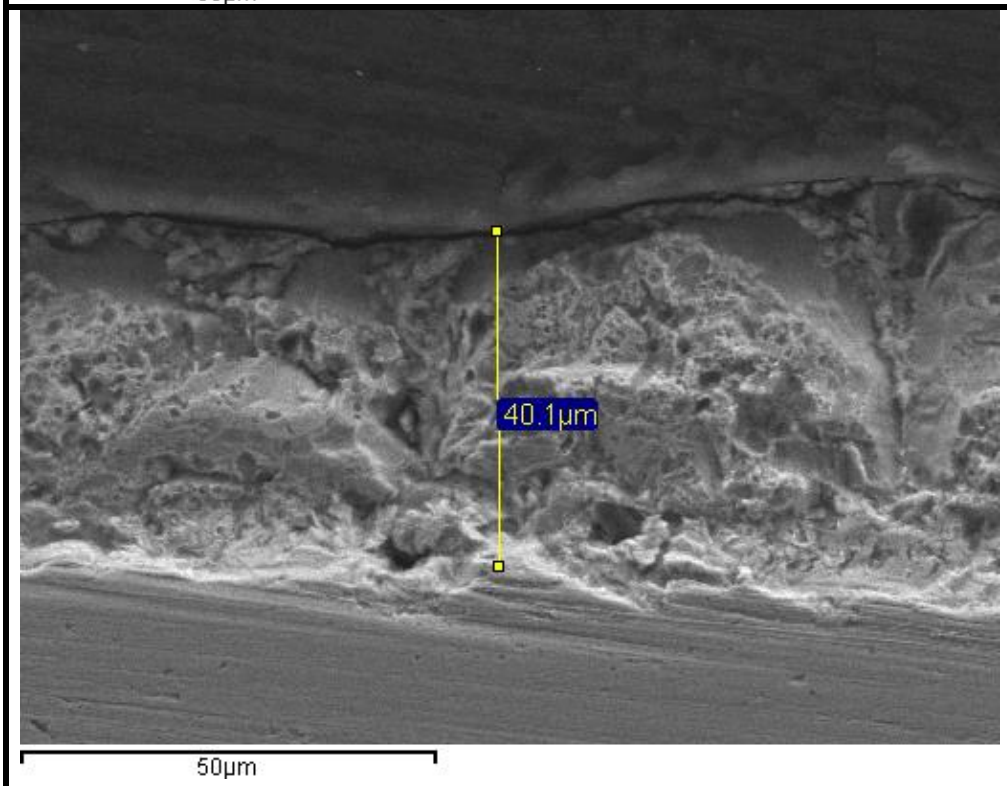

Figure 38

Mag = X1000

Voltage = 20kV

Comment:
C-HDG II
60-Cycles

Location 2
zoom in on the
area in Figure 28

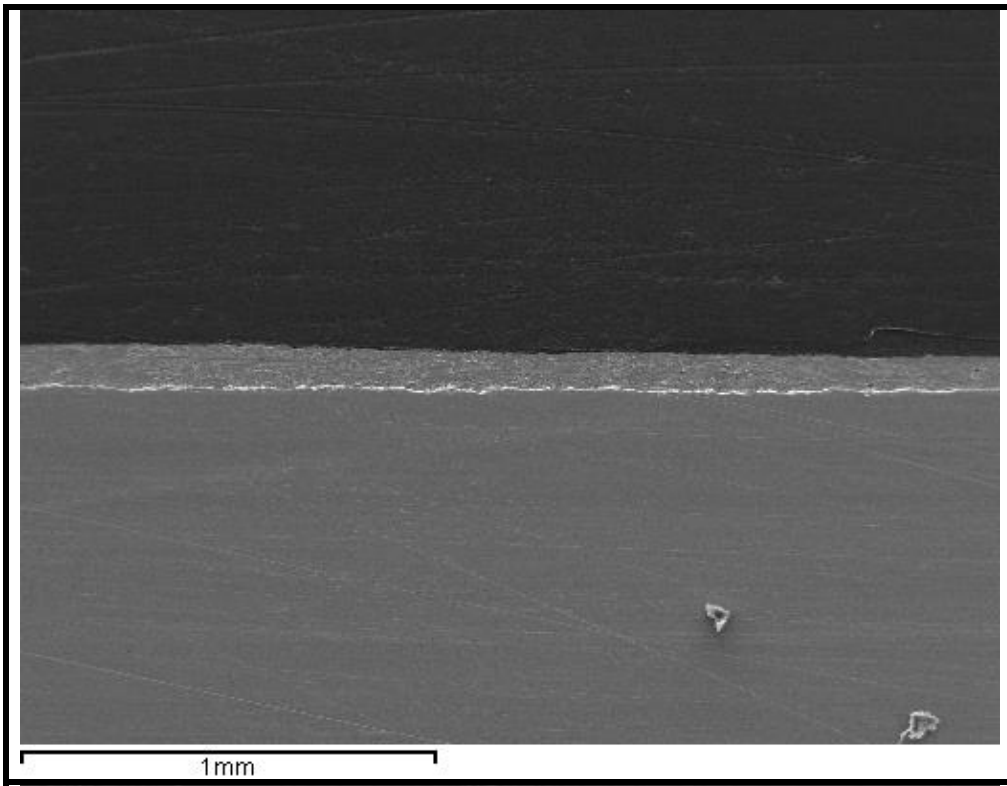

Figure 39

Mag = X50

Voltage = 20kV

Comment:
C-HDG I
Pre-exposure

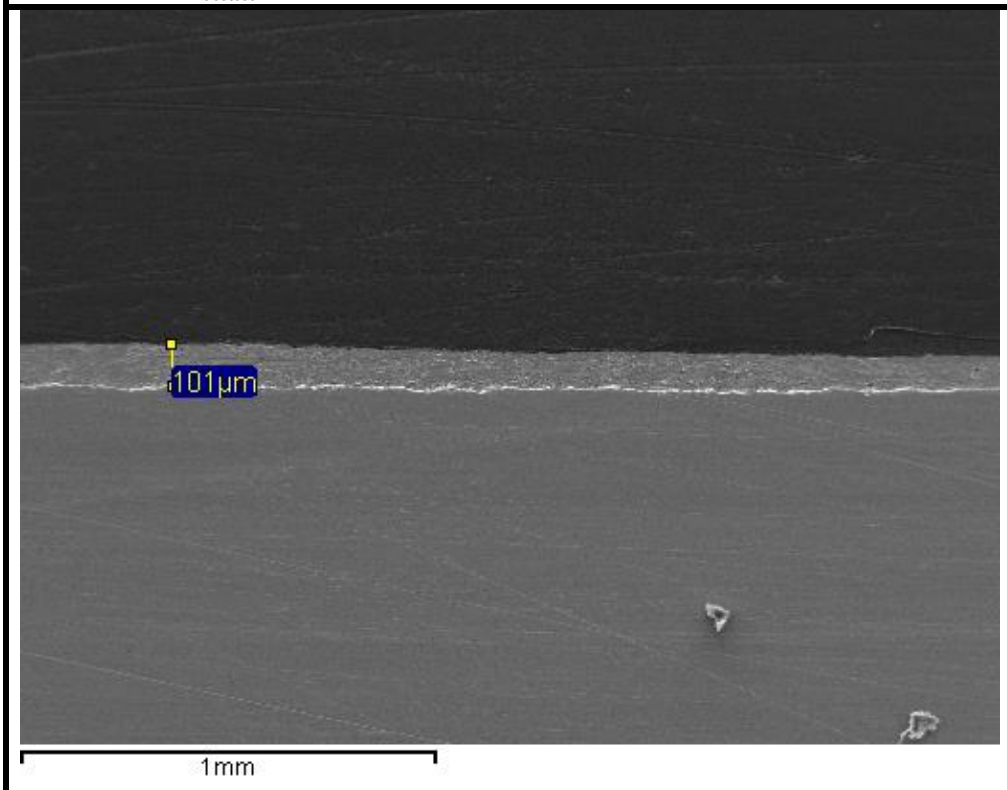

Figure 40

Mag = X50

Voltage = 20kV

Comment:
C-HDG I
Pre-exposure

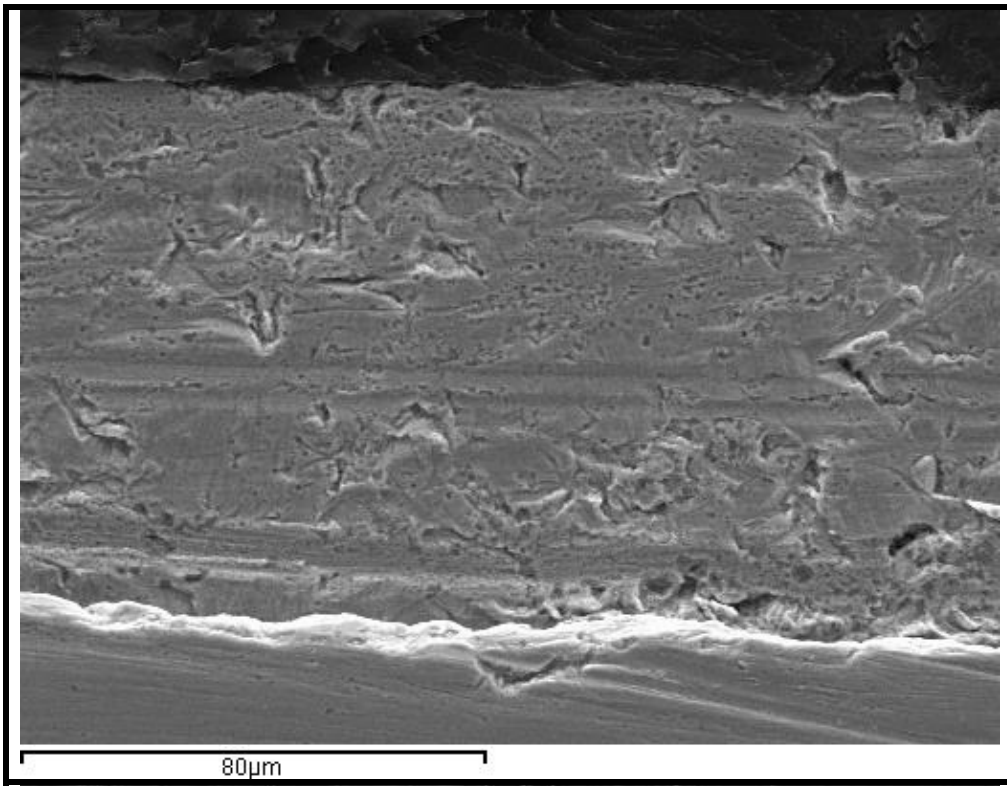

Figure 41

Mag = X700

Voltage = 20kV

Comment:
C-HDG I
Pre-exposure

Location 1

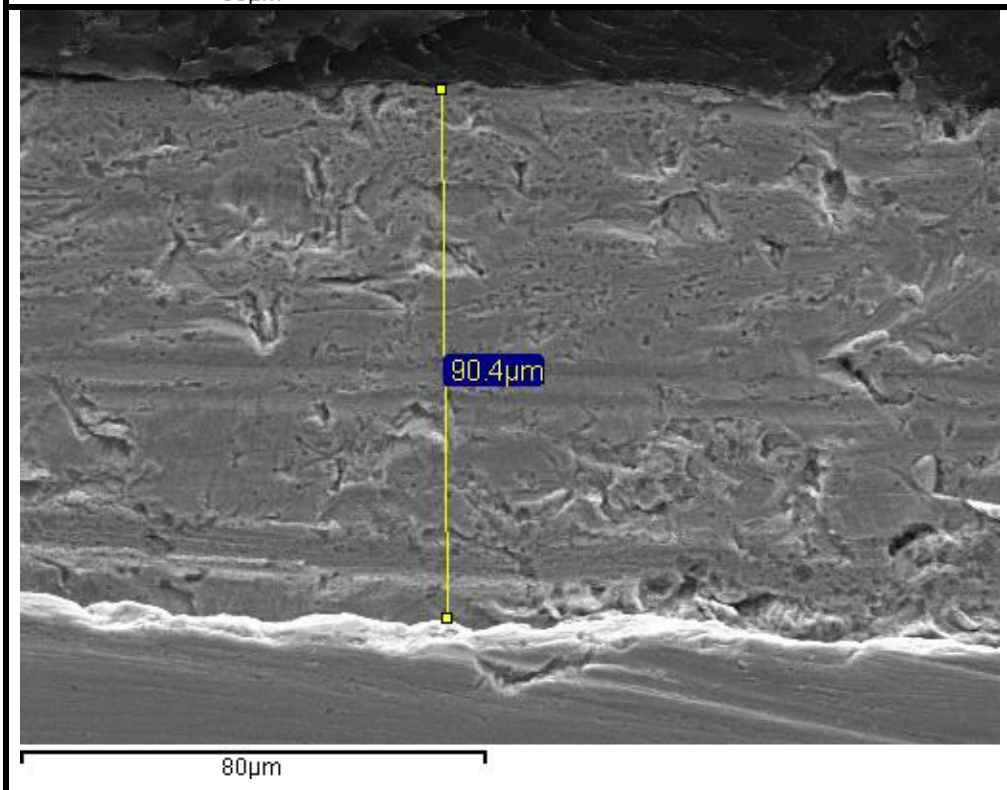

Figure 42

Mag = X700

Voltage = 20kV

Comment:
C-HDG I
Pre-exposure

Location 1

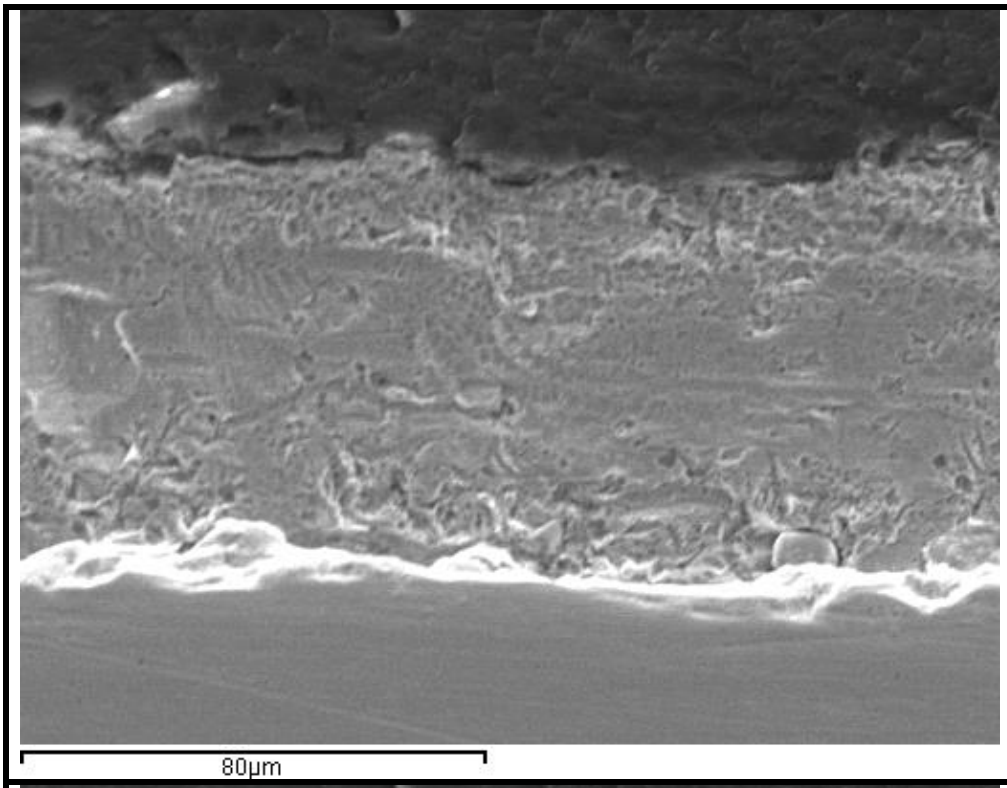

Figure 43

Mag = X700

Voltage = 20kV

Comment:
C-HDG I
Pre-exposure

Location 2

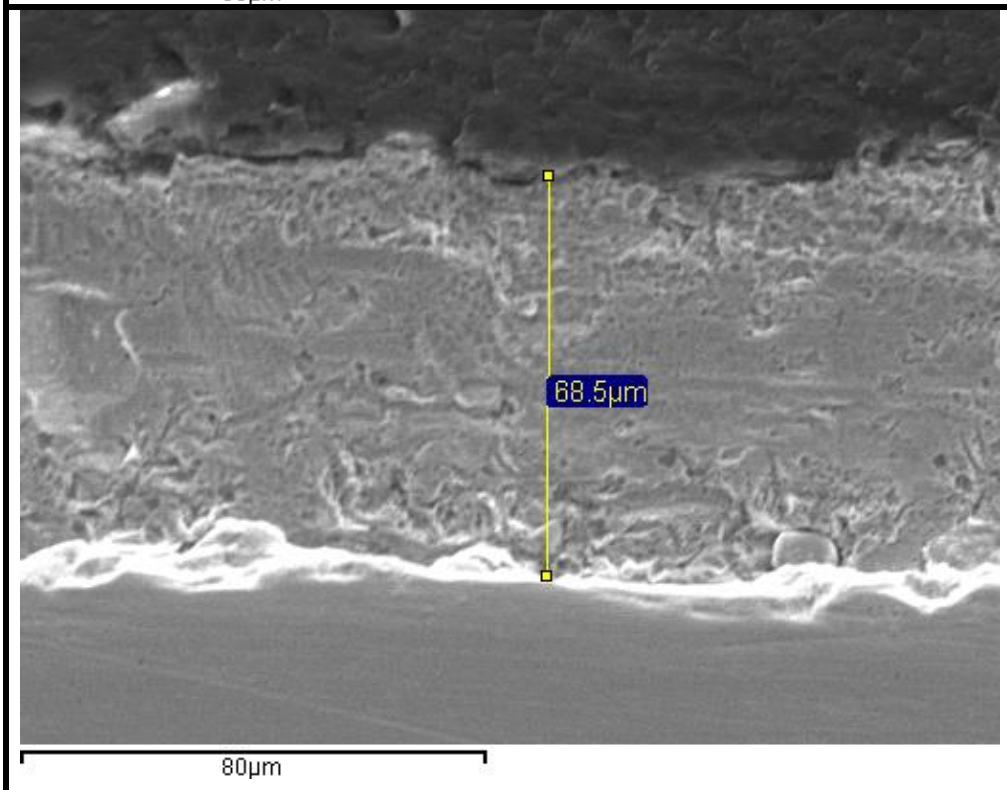

Figure 44

Mag = X700

Voltage = 20kV

Comment:
C-HDG I
Pre-exposure

Location 2

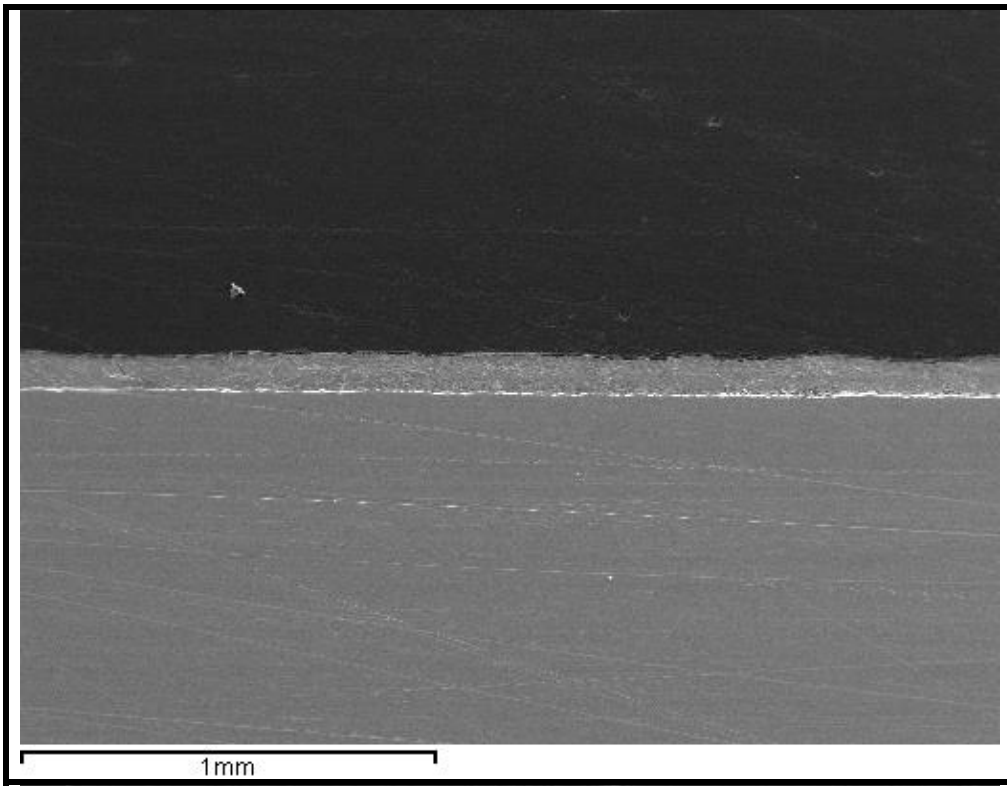

Figure 45

Mag = X50

Voltage = 20kV

Comment:
C-HDG II
Pre-exposure

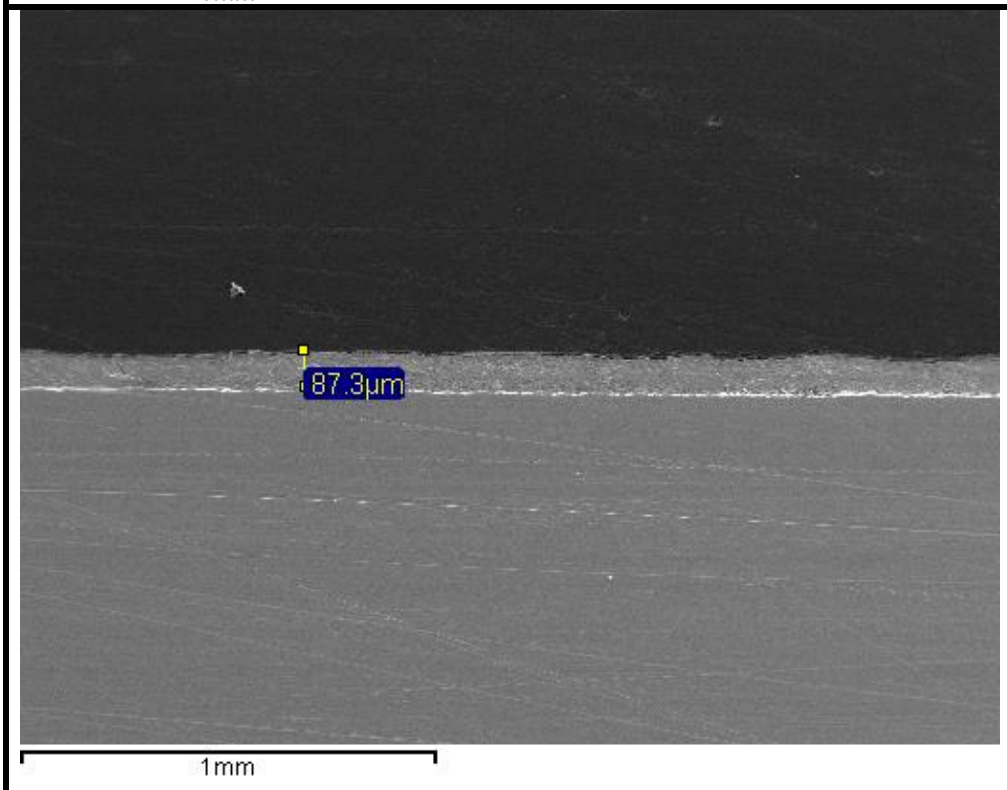

Figure 46

Mag = X50

Voltage = 20kV

Comment:
C-HDG II
Pre-exposure

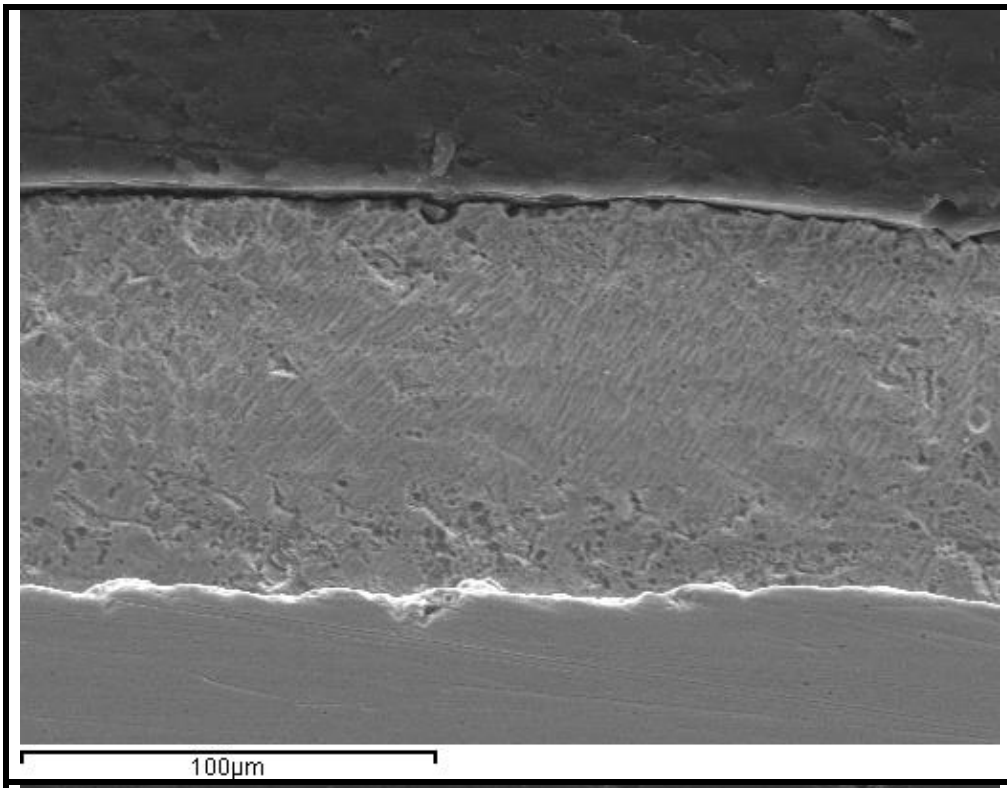

Figure 47

Mag = X500

Voltage = 20kV

Comment:
C-HDG II
Pre-exposure

Location 1

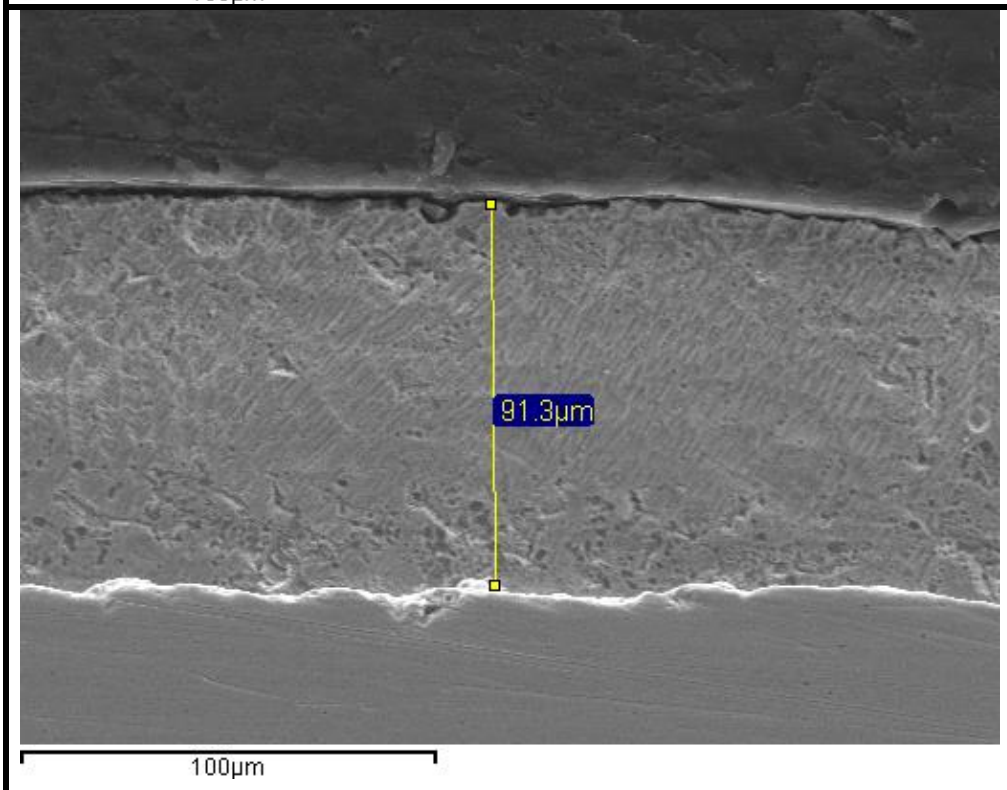

Figure 48

Mag = X500

Voltage = 20kV

Comment:
C-HDG II
Pre-exposure

Location 1

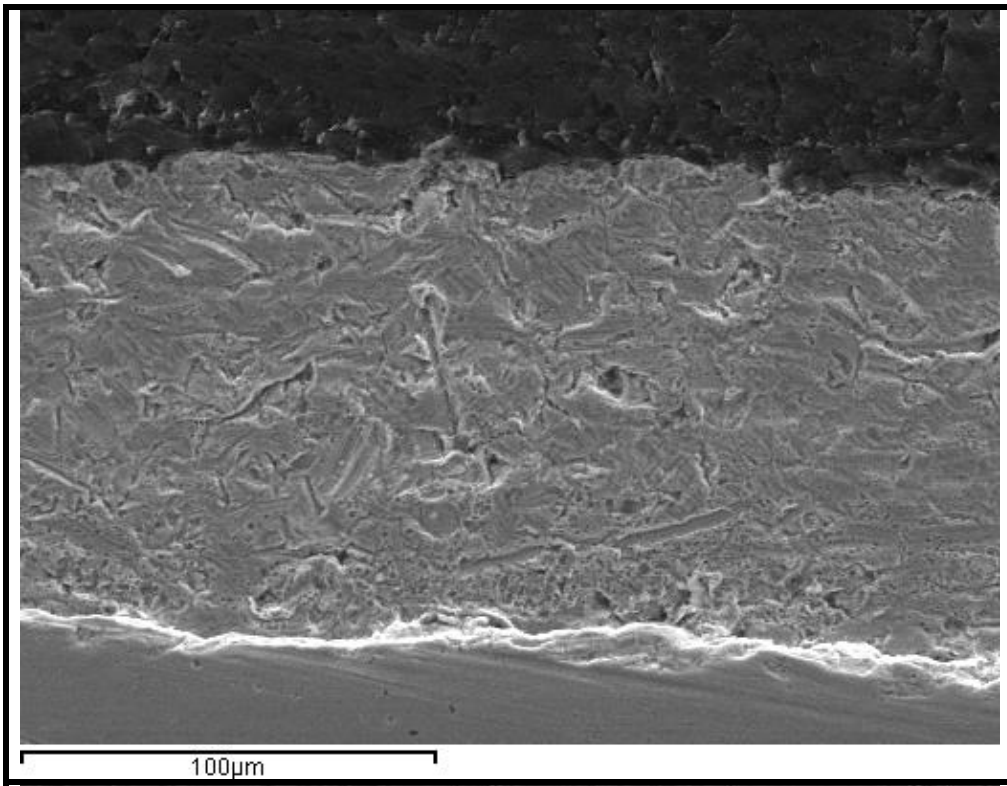

Figure 49

Mag = X500

Voltage = 20kV

Comment:
C-HDG II
Pre-exposure

Location 2

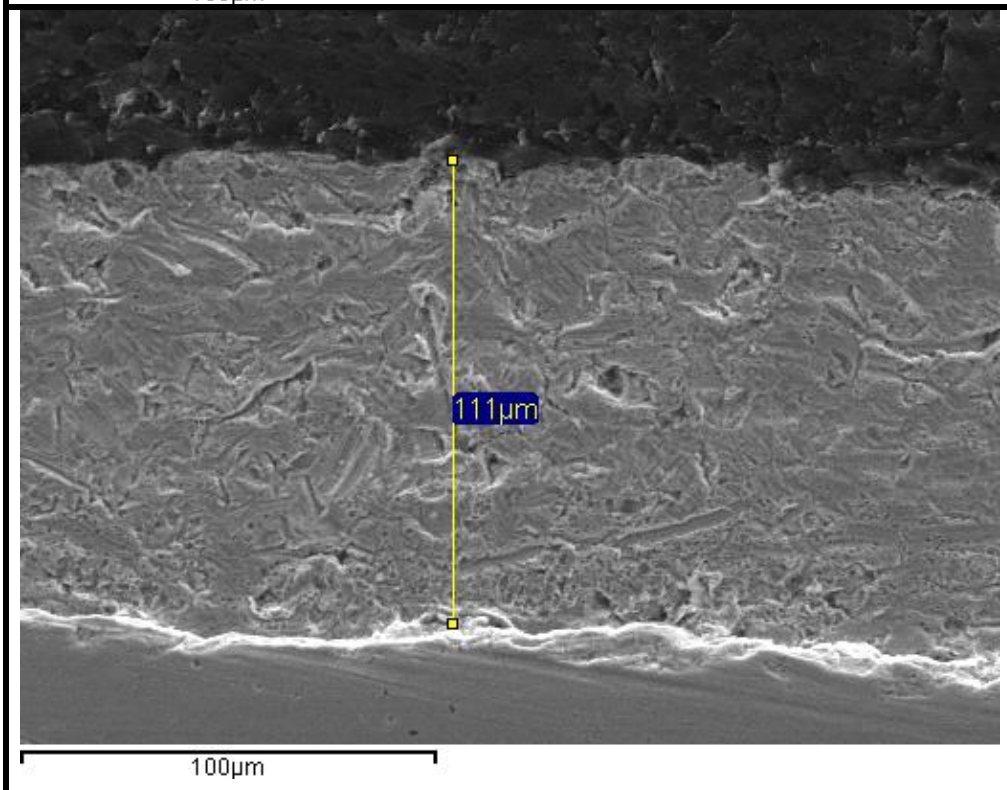

Figure 50

Mag = X500

Voltage = 20kV

Comment:
C-HDG II
Pre-exposure

Location 2